Technische Universität München
Wissenschaftszentrum Weihenstephan für Ernährung, Landnutzung und Umwelt
Lehrstuhl für Systemverfahrenstechnik

New Paths in Filtration – Optimal Control Approaches Based on Continuum Models

Michael Kuhn

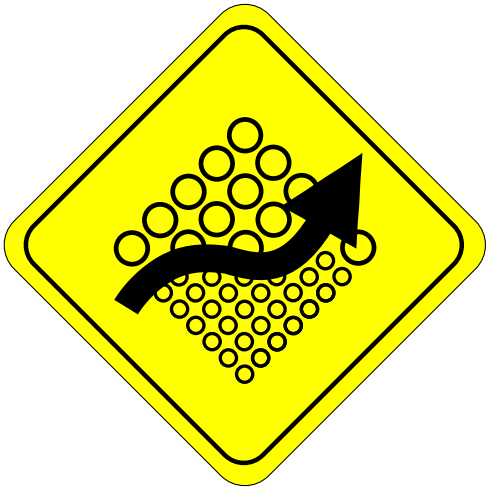

Technische Universität München
Wissenschaftszentrum Weihenstephan für Ernährung, Landnutzung und Umwelt
Lehrstuhl für Systemverfahrenstechnik

New Paths in Filtration – Optimal Control Approaches Based on Continuum Models

Michael Kuhn

Vollständiger Abdruck der von der Fakultät Wissenschaftszentrum Weihenstephan für Ernährung, Landnutzung und Umwelt der Technischen Universität München zur Erlangung des akademischen Grades eines Doktor-Ingenieurs (Dr.-Ing.) genehmigten Dissertation.

Vorsitzende: Prof. Dr. Mirjana Minceva

Prüfer der Dissertation:
1. Prof. Dr.-Ing. Heiko Briesen
2. Prof. Dr.-Ing. Sergiy Antonyuk, Technische Universität Kaiserslautern

Die Dissertation wurde am 10.10.2017 bei der Technischen Universität München eingereicht und durch die Fakultät Wissenschaftszentrum Weihenstephan für Ernährung, Landnutzung und Umwelt am 06.02.2018 angenommen.

Abstract

This dissertation explores the use of optimal control methods in the field of filtration. All simulation and optimization approaches are based on continuum models because this model type provides the required computational efficiency. Two case studies are considered in detail. First, the design of depth filters is optimized with respect to the spatial distribution of deposit within the filter and achievable filtration times. The control variable is the local filtration performance as described by the filter coefficient. For a simplified problem, an analytical optimal control solution is derived and the numerical algorithm is validated against this solution. Furthermore, a method to derive discrete filter layers from the continuous optimal control trajectories, as required for practical filter design, is presented.

The second case study considers filter-aid filtration. In a first step, a mechanistic model is derived which takes the contributions of surface and depth filtration to the total separation into account. Appropriate mathematical and numerical tools for solving the model equations, a moving boundary problem with sharp discontinuities, are identified. Secondly, an analytical optimal control solution for the dosage of filter aids is presented for a simplified problem, where all separation takes place due to surface filtration. In a third step, optimal filter-aid dosage is computed numerically for the full model. Goal of both optimal control approaches is to minimize energy consumption.

Furthermore, a broader historical and systematic framework is developed in which the two case studies on depth filtration and filter-aid filtration are embedded. Using systematic analogies, it is argued that the methods and results of the two case studies can be transferred to related applications. Flow through compressible porous media and processes based on intraparticle diffusion are discussed as promising candidates for such a transfer. The conducted historical analysis shows that we are entering a period in which, for the first time, the microstructure of filters can be tailored according to given specifications, e.g., using 3D printing technologies. It is asserted that the developed optimal control methods can play an important part in determining spatially-distributed microstructural properties and that they, therefore, aid a multi-scale approach to filter design and control.

Kurzzusammenfassung

Diese Dissertation erschließt Optimalsteuerungsmethoden für das Feld der Filtration. Alle Simulations- und Optimierungsansätze beruhen auf Kontinuumsmodellen, da dieser Modelltyp die benötigte Recheneffizienz gewährleistet. Zwei Fallstudien werden detailliert behandelt. In der ersten Studie wird der Aufbau von Tiefenfiltern in Bezug auf die örtliche Verteilung von Abscheidungen im Filter und erzielbare Filtrationszeiten optimiert. Die Kontrollvariable ist die lokale Filtrationsleistung, wie sie durch den Filterkoeffizienten beschrieben wird. Für ein vereinfachtes Modell wird eine analytische Optimalsteuerungslösung hergeleitet und der numerische Algorithmus damit validiert. Außerdem wird eine Methode vorgestellt, um diskrete Filterschichten, wie sie für das praktische Auslegen von Filtern benötigt werden, aus den kontinuierlichen Optimalsteuerungstrajektorien abzuleiten.

Die zweite Fallstudie behandelt das Verfahren der Anschwemmfiltration. Hierbei wird als erstes ein mechanistisches Modell hergeleitet, das Beiträge von Oberflächen- und Tiefenfiltration an der gesamten Trennung berücksichtigt. Geeignete mathematische und numerische Werkzeuge zur Lösung der Modellgleichungen, die ein Moving-Boundary-Problem mit scharfen Diskontinuitäten bilden, werden identifiziert. Weiterhin wird eine analytische Optimalsteuerungslösung der Dosierung von Filterhilfsmitteln für ein vereinfachtes Model präsentiert, in dem nur Oberflächenfiltration berücksichtigt wird. Außerdem wird die Filterhilfsmitteldosierung numerisch für das volle Modell optimiert. Ziel der Optimalsteuerung ist je die Minimierung des Energieeinsatzes.

Die beiden zentralen Fallstudien dieser Arbeit werden zudem in einen umfassenderen historischen und systematischen Rahmen gestellt. Basierend auf systematischen Analogien wird dafür argumentiert, dass die Methoden und Ergebnisse der Fallstudien auf verwandte Anwendungen übertragen werden können. Als zwei vielversprechende Beispiele für eine solche Übertragung werden die Durchströmung kompressibler poröser Medien und diffusionsgetriebene Prozesse diskutiert. Die durchgeführte historische Analyse zeigt, dass gerade eine Phase beginnt, in der es zum ersten Mal möglich ist, Filtermikrostrukturen nach gegebenen Anforderungen herzustellen, z.B. unter Verwendung von 3D-Drucktechnologien. Es wird vermutet, dass die entwickelten Optimalsteuerungsmethoden einen wichtigen Beitrag zur Ermittlung örtlich verteilter Mikrostruktureigenschaften leisten können und damit einen Multiskalen-Ansatz im Bereich Filterauslegung und -steuerung unterstützen.

Acknowledgments

My deepest gratitude goes to Prof. Dr.-Ing. Heiko Briesen for supervising this work. He always had an open ear and was singularly helpful and encouraging. Professor Briesen is also thanked for providing a uniquely inspiring and creative environment in which new ideas can be developed and openly discussed. I am very grateful to Prof. Dr.-Ing. Sergiy Antonyuk for examining this dissertation and to Prof. Dr.-Ing. Mirjana Minceva for presiding over the examination committee.

For proof reading parts of the work and providing many helpful hints, I thank Jörg Engstle, Moritz Kindlein, Christoph Kirse, Dimitrios Kokkinos, Marco Meixner, and Thomas Riller. Peter Bandelt read the whole dissertation and made various helpful comments. Obviously, all remaining mistakes are mine.

Special thanks go, again, to Christoph Kirse for many fruitful discussions on optimal control. I am grateful to Jörg Engstle, again, and Alexander Scheidel (former employee of the Chair for Process Engineering of Disperse Systems) for beneficial exchange on the more practical aspects of filtration. I further thank all students who were supervised by me over the years and who, directly or indirectly, all contributed to this work.

I thank Wiley for the kind permission to use parts of the text in Chapter 1 from Kuhn et al. (2017c), to reuse Kuhn and Briesen (2016b) for Chapter 4 and large parts of Kuhn and Briesen (2016b) for Chapter 5. All helpful comments on my publications, provided by various anonymous reviewers, are acknowledged.

For a great shared time in the office EG30, I thank Jörg Engstle and Tijana Kovačević. Equally, I am grateful to all other former and current employes of the Chair of Process Systems Engineering for creating such a pleasant working atmosphere. Finally, I deeply thank my parents and friends. My parents supported my education and provided general encouragement during the last years. Also, I am very grateful to my girlfriend Veronika for her great support and her patience during many a stressful period.

Contents

List of Figures

List of Tables

Symbols and Abbreviations

In the following, the notation of this dissertation is summed up. Some of the variables are used in vector as well as scalar form. They are not listed twice, vectors are simply shown as bold letters in this thesis. Indices are only listed separately if the same variables are complemented by different indices; if they are used to denote separate variables or quantities, they are introduced together with the corresponding letters. Units are only supplied where they are meaningful. The few ambiguities in symbol use are clearly marked in the following lists.

Latin Symbols

A	Area [m^2]
a, b	Parameters in constitutive equations; a also denotes an integration constant in Section 5.3
c	Volume concentration [-], mass concentration [kg/m^3] (only in Section 6.2)
D	Diffusion coefficient, diffusivity (synonymous) [m^2/s]
d	Diameter [m]
E	Young's modulus [N/m^2]
e	Specific energy consumption, i.e. energy per filter area [kg/s^2]
e_c	Strain [-]; in this work only used as compression
F	Function in depth filtration model, force [N] (only in Chapter 6)
f, g, h	Unspecified functions; g and h denote also constraints in Section 3.2
g	Gravitational constant [m/s^2], if not used as an unspecified function
H	Hamiltonian
I	Phase function [-]
k	Permeability [m^2]
L	Length, total height [m]
M	Boundary detection function [-]
m	Mass [kg]
n	Arbitrary number
p	Pressure [N/m^2]
P	Parameter vector
Q	Volume flow [m^3/s]

q	Superficial velocity [m/s]
R	Total filter cake resistance [m], overall radius [m] (only in Chapter 6)
r	Filter cake resistance [m^2], radial coordinate [m] (only in Chapter 6)
r_i	Ratio between neighboring gradients
r_a	Reactive term
s	Source term, characteristic variable (only in Appendix 4.1)
s_p	Specific surface [1/m]
t	Time [s]
u	Control variable [-]
V	Volume [m^3]
v	Velocity [m/s]
x	Spatial location [m], unspecified independent variable [-]
y	Unspecified dependent variable [-]
z	Spatial location [m]

Greek Symbols

Δ	Difference
ε	Porosity [-]
ε_p	Machine precision [-]
ε_s	Solidosity [-]
η	Dimensionless spatial coordinate [-]
ρ	Density [kg/m^3]
λ	Filter coefficient [1/m]
μ	Dynamic viscosity [kg/(m s)]
μ_w	Friction coefficient at the wall [-]
ν	Poisson's ratio [-]
σ	Specific deposit [-]
σ_c	Compressive stress [N/m^2]
ψ	Costate state, adjoint state, Lagrange multiplier (synonymous)
ϕ	Volume fraction (Section 2.1.2), limiter function (Section 3.1.2)

Subscripts

0	Initial state
41…55	Parameters in constitutive equations; the first number denotes the chapter, i.e., 4 or 5, the second the number of the corresponding parameter
c	Component

d	Deposit
DF	Depth filtration
DF-A	Depth filtration, analytical optimal control solution
DF-OC1	Depth filtration, first numerical optimal control scenario
DF-OC2	Depth filtration, second numerical optimal control scenario
e	End state
eff	Effective value
FA	Filter aid
FA-A	Filter-aid filtration, analytical optimal control solution
FA-Opt	Filter-aid filtration, optimization scenario
FA-OC	Filter-aid filtration, optimal control scenario
h	Homogeneous
L	Lagrange (type of objective functional)
m	Mass
M	Mayer (type of objective functional)
Opt	Optimum
p	Reference to pore space
PC	Precoat
s	Solid, stop, system (only in Section 2.3)
v	Volume
vessel	Reference to whole vessel
α	Reference to arbitrary phase

Superscripts

p	Reference to pore space

Accents

$\tilde{}$	Fluctuations around average (only in Section 2.1.2), nondimensional variable
$\hat{}$	Variable in transformed coordinate system
$\bar{}$	Average

Abbreviations

1D, 2D, 3D	One-, two-, three-dimensional

CFD	Computational fluid dynamics
CLSM	Confocal laser scanning microscopy
CT	Computed tomography
DF-0	Depth filtration, reference case for comparison
DF-A	Depth filtration, analytical optimal control solution
DF-OC1	Depth filtration, first numerical optimal control scenario
DF-OC1-3L	Depth filtration, first numerical optimal control scenario, 3 layers
DF-OC2	Depth filtration, second numerical optimal control scenario
DF-OC2-3L	Depth filtration, second numerical optimal control scenario, 3 layers
FA-0	Filter-aid filtration, reference scenario for model exploration
FA-1	Filter-aid filtration, first model exploration scenario
FA-2	Filter-aid filtration, second model exploration scenario
FA-A	Filter-aid filtration, analytical optimal control solution
FA-Opt	Filter-aid filtration, numerical optimization scenario
FA-OC	Filter-aid filtration, numerical optimal control scenario
FDM	Finite difference method
FEM	Finite element method
FGM	Functionally graded materials
FVM	Finite volume method
MRI	Magnetic resonance imaging

Chapter 1

Introduction

1.1 Introducing the Topic by an Explication of the Title

In this section, a first outline of the topic is provided by a word-by-word comment on the title. All of these points will be discussed in much more depth later on.

Filtration denotes the unit operation in process engineering where dispersed matter, often solid, is separated from a fluid phase. In this thesis, the considered fluid is always a liquid, as opposed to gas filtration. Furthermore, all discussed filtration processes aim at clarification of the liquid phase, in contrast to other processes where the separated solids are of primary interest.

Optimal control, generally speaking, is the systematic search for functions that minimize a given cost measure. These functions can be conceived of as paths, usually in space or time, hence the **path** label in the title. Additionally, possible developments resulting from this thesis can be interpreted as **new paths**.

Continuum models are based on continuum mechanics. This implies that matter is treated as a continuum in contrast to being composed of parts. In particular, the continuum label is used to demarcate the porous media and filtration models used in this work from other methods such as pore-scale models, where the true geometry of pores is considered, and pore-network models, where the pores are represented by simplified networks. Continuum models are used in this dissertation mainly due to their computational efficiency compared to the other two approaches.

Next, some historical background is provided, followed by a discussion of the epistemological stance of this work. Both sections flesh out some general foundation of the following material. The introductory chapter ends with a detailed outline of the remaining thesis.

1.2 Filtration and Control: A Short History of Practice and Theory

Filtration and control are now briefly reviewed from a historical perspective. This allows to introduce some central concepts and to locate this dissertation with respect to the broad background of the two fields. It will be seen that practice mostly preceded theory in the history of filtration and control; for that reason, practice is also mentioned first in the title of this section. The historical account of filtration along with the reflection on paradigms in engineering follows Kuhn et al. (2017c).

1.2.1 Paradigms in Filtration

Writing history consists not only in an enumeration of facts, the historical facts also have to be organized in some way. A very influential model for structuring the historical development of scientific disciplines was provided by the physicist and historian of science Thomas Kuhn[1] in his highly influential 1962 book, "The Structure of Scientific Revolutions" (Kuhn, 1970). In that work, the concept of research paradigms plays a central role. A paradigm comprises all aspects of scientific practice including theories, laws, methods, and applications. It is a set of shared believes among scientists, as to what counts as proper science and what does not. Notably, paradigms include prototypical problem solutions that inspire further research and pose follow-up problems considered interesting and relevant by the scientific community. As seen by Kuhn, Newtonian mechanics, Einsteinian relativity, or Darwin's theory of evolution are typical examples of paradigms in different disciplines.

According to Kuhn's model, each discipline undergoes a preparadigmatic phase, followed by the establishment of a paradigm in which "normal science" is conducted, i.e. problems are solved using the means provided by the paradigm. If too many unsolved problems accumulate, i.e. if problems continuously resist a solution within the framework of a given paradigm, it is abandoned resulting in a scientific revolution, which leads to the establishment of a new paradigm replacing the old one. This scheme is now briefly applied to the history of liquid filtration. A schematic of the identified paradigms, including the rough time frames, is shown in Figure 1.1.

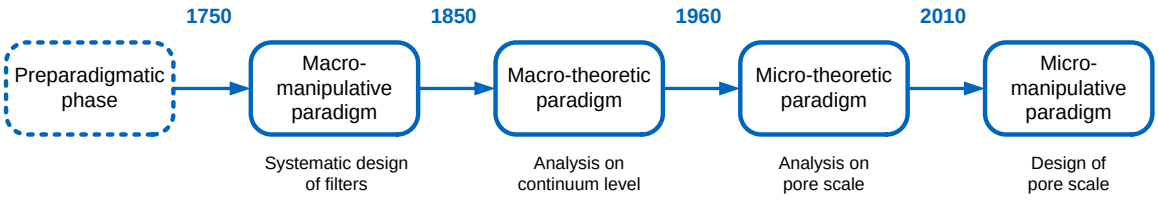

Figure 1.1: Paradigms in filtration research with corresponding characteristics; years of paradigm shifts are understood only as rough estimates.

[1] In no way affiliated with the author of this thesis.

Filtration in its **preparadigmatic phase** is characterized by trial-and-error approaches. Results were not published systematically, there were no explicit filtration researchers and no scientific community focusing on filtration. No coherent framework of established methods, unified goals, prototypical problems, etc. existed. One only finds largely unconnected empirical results and evidence from practically applied filtration approaches scattered across different times and locations. Typical examples are the filtration of water utilizing porous vessels as filter media in ancient Egypt (Anlauf, 2003) and "Hippocrates' sleeve", cloth bags used to clarify rain water, suggested by the ancient Greek physician Hippocrates (c. 460- c. 380 BC) (Baker, 1948, p. 5).

The first coherent research endeavor that eventually emerged could be termed the **macro-manipulative paradigm**. The main characteristic of this paradigm is systematic experimentation at the level of whole filters or filter components, i.e. macroscopically. Different design variables, such as filter geometries and filter media, were manipulated and the filter performance was evaluated. In this phase, a scientific community existed that discussed about filtration problems in view of certain experimental findings and published their results. This first paradigm was established around the middle of the 18th century as indicated by the first patent for a filter design in 1745 and the first book on filtration published in 1750, both by Joseph Amy (1696-1760) (Baker, 1948, p. 30). The macro-manipulative paradigm is a powerful illustration of the dictum by Ian Hacking (*1936), an American philosopher of science, that "experimentation has a life of its own" (Hacking, 1983, p. 150), implying that detailed theory is often not necessary for successful experimentation. Nevertheless, many problems could not be solved within the macro-manipulative paradigm, e.g., scale-up issues of linking laboratory filtration experiments to full-scale filters. Such defects finally induced a paradigm shift.

A next paradigm can be identified when mathematical analysis is introduced to filtration. It might be called the **macro-theoretic paradigm**, due to the fact that in this period filtration was mathematically described on the macroscopic level, i.e. by global variables, such as flow rate or pressure drop, as well as continuum approaches. The pore-level of the filter or the exact nature and separation mechanisms of impurities were not yet addressed. The paradigm already dawned in the work of Reinhard Woltman (1757-1837), who, e.g., introduced the notion of volume fractions, such as porosity, to characterize porous media on a continuum scale (De Boer, 1992). The first prototypical example, however, is Darcy's law. It was developed by Henry Darcy (1803-1858) during his design of the Dijon water works in France and was published in 1856 (Darcy, 1856; Brown, 2002). In its modern formulation, Darcy's law reads

$$Q = -\frac{k}{\mu} \cdot \frac{\Delta p}{L} \cdot A\,, \tag{1.1}$$

where Q is the volumetric flow rate, k is the permeability, μ the fluid's dynamic viscosity, Δp the pressure difference across the porous layer, L its height, and A is the cross-sectional area. Darcy's law, for the first time, yielded a quantitative and mechanistic description of filter behavior. For example, the equation was successfully employed for up-scaling of filters which solved problems that could not be addressed within the previous paradigm. Once the permeability k of a filter material is determined and the fluid viscosity μ is known, Darcy's law yields the pressure-flow

relationship for any filter dimension, i.e., height L and cross-sectional area A. In the phase of "normal engineering", a term that could be used in analogy to Kuhn's notion of "normal science", many further problems resulted and were solved by such macro-scale equations. Another very influential example is the treatment of depth filtration by Iwasaki (1937). He developed a differential equation that describes the separation of impurities within filter materials. However, in this approach, impurities are only described by their concentration, i.e., by a continuum-mechanical approach, and the separation is modeled as a reduction of that concentration in the fluid phase. The exact mechanisms on the pore scale could not be addressed with Iwasaki's method. In this manner, unanswered questions concerning micro-scale separation mechanisms accumulated and eventually led to a paradigm shift.

The macro-theoretic paradigm was followed by the **micro-theoretic paradigm**. In this phase, the separation of impurities in filters was investigated on the micro scale, empirically as well as theoretically. Hypotheses concerning elementary separation mechanisms were formulated and tested. This paradigm was strongly influenced by the new discipline of colloid science, initiated around 1950, which is concerned with the study of interactions between small particles suspended in liquids and solid surfaces (Israelachvili, 2011, p. 17). The results of colloid science were adapted to filtration problems from around 1960 onwards, a transition reflected in publications such as Herzig et al. (1970) and Ives (1975). New imaging technologies, e.g., micro-computed tomography, are another key element in the micro-theoretic paradigm. These imaging technologies allow for a detailed analysis of the microstructure of different filter media, such as the determination of true pore size distributions and the characterization of deposited impurities, including their location on or within different filter media. Also large-scale computer simulations play an important role in this paradigm. An example is the study of flow in complicated 3D pore geometries of filters by computational fluid dynamics (CFD) (Mirabolghasemi et al., 2015). All this micro-scale information is valuable for selecting appropriate filter materials and designing new filters. Additionally, this paradigm raised many related problems which were subsequently addressed in another phase of "normal engineering". However, the micro-scale analysis eventually led to novel ideas concerning pore-scale properties which go beyond the micro-theoretic paradigm.

We might thus be facing once again the beginning of a novel research phase which could be called the **micro-manipulative paradigm**. It is characterized by chemically and nanotechnologically functionalized filter surfaces, e.g., membranes that are sensitive to temperature or pH shifts (Liu et al., 2016). Equally, it is marked by the advent of novel technologies like the 3D printer which allow to exactly tailor the microstructure of filters according to given specifications (Low et al., 2017; Nawada et al., 2017).

All paradigms introduced here are based on methods used in filtration research. Of course, the proposed classification is just one out of a number of possibilities. One could, for example, also define paradigms based on apparatus concepts, such as the slow sand filter, the rapid filter, the vacuum drum filter, etc. However, this would lead to a multitude of paradigms with no

clear temporal order; also, the comparison between different areas of application, such as water treatment and chemical engineering, would be difficult due to the different apparatuses used in these fields. Such a classification, thus, gives no real structure to the overall history of filtration. It is asserted that the proposed classification does better in this respect and that it is, therefore, a good starting point to approach the history of filtration.

Additionally, two major differences to Kuhn's approach are worth mentioning. Paradigms in engineering differ in some important aspects from Kuhn's notion. Namely, engineering is never as isolated as the fundamental research in physics that was Kuhn's main object of study. A specific field in technology is always embedded in a broader technological, scientific, and social context which renders it difficult to determine what to include in the corresponding paradigms and what to leave out. For example, it depends on the perspective, if the wide-spread combination of filtration with other technological developments, such as flocculation, is to be regarded as a paradigmatic move, or how the effect of data-science methods on filtration is evaluated.

Furthermore, paradigm shifts in engineering are not as radical as the ones portrayed by Kuhn in physics. True revolutions hardly occur, paradigms usually exist in parallel, and old paradigms are rarely completely abandoned. For example, there is still macroscopic experimental research in filtration, benefiting, e.g., from improved measurement technologies. This stands in contrast to Kuhn's notion of a paradigm: After Einstein, physicists largely abandoned the paradigm of Newtonian mechanics and subsequently considered the theory of relativity as the better or more probable description of the phenomena. Paradigms in engineering differ from those in physics, for one reason, due to a different function of theory in these disciplines. Contrary to natural science, theory in engineering does not primarily strive for truth, but mainly aims to be functional in a given context. Thus, even superseded theories can be exact enough for some tasks and are, for that reason, also used in later paradigms. A more detailed discussion on the specifics of engineering knowledge is provided in Kuhn et al. (2017c).

1.2.2 Developments in Process Control

After the comparatively detailed assessment of filtration history in the last section, a much shorter overview of the development of process control is given now. Filtration was treated in greater detail because this work is primarily considered as a work of filtration research; optimal control methods, on the contrary, are mainly applied as tools here.

Whereas mechanically realized feedback control devices existed since antiquity, e.g., in the form of float valve regulators (Bissell, 2009), theory on feedback control developed mainly in the 20th century. This development is closely related with the more widespread availability of instruments for measuring, indicating, and recording the states of various processes such as voltage, current, temperature, pressure, or flow velocity – the latter two being also important in the context of filtration. In this manner, the beginning of the 20th century saw a pronounced increase in the ratio of instrument to machinery sales (Bennett, 1996).

While classical control theory is concerned with the search for optimal points in some given state spaces, optimal control theory aims at optimal paths. Having precursors in the calculus of

variations that emerged in the late 17th century (Sussmann and Willems, 1997), optimal control theory essentially developed since the 1950s. Modern optimal control theory was mainly influenced by the will to control missiles and space vehicles as well as the advent of digital computers (Bennett, 1996). The terms “optimal control” and “dynamic programming” are mostly used synonymously, whereas “calculus of variations” denotes only one method to solve optimal control problems. For political reasons, the label “dynamic programming” was chosen in the context of Richard Bellman’s research on the allocation of missiles to maximize overall damage around 1950 due to the positive connotations of “dynamic” and the preference of “programming” over “planning” (Bennett, 1996).

In the pre-WWII period, filters were primarily controlled manually or by simple mechanical control devices. For example, the differential pressure from Venturi flow-meters was used as a signal for flow valves which were counteracted by beams with weights attached to achieve the desired flow rate. As a next step, pneumatic control was introduced, followed by electronic control. In water treatment, variable flow rate control was first introduced in the 1960s (Fulton, 1981, pp. 67-69). Recently, data-driven methods were investigated for the control of filtration. Data mining was tested by Eberhard (2006); the practical application of a fuzzy-logic control for beer filtration was introduced in Fellner et al. (2012). Some studies also applied optimal control in the context of filtration; they will be introduced in Section 2.3.4.

1.2.3 Lessons from History

Some conclusions from the historical developments discussed in the last two sections are drawn now. If the assessment of developments in filtration research is essentially correct, the stage is set for specifically tailored filter microstructures. This recently emerging movement was labeled the micro-manipulative paradigm. However, the ability to manipulate filter microstructures also requires detailed information on what microstructural properties are actually desirable. In this respect, it is also imaginable that there is not a unique optimal microstructure for a given filter but that local variations on the micro level offer some benefits.

Using a few examples, it was illustrated that within the last ten years advanced control methods have also been tentatively tried out in the field of filtration. Optimal control, as one such method, seems a new and promising tool in the context of microstructure design; even though, usually, it is not yet applied for that purpose. As the goal of optimal control is to determine optimal paths, these paths can also be optimal distributions in space and thus guide the design of filter microstructures. In this respect, the developments in filtration research and control engineering converge and possibly exhibit some synergistic effects.

That there are such synergistic effects is one of the main working hypotheses of this dissertation. Based on continuum models, optimal spatial trajectories of filter properties are derived. Methods to bridge the gap between pore scale and continuum scale are known and introduced in Section 2.1.2, a complete agenda for multi-scale filter optimization is sketched in the outlook provided in Chapter 7. Note that the use of continuum models in this thesis, which were a key element of the macro-theoretic paradigm, illustrates the observation of Section 1.2.1 that

paradigms in engineering are rarely completely abandoned. It is asserted here that continuum approaches also provide an important tool within the micro-manipulative paradigm.

1.3 Epistemological Positioning

1.3.1 Scientific Stance

After the historical background was outlined in the last section, the epistemological position of the dissertation is explained now. The current work is a scientific analysis of some engineering problems, namely in the field of solid-liquid separation. As in all science, its empirical claims need to be tested experimentally. Since this is a theoretical work, some models and strategies are proposed but not validated yet. Different aspects, therefore, still remain in the state of "bold conjectures" (Popper, 2002b, pp. 278, 280). Also, the mathematical parts contain open hypotheses, however, without empirical content but rather structural claims of the form "solution method X is suitable for problem Y". All hypotheses, of either type, are clearly indicated in this work so that further research may challenge these claims and can continue from there. These "conjectures" that are prone to future "refutations" (Popper, 2002a) are, however, no disadvantage of this particular work. It rather is a general characteristic of the scientific method, which can be seen as "an evolutionary approach" (Popper, 1972). This being said, the "paths" in the title still gets a further meaning, namely that this dissertation does not present final and fixed results, but rather is seen as an exploration of some paths opened up by the synthesis of modern optimal control theory and filtration modeling.

1.3.2 Technological Stance

Even though scientific methods are used, this dissertation is not a work of natural science or mathematics, but primarily of engineering. Engineering differs from natural science in that its main focus is not on true descriptions of the world as it is, but rather on changing the world technologically. Engineers invent new artifacts, they develop and improve processes and technological strategies. Development, invention, and improvement all imply that the current state of the world is changed. This raises the question how engineers go about to change the *status quo*. The author has argued elsewhere that engineering can be interpreted as a form of fiction (Kuhn, 2015, 2017); a similar thesis was formulated by Dunne and Raby (2014) for the discipline of design. Engineers develop visions of a different world and they go about it in a similar manner than writers making up imaginary worlds.

As in literature, new technology is a combination of previously existing elements (Arthur, 2009; Kuhn, 2017). In literature, on the one hand, these elements are, e.g., words, phrases, basic plots, etc. Engineers, on the other hand, use simple parts, such as the screw or the electrical resistance, and causal mechanisms, such as the lever, to generate new solutions. Also similar to literature, technology does not only exist within the heads of individuals but is facilitated by external media. In the case of literature, the primary medium is language; engineers, on the

contrary, develop their visions primarily by means of models, which are understood here in a broad sense, comprising hand sketches, technical drawings, scale models, and computer models of different sorts. Ludwig Wittgenstein (1889-1951), a philosopher of language, has famously remarked: “The limits of my language mean the limits of my world.” (Wittgenstein, 2001, 5.6). In a similar manner, the models and modeling strategies available to engineers limit their world – or, to be more precise, their ability to explore possible worlds. Thus, two important driving forces for technological innovation are new combinations of conceptual building blocks as well as new general models.

The benefit of the present work can be seen as developing itself visions of a technologically different world. In this technologically different world, filtration processes allow for spatial and temporal variation of control variables which were previously kept constant. Therefore, a new combination of previously separate concepts is introduced which is, as already mentioned in the last section, a synthesis of modern optimal control theory and filtration modeling. Furthermore, the methods and models developed in this dissertation, may benefit the “technical imagination” (Dunne and Raby, 2014, p. 70) generally. The developed models, understood as media, could be able to broaden the scope of what is conceivable. Also, the applied optimal control strategies may, by analogy, help to question the technological *status quo* in other areas than solid-liquid separation; examples are provided in Chapter 6. This claim could be summed up by the imperative: May there be variable functions where previously there were only constants.

1.4 Outline of the Thesis

After the quick sweep over the historical and epistemological position of this dissertation in the introduction, the theoretical background is discussed in **Chapter 2**. In detail, the continuum treatment of porous media is introduced and demarcated from pore scale models and pore-network models. Volume averaging is presented as a way to move from the pore scale to the continuum scale, a method that is required if microscale design is to be coupled with optimal control on the continuum scale. Also, basics of filtration and optimal control theory are discussed.

Chapter 3 provides some background on the numerical methods used in this work. The material is mainly included as a separate chapter in order to avoid repetition of these themes in the two subsequent case studies for which essentially the same methods were used. In detail, numerical methods for partial differential equations are introduced and the method of lines, as the chosen option, is discussed. Furthermore, strategies to treat sharp moving fronts and moving boundary problems are discussed.

The two case studies of Chapters 4 and 5 form the main body of the present work. In **Chapter 4** depth filtration is considered. Based on some phenomenological observations from filtration practice, optimal control scenarios are identified and solved using mainly models from the literature. The results are optimized depth filter designs in which the local filtration performance is the control variable. From the continuous optimal control solutions, layered filter

designs are derived that are useful for practical filter design. However, it is also highlighted that within the micro-manipulative paradigm also continuous solutions may prove useful.

Chapter 5 addresses filter-aid filtration. Whereas the focus of Chapter 4 is clearly on the optimization of filter design, the focus of this chapter is primarily on the derivation of a mechanistic and fully dynamical model. Subsequently, an analytical optimal control solution is derived based on a simplified model from the literature. Also, numerical optimal control solutions for the full model are shown. All results are temporal trajectories of filter-aid dosage. However, even though the control variables are determined in time, the indirect goal is also optimization of filter's microstructure because the dosage of filter aids affects the dynamically created filter cake structure.

In **Chapter 6**, further fields of application are discussed in which ideas and methods developed in this dissertation could be beneficial. These further fields are broadly divided into flow through compressible porous media, such as encountered in preparative chromatography, and processes based on intra-particle diffusion, such as coffee extraction. Also some further applications that do not fit into these two categories are mentioned. Chapter 6 does not provide numerical modeling or optimization results; the potential benefits are only discussed with respect to the underlying physical theory and by means of analogy to the conducted optimal control calculations.

Chapter 7 provides a general conclusion of the whole thesis and a broad outlook. The earlier threads of the introduction concerning a multi-scale method for filter control and design are picked up and developed further. Open points are highlighted, notably, possible problems in transferring the optimal control results from the case studies of Chapters 4 and 5 to actual filtration practice as well as using the methods of this thesis for new applications such as the ones discussed in Chapter 6. Also, further challenges regarding the applied numerical methods are discussed.

Note that throughout this work, some redundancies are intended. The most important points are highlighted in various places to keep the common theme in focus. Also, some theoretical building blocks are repeated, e.g., when treating the theory in Chapter 2 as well as in the case studies of Chapters 4 and 5, to allow the results chapters to stand for themselves to some degree and prevent the reader from turning back to the theory part too often.

Chapter 2

Theoretical Background

In this chapter, the theoretical background is introduced, namely the continuum treatment of porous media as well as some basics on filtration and optimal control. The theory is kept as concise as possible; for more information, references to the corresponding literature are included.

2.1 Continuum Treatment of Porous Media

Filters, in whatever form, always consist of porous materials. For that reason, porous media and their mathematical description are discussed first. Simply put, a porous medium is a "solid with holes" (Bear, 1988, p. 14). However, this definition is still too simple, because a tube, which can be also considered a solid with a hole, is usually not classified as a porous medium. Therefore, a porous medium is defined as a multiphase material of which at least one phase is solid and one phase is not solid. Additionally, all phases are required to be spatially distributed within the domain of interest in such a way that stable averaged quantities can be derived, as will be explained below. All regions that are not part of the solid phase are called void space or pore space. If convective transport is to take place in porous media, the pore space needs to be at least partially connected. Convection denotes the ordered collective movement of molecules in fluids as opposed to their random movement that takes place during diffusion.

2.1.1 Micro, Meso, and Macro Scale

Different levels of detail are of interest in the study of porous media, each with their own methods and research traditions. These detail levels are referred to in this work as the micro, meso, and macro scale.

On the micro scale or pore scale, the true geometry of porous media is the basis of investigation, i.e., the "solid with holes". A two-dimensional illustration of the micro scale is given in Figure 2.1. Studies on the micro scale belong to the newest movements in research which correspond to the micro-theoretic paradigm and micro-manipulative paradigm in filtration as described in Section 1.2.1. Micro-scale information is obtained by 3D imaging technologies, such as X-ray computed tomography (CT), magnetic resonance imaging (MRI), or confocal laser

scanning microscopy (CLSM). Other means to obtain pore-scale information with a lower level of detail are, e.g., mercury intrusion porosimetry and gas adsorption (Xiong et al., 2016). In some studies, also idealized micro-scale geometries are used, such as simplified model pores (Lee and Koplik, 1999). Micro scale information can be used for purely geometrical characterizations such as the determination of pore size distributions. Also mass transport can be studied on the pore scale, be it purely flow or reaction and deposition phenomena (Mirabolghasemi et al., 2015). Analyses on the micro scale are important to gain insights into prevailing mechanisms. However, they are always computationally expensive, both in terms of required storage as well as computational times necessary for analysis and simulation.

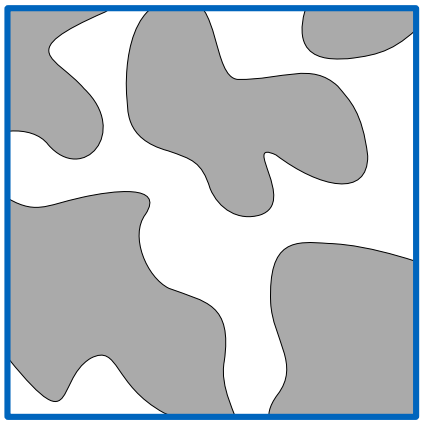

Figure 2.1: Two-dimensional illustration of porous-media micro scale. The solid phase is depicted in gray, the pore space in white.

To counteract these computational costs while keeping some geometrical details, pore-network methods were introduced. Historically, they appeared in the transition from the macro-theoretic to the micro-theoretic paradigm, as they were introduced for filtration in Section 1.2.1. Pore-network methods are located at the meso scale (Xiong et al., 2016). They, thus, conceptually, not only historically, bridge the gap between micro and macro scale. From the full micro-scale information, pore networks are extracted by identifying pore bodies and pore throats, as illustrated in Figure 2.2. The result is a graph, where the throats are the edges and the pores are the nodes. These graphs can be analyzed by mathematical graph theory and can be used for further computations, e.g., of mass transport phenomena. However, there is a plethora of variants of pore network models (Tansey and Balhoff, 2016; Xiong et al., 2016). In very simple cases, pores are simply seen as connections of throats without an own contribution, and flow in each throat is modeled, e.g., by the Hagen-Poiseuille equation (Gostick et al., 2016). Due to the computational efficiency of pore network models, it is possible to simulate thousands of pores simultaneously, which is impossible so far at the micro scale.

The lowest level of detail is retained on the macro scale which refers in our case to the continuum treatment of porous media. The term continuum is understood here in the same sense as in classical continuum mechanics, i.e., matter is not treated as composed of discrete parts

but as a continuum which, therefore, can be described by continuous variables and functions (Malvern, 1969, pp. 1-2).

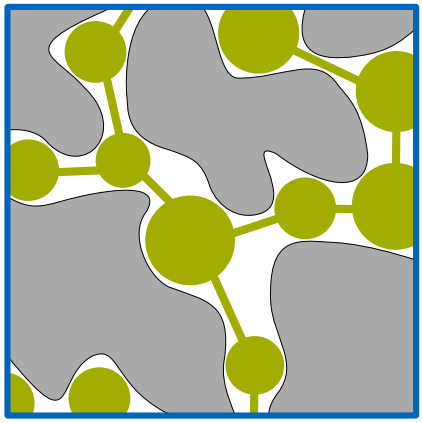

Figure 2.2: Two-dimensional illustration of pore-network models. The solid phase is depicted in gray, the pore space in white; the pore network structure is shown in green, comprising pore bodies (circles) and throats (lines).

The continuum scale corresponds to the macro-theoretic paradigm in filtration, as introduced in Section 1.2.1. On the macro scale, porous media are only described by averaged qualities, such as the relative volumetric concentration of pores, i.e., the porosity. Averaging as a way to arrive at continuous variables is introduced in the next subsection. Due to the low level of detail, macro-scale approaches allow for most efficient computations of the three discussed scales. The continuum treatment, although the oldest method, is, therefore, still the method of choice when computational efficiency is required, such as in optimization and optimal control, which are addressed in this work.

Obviously, the relevant scales strongly depend on the problem at hand and the perspective under which it is considered. What was here referred to as the micro scale results already from a scale-up from the atomistic level, as it is considered, e.g., in molecular dynamics (MD) simulations. Also, the macro scale, as it was just discussed, is not the largest possible scale; one can also analyze the whole-plant level, as it is done, e.g., in flow-sheet simulations.

2.1.2 From Micro to Macro Scale by Spatial Averaging

Spatial averaging is a means to derive continuum-scale information from the pore scale. It is, therefore, an indispensable tool for multi-scale approaches. As the name indicates, variables on the micro scale are averaged across space, leading to new integral variables. The minimal size of spatial regions used for averaging is denoted as representative elemental volume (REV).

If the regions to be analyzed are taken from larger samples, the criteria proposed by Brun et al. (2009) and Huang et al. (2015) are applicable to determine the size of a representative elemental volume, i.e., a volume that is statistically representative of the bigger sample. Required REV sizes are given by the convergence of the variable of interest and are, therefore, no universal constants of a given system. Figure 2.3 illustrates the convergence behavior with

increasing sampling volume. As also shown in the figure, if the size of the averaging volume is further enlarged, macroscopic inhomogeneities affect the averaged variables.

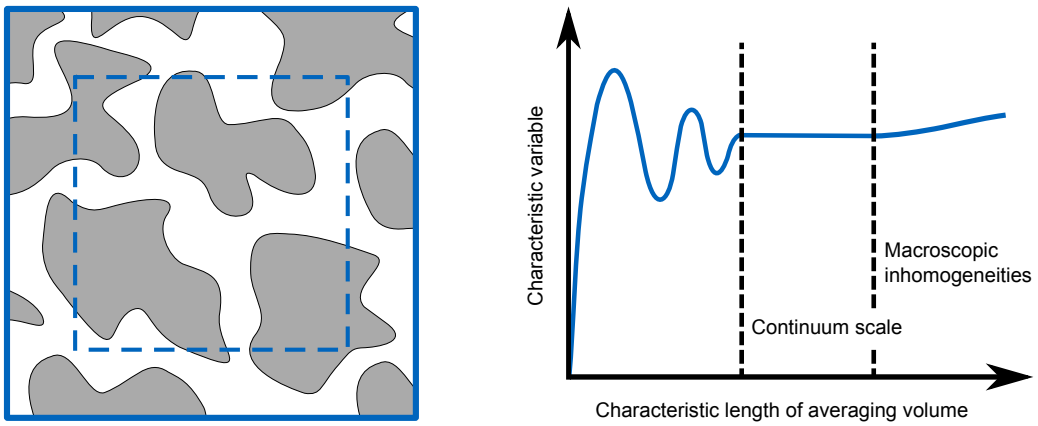

(a) (b)

Figure 2.3: Two-dimensional illustration of representative elementary volume (REV), marked by dashed line; the solid phase is shown in gray (a). Convergence behavior of variable of interest with increasing REV size, adapted from Bear (1988, p. 20) (b).

Spatial averages of some functional variable $f(t,\mathbf{x})$ are denoted as $\langle f(t,\mathbf{x})\rangle$ and follow from

$$\langle f(t,\mathbf{x})\rangle = \frac{1}{V}\int_V f(t,\mathbf{x})\, dV'. \tag{2.1}$$

Some of the quantities and equations used later on are now derived by spatial averaging. For this reason, the phase function $I_\alpha(\mathbf{x},t)$ is introduced (Lu and Torquato, 1993; Torquato, 2002):

$$I_\alpha(t,\mathbf{x}) = \begin{cases} 1 & \text{if } \mathbf{x} \text{ lies within phase } \alpha \\ 0 & \text{otherwise.} \end{cases} \tag{2.2}$$

$I_\alpha(t,\mathbf{x})$ refers to any phase α within a multi-phase domain and indicates that α is found at a given location $\mathbf{x}$ at time t by the value 1. For now, the temporal dependency of I_α is neglected. Phase fractions are denoted by ϕ_α. Assuming the phase of interest is the pore space p of a porous medium, the volume fraction of the pore space ϕ_p, respectively the **porosity** ε, is defined as

$$\phi_p = \varepsilon = \langle I_p(\mathbf{x})\rangle = \frac{1}{V}\int_V I_p(\mathbf{x})\, dV' = \frac{V_p}{V}. \tag{2.3}$$

In depth filtration, solid matter is separated and, therefore, deposited within some filter medium. The **specific deposit** σ is defined as

$$\phi_d = \sigma = \langle I_d(\mathbf{x})\rangle = \frac{1}{V}\int_V I_d(\mathbf{x})\, dV' = \frac{V_d}{V} \tag{2.4}$$

where the index d refer to the phase created by the deposited material.

Another property, used in many filtration equations, is the **specific surface**, i.e., surface area between phases per volume. For detecting phase boundaries, the function M_p is introduced, defined as

$$M_p(\mathbf{x}) = |\nabla I_p(\mathbf{x})|\,; \tag{2.5}$$

the specific surface s_p then is

$$s_p = \langle M_p(\mathbf{x}) \rangle = \frac{1}{V} \int_V M_p(\mathbf{x})\; dV' = \frac{S_p}{V}\,. \tag{2.6}$$

Imagining, as a thought experiment, a 3D imaging process with a sufficiently high temporal and spatial resolution, e.g., an X-ray micro-tomography device, all information to describe the process would be given. In case of filtration, the distribution of the relevant phases, i.e., the filter material, the pore space, and the separated impurities, would be known exactly. These information could be averaged subsequently according to the above rules yielding a complete dynamic description of the process. However, not all processes at all scales can be imaged online due to practical limitations such as limited resolution in time and space as well as accessibility of the relevant process operations. Furthermore, the goal is not only a true description of processes but also prediction of phenomena under different boundary conditions. For these reasons, descriptive variables are linked by mechanistic equations.

Mechanistic equations on the macro scale comprise spatially averaged variables and are themselves derived by volume averaging. As an example on how to arrive at spatially average equations, an advection-reaction equation is considered. Its averaged form will be further developed below in Section 2.2.3 and it will be also used in the case studies of Chapters 4 and 5. The derivation is presented in some detail in the main text because the method of volume averaging, which is thereby shown in action, directly links this dissertation to the now often-used pore-scale approaches. Also, the perspective for a multi-scale method of filter design and control directly hinges on this method.

The one-phase advection-reaction equation results from a mass balance of the component under consideration and reads

$$\frac{\partial c}{\partial t} + \nabla \cdot (\mathbf{v}\; c) = r_a\,, \tag{2.7}$$

where c is the component concentration in the liquid phase and $\mathbf{v}$ is the transport velocity of this phase. This equation is now considered in a porous domain where the pore space is completely filled with the liquid phase. Averaging it spatially gives

$$\frac{1}{V} \int_V \left(\frac{\partial c}{\partial t} \right)\; dV' + \frac{1}{V} \int_V \nabla \cdot (\mathbf{v}\; c)\; dV' = \frac{1}{V} \int_V r_a\; dV'\,, \tag{2.8}$$

which is equal to

$$\frac{\partial \langle c \rangle}{\partial t} + \langle \nabla \cdot (\mathbf{v}\, c) \rangle = \langle r_a \rangle \,. \tag{2.9}$$

In case of the first term, integration and derivation can be exchanged because the averaging volume V is independent of time; additionally only the definition of

$$\langle c \rangle = \frac{1}{V} \int_V c \; dV' \,. \tag{2.10}$$

is used. The spatial averaging theorem (Whitaker, 1999, p. 126) states that

$$\langle \nabla \cdot (\mathbf{v}\, c) \rangle = \nabla \cdot \langle (\mathbf{v}\, c) \rangle + \frac{1}{V} \int_A \mathbf{n} \cdot (\mathbf{v}\, c) \; dA' \,, \tag{2.11}$$

$\mathbf{n}$ is the normal vector on the phase boundary. Neglecting interfacial fluxes, i.e., considering the solid phase as rigid and impermeable, thus gives

$$\langle \nabla \cdot (\mathbf{v}\, c) \rangle = \nabla \cdot \langle \mathbf{v}\, c \rangle \tag{2.12}$$

To treat the convective term, the following decomposition is performed (Whitaker, 1999, p. 127):

$$\mathbf{v} = \langle \mathbf{v} \rangle^p + \tilde{\mathbf{v}} \tag{2.13}$$

$$c = \langle c \rangle^p + \tilde{c} \,, \tag{2.14}$$

where $\langle f \rangle^p$ are the spatially averaged quantities with respect to the pore phase p:

$$\langle f \rangle^p = \frac{1}{V_p} \int_V f \; dV' \,; \tag{2.15}$$

$\tilde{f}$ are spatial deviations, i.e., the fluctuations around the average (Whitaker, 1999, p. 15). Substitution gives

$$\langle c\, \mathbf{v} \rangle = \langle \langle \mathbf{v} \rangle^p \langle c \rangle^p + \langle \mathbf{v} \rangle^p \tilde{c} + \tilde{\mathbf{v}} \langle c \rangle^p + \tilde{\mathbf{v}} \tilde{c} \rangle \,. \tag{2.16}$$

Using the averaging rules

$$\langle f + g \rangle = \langle f \rangle + \langle g \rangle \tag{2.17}$$

$$\langle \langle f \rangle^p g \rangle = \langle f \rangle^p \langle g \rangle \tag{2.18}$$

according to Drew (1983) and Civan (2011, p. 66) yields

$$\langle c\, \mathbf{v} \rangle = \langle \langle \mathbf{v} \rangle^p \langle c \rangle^p \rangle + \langle \mathbf{v} \rangle^p \langle \tilde{c} \rangle + \langle \tilde{\mathbf{v}} \rangle \langle c \rangle^p + \langle \tilde{\mathbf{v}} \tilde{c} \rangle \,. \tag{2.19}$$

If the term $\langle \langle \mathbf{v} \rangle^p \langle c \rangle^p \rangle$ is treated consecutively by the following relationships (Civan, 2011, p. 66)

$$\langle \langle f \rangle^p \langle g \rangle^p \rangle = \varepsilon \langle \langle f \rangle^p \rangle^p \langle \langle g \rangle^p \rangle^p + \varepsilon \langle \langle \tilde{f} \rangle^p \langle \tilde{g} \rangle^p \rangle^p \tag{2.20}$$

$$\langle \langle f \rangle^p \rangle^p = \langle f \rangle^p \tag{2.21}$$

$$\langle \tilde{f} \rangle^p = 0\,, \tag{2.22}$$

the result is

$$\langle c\ \mathbf{v} \rangle = \varepsilon \langle \mathbf{v} \rangle^p \langle c \rangle^p + \langle \mathbf{v} \rangle^p \langle \tilde{c} \rangle + \langle \tilde{\mathbf{v}} \rangle \langle c \rangle^p + \langle \tilde{\mathbf{v}} \tilde{c} \rangle\,. \tag{2.23}$$

Again, by definition, the fluctuations vanish when averaged, i.e., $\langle \tilde{\mathbf{v}} \rangle = 0$ and $\langle \tilde{c} \rangle = 0$ (Whitaker, 1999, p. 128), therefore

$$\langle c\ \mathbf{v} \rangle = \varepsilon \langle \mathbf{v} \rangle^p \langle c \rangle^p + \langle \tilde{\mathbf{v}} \tilde{c} \rangle\,. \tag{2.24}$$

Substitution in the main balance equation gives

$$\frac{\partial \langle c \rangle}{\partial t} + \underbrace{\nabla \cdot (\varepsilon \langle \mathbf{v} \rangle^p \langle c \rangle^p)}_{\text{convection}} + \underbrace{\nabla \cdot \langle \tilde{\mathbf{v}} \tilde{c} \rangle}_{\text{dispersion}} = \langle r_a \rangle\,, \tag{2.25}$$

with the **convection** and **dispersion** terms marked in Eq. (2.25). Combining Eqs. (2.1) and (2.15) yields

$$\langle c \rangle = \varepsilon \cdot \langle c \rangle^p\,. \tag{2.26}$$

Porosity ε is assumed to be constant and dispersion is neglected. Using furthermore the chain rule together with the volume-averaged continuity equation (Whitaker, 1999, p. 132)

$$\nabla \cdot \langle \mathbf{v} \rangle = 0\,, \tag{2.27}$$

the result is

$$\varepsilon \frac{\partial \langle c \rangle^p}{\partial t} + \varepsilon \langle \mathbf{v} \rangle^p \cdot \nabla \langle c \rangle^p = \langle r_a \rangle\,. \tag{2.28}$$

This form of the transport equation will be further used in Section 2.2.3 when the basic equations of filtration will be introduced. Note that often $\langle c \rangle^p$ is treated like c. However, whereas c is the point value at some given location $\mathbf{x}$ within the pore space, $\langle c \rangle^p$ is a spatially averaged or filtered value determined using the averaging volume V. Having emphasized this here, also simply c will be used in the remaining work for reasons of readability.

2.2 Filtration

This section explains some terminology and introduces some basic building blocks to mathematically describe filtration. These information form the basis for the case studies presented in Chapters 4 and 5.

2.2.1 Nomenclature and Classifications

As noted in the introduction, filtration is a unit operation in process engineering that aims at separating a dispersed phase (solids, cells, droplets) from a fluid phase. Because in all processes considered in this thesis clarification of the liquid is the goal, the dispersed phase is also referred to as the impurities. Figure 2.4 shows how filtration operations can be classified with respect to the sizes of impurities to be separated; note that often reverse osmosis is not counted as filtration, but it is listed here nevertheless for reasons of completeness. The two applications presented in the case studies of Chapters 4 and 5, namely depth filtration and filter-aid filtration, are usually operated as particle filtration with mainly particles in the range of $1 \ldots 100$ µm to be separated.

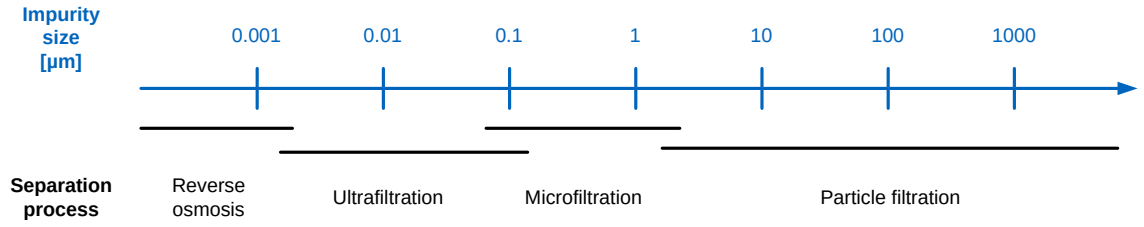

Figure 2.4: Filtration operations classified according to sizes of impurities to be separated; figure adapted from Svarovsky (2000, p. 27).

In all modes of filtration, the elements of the dispersed phase are captured on or within some material structure which is referred to as the **filter medium** or **septum**. In order to introduce movement to the fluid phase and thereby facilitate the separation process, a pressure difference across the filter medium needs to be applied. In this thesis, only liquid filtration is considered. The liquid entering the filter is called **suspension**, the liquid leaving the filter is denoted as **filtrate**.

Besides the classification of Figure 2.4, filtration operations can be sorted according to various other criteria. Ripperger et al. (2012) mention classifications according to the following characteristics:

- **Location of particle retention**: surface filtration, depth filtration, ...
- **Generation of pressure difference**: pressure filtration, vacuum filtration, ...
- **Mode of operation**: continuous filtration, discontinuous filtration, ...
- **Application**: water filtration, beer filtration, ...

Of these possibilities, classification according to location of particle retention is used here. The location of particle retention is closely linked to the prevailing separation mechanism. Due to the methodological focus of this work, prevailing mechanisms are most important. In contrast, it does not matter if the pressure is applied as excess pressure on the upstream side or suction

at the downstream side of the filter; also, the concrete application is of secondary importance due to the methodological focus of the present work.

Surface filtration, also called cake filtration, denotes the mode where particles are completely captured at the surface of the filter cake, no impurities penetrate the already existing cake. In pure cake filtration, the particles to be separated are usually larger than the pores of the already existing filter cake; however, particle bridges over pores of the filter medium are often decisive at the beginning of filtration (Rainer, 2003; Tichy, 2007). In **depth filtration**, on the contrary, particles are solely separated within the filter medium. For pure depth filtration, the particles to be separated need to be smaller than the pores of the filter medium, at least than the pores at the entry. Sometimes deep bed filtration is synonymously used to depth filtration. However, in most cases, deep bed filtration is only used when the filter bed consists of a particle packing of a depth in the order of meters, as encountered, e.g., in water treatment. The mechanisms of surface filtration and depth filtration are illustrated in Figure 2.5.

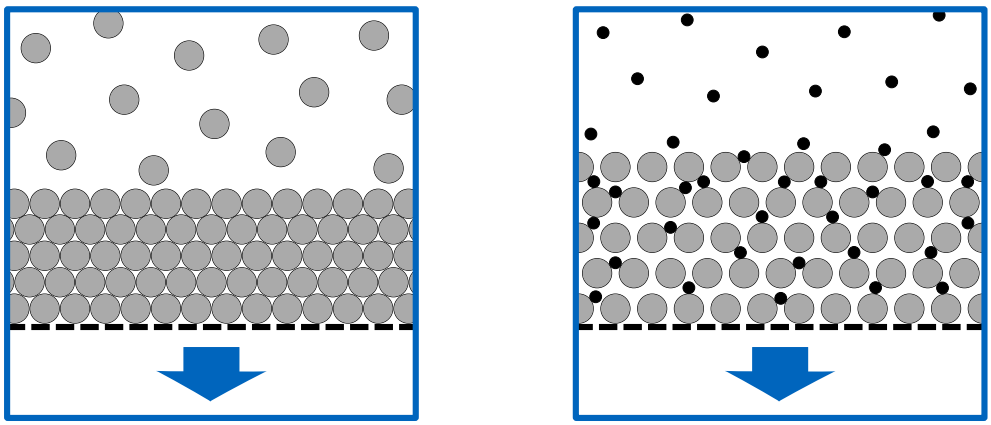

(a) (b)

Figure 2.5: Illustration of filtration mechanisms: surface filtration (a) and depth filtration (b). The main particles, composing the porous structure, are shown in gray, impurities in (b) are depicted in black; the blue arrow indicates the flow direction.

Note that pure surface and depth filtration are idealizations that are seldom encountered in practice. Often, some small particles are able to penetrate the already existing cake in surface filtration and some particles are already retained on the filter surface in depth filtration. However, the nomenclature is still used to describe the process as a whole if the corresponding location of particle retention clearly dominates. Besides these non-pure forms, there are also processes where both mechanisms are at work to a significant degree. This is often the case in **filter-aid filtration**, addressed in the case study of Chapter 5. Filter aids are inert materials that are added to the suspension in order to prevent a complete blocking of the filter medium and facilitate the build-up of permeable filter cakes. More details are provided in the case study.

2.2.2 Separation Mechanisms

In filtration, separation of dispersed matter from a liquid phase is caused by different mechanisms. Dispersed matter is here simply referred to as particles. In general, for a successful separation two steps are necessary: first, particles must come into contact with filter surfaces; second, particles need to be captured there. Commonly, the following causes for contact between particles and filter surfaces are distinguished (Herzig et al., 1970; Ives, 1975; McDowell-Boyer et al., 1986; Tien and Ramarao, 2007; Zamani and Maini, 2009):

- **Interception**: Particles follow the stream lines of liquid flow and thereby touch filter surfaces due to their geometrical extension.
- **Sedimentation**: Particles with densities that differ from the fluid phase can deviate from the fluid flow due to the influence of gravity, thus causing contact with filter surfaces.
- **Inertia**: Trajectories between particles and fluid can deviate due to the inertia of particles. Note that inertia and gravity, even though physically identical forces, lead to phenomenologically separate effects in filtration because the latter only acts in the direction of the gravitational field created by the earth, whereas the former counteracts any changes in direction of particle movement.
- **Hydrodynamic action**: Shear forces in the fluid can cause rotational movements in non-spherical particles; these so called hydrodynamic actions are a possible cause of contact. The term "hydrodynamic action" might be somewhat confusing because, e.g., interception is also caused by fluid-induced forces. It is used here nevertheless to denote rotational effects to keep the nomenclature in agreement with literature.
- **Diffusion**: Brownian motion can cause particles to touch filter surfaces.
- **Electrostatic forces**: Short-ranged forces, such as the Van-der Waals force, can attract particles to filter surfaces.
- **Straining**: Particles are captured within constrictions of the filter geometry; this is a purely geometrical effect and is also referred to as sieving.

Figure 2.6 gives an illustration of three mechanisms. Similar figures are found in a row of publications, e.g., Ives (1975, p. 195), McDowell-Boyer et al. (1986), and Sutherland (2008, p. 16). Whether particles are permanently captured on filter surfaces depends on the prevailing forces; however, a simple and general treatment is not possible due to the complexity of the problem. Therefore, the underlying logic will only be illustrated briefly. If the filter surface is not itself pushing off the particles, e.g., due to repelling electrostatic forces, and the particles have a certain tendency to stick to the surface, e.g., due to surface friction or attractive electrostatic forces, the particle-surface connection needs to withstand mainly forces exerted by the fluid flow. These are drag and lift forces. Trivially, if the attractive forces are larger than the repulsive ones, the particles will be captured on the filter surface (Bai and Tien, 1997; Molnar et al.,

2015). Usually, the most stable mechanism of particle capture is by straining; in this case, the particles are strongly bound in constrictions. Experimental characterization of relevant particle properties and interactions between particles is discussed in Hintz et al. (2008).

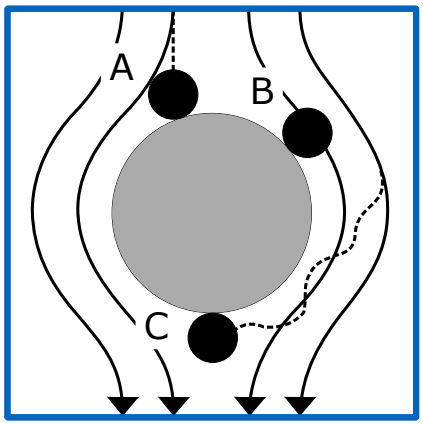

Figure 2.6: Three important mechanisms for contact between impurity particles (black) and filter surfaces (gray): inertia (A), interception (B), and diffusion (C).

The different causes for contact and capture are prevailing to different degrees in surface and depth filtration. Usually, straining is the dominant mechanism in surface filtration; particles are captured on the existing filter cake, where the previously separated matter therefore acts as the effective filter medium; they usually move until they are in a geometrically stable position. However, also surface friction and electrostatic forces can play an important role, especially when forces exerted by the fluid are comparatively small as is the case, e.g., in gas filtration (Tien, 2006, pp. 117-147).

2.2.3 Basic Equations

Filtration can be modeled on the pore scale, using pore networks, and on the continuum scale. A continuum treatment has the advantage of computational efficiency, which is important for optimization as well as optimal control approaches because, in these cases, simulations need to be performed many times. For this reason, continuum models are used in this work. All shown equations can be derived by spatial averaging from micro-scale information as illustrated above.

First, **depth filtration** is introduced because it directly continues the discussion of Section 2.1.2. If Eq. (2.28) is picked up and the pore-space averages are omitted for reasons of readability one gets

$$\varepsilon \frac{\partial c}{\partial t} + \varepsilon \mathbf{v} \cdot \nabla c = \langle r_a \rangle . \tag{2.29}$$

Converting it to a 1D formulation, often used for basic modeling approaches in filtration research, gives

$$\varepsilon \frac{\partial c}{\partial t} + \varepsilon v \cdot \frac{\partial c}{\partial z} = \langle r_a \rangle . \tag{2.30}$$

The 1D pore-space velocity v is often expressed in terms of the superficial velocity q, defined as

$$q = \frac{Q}{A}, \tag{2.31}$$

where Q is the volumetric flow rate and A is the cross-sectional area. Further, it holds that

$$v = \frac{q}{\varepsilon}. \tag{2.32}$$

Substituting v in Eq. (2.4) yields

$$\varepsilon \frac{\partial c}{\partial t} + q \cdot \frac{\partial c}{\partial z} = \langle r_a \rangle. \tag{2.33}$$

The source term $\langle r_a \rangle$ is in case of depth filtration expressed as $-\partial\sigma/\partial t$, i.e., as a sink term, where σ is the specific deposit as defined earlier. $\partial\sigma/\partial t$, therefore, directly conforms to the volume averaged form of $\langle r_a \rangle$ as derived in Section 2.1.2. Thus, the final equation is

$$\varepsilon \frac{\partial c}{\partial t} + q \cdot \frac{\partial c}{\partial z} = -\frac{\partial \sigma}{\partial t}; \tag{2.34}$$

$\partial\sigma/\partial t$ is usually described by

$$\frac{\partial \sigma}{\partial t} = \lambda \cdot q \cdot c, \tag{2.35}$$

with λ being the filter coefficient, which describes the efficiency of local filtration performance. On the continuum level, λ comprises all the diverse effects of particle capture discussed in Section 2.2.2. Values of the filter coefficient for a broad variety of applications are listed in Herzig et al. (1970). Note that due to deposition within the filter, ε is no longer constant as assumed in the derivation of Section 2.1.2. A mathematical argument why, nevertheless, ε appears outside of the time derivative in Eq. (2.34) was given by Civan and Rasmussen (2005) and Civan (2015). Furthermore, it is often argued on physical grounds that the changes of ε are comparatively small (Civan and Rasmussen, 2005). If λ is assumed to be independent of σ, Eq. (2.35) is introduced into Eq. (2.34), and stationary behavior is considered, Eq. (2.34) reduces to the well-known relationship first formulated by Iwasaki (1937):

$$\frac{dc}{dz} = -\lambda \cdot c. \tag{2.36}$$

Note that in depth filtration models usually the origin of the coordinate system is located at the filter inlet and the spatial coordinate points in the same direction as the flow direction.

Darcy's law relates pressure gradient ∇p in the fluid phase and flow rate $\mathbf{q}$ in porous media and, therefore, also in filters. It is one of the oldest and most basic continuum laws in porous media studies and is really a paradigmatic example for the macro-theoretic research period as discussed in Section 1.2.1. Darcy's law can also be derived by spatial averaging along similar lines as the transport equation just discussed. However, the derivation is more lengthy and is well documented in the literature (Whitaker, 1966, 1986). For this reason, only the result is shown here:

$$\mathbf{q} = -\frac{\mathbf{k}}{\mu} \cdot (\nabla p - \rho \mathbf{g}) \,. \tag{2.37}$$

$\mathbf{k}$ is the permeability; μ and ρ are the fluid's dynamic viscosity and density, respectively; $\mathbf{g}$ is the gravitational constant. In 3D, $\mathbf{k}$ takes the form of a tensor. As in filtration liquid heights are often small, gravitation can be usually neglected. Also, as already mentioned, basic modeling approaches are often conducted in 1D. Under these assumptions, Darcy's law reads

$$q = -\frac{k}{\mu} \cdot \frac{dp}{dz} \,. \tag{2.38}$$

Permeability k is a property of the solid phase only. It can be spelled out by different models. One of the most popular expressions for k is the **Kozeny-Carman equation** (Kozeny, 1927; Carman, 1997) which is derived from an analogy between porous media flow and flow in pipes governed by the Hagen–Poiseuille equation (Epstein, 1989). The model is formulated as

$$k = \frac{d^2}{9 \cdot b \cdot \tau^2} \cdot \frac{\varepsilon^3}{(1-\varepsilon)^2} \,, \tag{2.39}$$

where d is the mean particle diameter, b is some shape factor, and τ is the **tortuosity**. Tortuosity is defined as

$$\tau = \frac{L_{\text{eff}}}{L} \,, \tag{2.40}$$

with L_{eff} being the effective pore length, i.e., the path actually traveled by fluid elements, and L the length of the porous medium, i.e., the length macroscopically accounted for. If b is assumed to be 40, i.e., the mean value between a circular flow cross section and an infinite slit, and τ is assumed to be $\sqrt{2}$ (Epstein, 1989), i.e., the flow paths are assumed to be on the average 45° inclined with respect to the shortest path, the result is:

$$k = \frac{d^2}{180} \cdot \frac{\varepsilon^3}{(1-\varepsilon)^2} \,. \tag{2.41}$$

Detailed derivations of the Kozeny-Carman model are shown in Bear (1988, p. 166) and Epstein (1989). It is important to note, however, that the concrete formulation of the formula deviates to some degree in different publications. Sometimes, Darcy's law with the model for k already introduced is referred to as the Kozeny-Carman equation. Also, the prefactor of $1/180$ often deviates due to different assumptions in the derivation or its direct adjustment to experimental data.

As seen from the Kozeny-Carman equation, porosity and particle size are the decisive influences on permeability. Some of the more complex interactions between these variables are briefly highlighted now. For monodisperse particles, ε is independent of the particle size and ranges from 0.26 to 0.48 for spheres in the idealized rhombohedral and cubical packing, respectively (Bear, 1988, p. 45). Typical porosity values in natural sedimentary materials such as sands or soils are $\varepsilon = 0.3 \ldots 0.6$ (Bear, 1988, p. 46). A range of $\varepsilon = 0.1 \ldots 0.9$ is reported in cake

filtration, where the high values are found in loose packings of fibers (Tiller and Cooper, 1962; Tien and Ramarao, 2013). As depth filters are also composed of particles or fiber beds, similar porosities are encountered. If particles are distributed in their sizes, ε is usually also a function of their size distribution. Especially the packing of bidisperse particles was studied intensively (Yang, 2003, Ch. 2) and it was found in most cases that the porosity of binary particle mixtures is lower than the monodisperse packing porosities of the two constituents because smaller particles occupy the voids between larger particles; an effect that is dependent on the size ratio of the two mixed particles (Shapiro and Probstein, 1992; Mota et al., 2001; Dias et al., 2004; Brouwers, 2013). Some works also addressed the effects of mixing more than two particle sizes as well as of continuous particle size distributions (MacDonald et al., 1991; Yu et al., 1992; Dias et al., 2005; Brouwers, 2014). Additional to size, particle shape influences the porosity and, therefore, the permeability of packings (Yu et al., 1992; Allen et al., 2013; Vollmari et al., 2015). The properties of the materials involved represent another important factor (Dong et al., 2012; Liu et al., 2017).

Next, **cake filtration** is considered. Contrary to the treatment of depth filtration and Darcy's law, cake filtration is directly introduced in 1D on the continuum level as usual in the literature (Stamatakis and Tien, 1991; Civan, 1998; Tien, 2006). An important variable in cake filtration is cake height. Following from a mass balance at the cake surface (Tien, 2006, p. 57), cake height L in case of compressible cake filtration can be expressed as

$$\frac{dL}{dt} = \frac{\varepsilon_s}{\varepsilon_s - c} \cdot \left(\frac{k}{\mu} \frac{\partial p}{\partial z} \right)_{(z=L)} + q(z=0) = -\frac{\varepsilon_s}{\varepsilon_s - c} \cdot q_{\text{eff}}(z=L) + q(z=0)\,, \tag{2.42}$$

where c is the volume concentration of impurities in the liquid phase and ε_s is the solidosity of the resulting filter cake. Solidosity is defined as solid volume per total volume and is the complement to porosity, i.e., $\varepsilon_s = 1 - \varepsilon$. In case of compressible cake filtration also the solid phase moves and, therefore, Darcy's law leads to some effective superficial velocity q_{eff} everywhere except at the filter medium at $z = 0$ where solid movement is prevented. However, this is not further discussed here because only incompressible cakes are considered in this work. Incompressible cake filtration can be interpreted as a special case of compressible cake filtration for which $q_{\text{eff}}(z=L) = q(z=0) = q$ because the solid phase remains stationary. Therefore

$$\frac{dL}{dt} = -\frac{c}{\varepsilon_s - c} \cdot q\,. \tag{2.43}$$

Often, $c \ll \varepsilon_s$; thus, the last equation is well approximated by

$$\frac{dL}{dt} = -\frac{c}{\varepsilon_s} \cdot q\,; \tag{2.44}$$

a relationship that is used, e.g., by Hackl et al. (1993, p. 18). Note that for a constant solid concentration in the suspension c and constant solidosity ε_s, the cake grows linearly with time in case of constant-rate filtration. This is contrary to compressible cake filtration where ε_s is locally increased due to compression which results in a non-linear cake growth. Different than in most

depth filtration models, the origin of the coordinate system is located at the filter medium and the spatial coordinate is opposed to the flow direction when cake filtration is modeled; thus, the minus sign in Eqs. (2.43) and (2.44).

The pressure drop-flow relationship in case of cake filtration is usually modeled by Darcy's law, as formulated above in Eq. (2.38). Combining the shown treatment of cake growth with Darcy's law leads to the classical equations of cake filtration (Verein Deutscher Ingenieure, 2006; Ripperger et al., 2012) which are, however, not presented here because they are not used in this thesis.

A special case of cake filtration is **filter-aid filtration**. In this case, the permeability of the filter cake is dependent on both the impurities to be separated and the filter aids dosed to the suspension. The classical model to account for this effect is known as the Sutherland equation. Before introducing the model, a preliminary remark is in order. Some descriptions, such as the Sutherland equation, use filter cake resistance r instead of permeability k. The two properties are simply inversely related, i.e.

$$r = \frac{1}{k}\,. \tag{2.45}$$

The Sutherland equation expresses the resistance of filter cakes composed of filter aids and impurities in case of pure surface filtration and was developed, as the name indicates, by Sutherland and Hidi (1966). An analogous expression was found by Heertjes and Zuideveld (1978c). Haba and Koch (1978) validated the model. Further uses appear in Berndt (1981, pp. 31-32), Wegner (1985, p. 24), Tittel (1987, pp. 8, 56), and Hackl et al. (1993, p. 30). The equation reads

$$r = r_0 \cdot \exp\left(K_S \cdot \frac{c}{c_{\mathrm{FA}}}\right)\,, \tag{2.46}$$

where r_0 is the resistance of a filter cake which is only composed of filter-aid particles; c and c_{FA} are the concentrations of impurities and filter aid, respectively; K_S is a model constant. r_0 is determined experimentally or estimated using Darcy's law; K_S is determined experimentally for a given system of substances. Expressed in terms of permeablities, the Sutherland equation reads

$$k = k_0 \cdot \exp\left(-K_S \cdot \frac{c}{c_{\mathrm{FA}}}\right)\,. \tag{2.47}$$

It is important to note that most practice-oriented works on filtration use **mass concentrations**, i.e., c as component mass per total volume. In this manner, the Sutherland equation was developed for mass concentrations of filter aids and impurities. On the contrary, most theoretical works use **volume concentrations**, i.e., c as component volume per total volume. For example, this treatment is more closely linked to the volumetrically defined variables of porosity and specific deposit as discussed in Section 2.1.2. Trivially, volume concentrations c_v and mass component concentrations c_m are linked by the component densities ρ_c, i.e.

$$c_v = \frac{c_m}{\rho_c}\,. \tag{2.48}$$

Throughout this thesis, only volume concentrations are used when filtration is treated. For reasons of readability, therefore, the index v is omitted.

As indicated by the title of the section, only basic equations were introduced at this point. In order to obtain a closed description, additional relations are needed. However, these constitutive equations are introduced directly in the case studies of Chapters 4 and 5.

2.3 Optimal Control

Optimal control is a broad field, spanning purely mathematical investigations as well as applications in many branches of engineering. The classical theory is summarized in various textbooks (Bryson Jr. and Ho, 1975; Kirk, 2004; Lewis et al., 2012; Papageorgiou et al., 2012; Upreti, 2013). For this reason, only those parts of optimal control theory that are actually used in this dissertation are reviewed here. Generally, the formulation of an optimal control problem requires

- A **system model**,
- A **performance criterion**, and
- **Physical constraints**, if applicable (Kirk, 2004, p. 4).

To be more precise, optimal control problems comprise state variables $\mathbf{y}$ and control variables $\mathbf{u}$ of the system under consideration; the system model usually has the form

$$\dot{\mathbf{y}} = f_S(x, \mathbf{y}, \mathbf{u}(x)) , \tag{2.49}$$

where x is the independent variable. However, also other system models are encountered, e.g., partial differential equations, as used in Chapters 4 and 5, which naturally comprise more than one independent variable. Solving optimal control problems consists in determining paths of the control variables $\mathbf{u}$ so that a given performance criterion or cost measure J is minimized, i.e. the optimal control task is

$$\min_{\mathbf{u}} (J(\mathbf{u})) . \tag{2.50}$$

2.3.1 Types of Objective Functionals

The cost or performance measures in optimal control are usually referred to as objective funtionals. They are named functionals because they assign scalars to input functions. Commonly, three types of objective funtionals are used in optimal control:

- **Lagrangian type**
- **Mayer's type**
- **Bolza's type**

The Lagrangian objective functional is defined as

$$J(\mathbf{u}) = \int_{x_0}^{x_e} f_L(x, \mathbf{y}(x, \mathbf{u}(x)), \mathbf{u}(x))\,\mathrm{d}x\,. \tag{2.51}$$

Thus, in this case an integral measure over the whole range of the independent variable $[x_0\ x_e]$ is minimized. Mayer's objective functional, on the contrary, implies only an optimization of some end state-dependent measure f_M. It is defined as

$$J(\mathbf{u}) = f_M(x_e, \mathbf{y}(x_e))\,. \tag{2.52}$$

Bolza's objective functional is a combination of the Lagrangian and the Mayer type, being defined as

$$J(\mathbf{u}) = f_M(x_e, \mathbf{y}(x_e)) + \int_{x_0}^{x_e} f_L(x, \mathbf{y}(x, \mathbf{u}(x)), \mathbf{u}(x))\,\mathrm{d}x\,; \tag{2.53}$$

it, thus, contains end state components f_M and integral components f_L which can be weighted differently.

2.3.2 Classification of Problems

Besides the type of objective functional, optimal control problems are further classified according to the following criteria (Upreti, 2013, pp. 153-184):

- **Range of independent variable**: fixed x_e vs. free x_e
- **Final states**: fixed final states $\mathbf{y}_e$ vs. free final states $\mathbf{y}_e$
- **Constraints**: on states $\mathbf{y}$ and/or controls $\mathbf{u}$

Note that due to the fact that often time is the independent variable, fixed x_e and free x_e are usually referred to as "fixed final time" and "free final time", respectively. If the control variables $\mathbf{u}$ are constrained, trajectories of $\mathbf{u}$ that satisfy these constraints over the entire interval of the independent variable are called **admissible controls**. Analogously, **admissible states** denote states satisfying any given state constraints (Kirk, 2004, pp. 7-8).

The introduced classifications are used in the derivation of conditions for optimality, as discussed in the next section. The same criteria also guide the selection of numerical methods to solve optimal control problems; they will be introduced in Section 3.2.2 of the next chapter.

2.3.3 Necessary Conditions

Optimal control problems can be solved by so called direct and indirect methods. The direct method that is used to numerically solve problems based on full models is presented in Section 3.2.2. Indirect methods employ the calculus of variations to derive a set of necessary and sometimes also sufficient conditions for optimality. Some basic conditions are introduced in this section and are used later on to derive analytical optimal control solutions for simplified models.

The conditions are introduced here for the simplest case, i.e., for a **fixed range of the independent variable** and a **free end state** (Upreti, 2013, p. 161). This is exactly the type of problem encountered in the derivation of the analytical solutions for the two case studies of Chapters 4 and 5.

To simplify the theoretical treatment, usually the **Hamiltonian** is introduced as a new combined function

$$H = f_L + \boldsymbol{\psi} \cdot f_S \,, \tag{2.54}$$

where $\boldsymbol{\psi}$ are the Langrange multipliers or costates. The three main necessary conditions are called state equation, costate equation, and control condition; all three are formulated in terms of the Hamiltonian. The **state equation** reads:

$$\frac{\partial H}{\partial \boldsymbol{\psi}} = \dot{\mathbf{y}} = f_S(x, \mathbf{y}, \mathbf{u}(x)) \,. \tag{2.55}$$

The **control condition** is

$$\frac{\partial H}{\partial \mathbf{u}} = \mathbf{0} \,. \tag{2.56}$$

The **costate equation** is given as

$$\frac{\partial H}{\partial \mathbf{y}} = -\dot{\boldsymbol{\psi}} \,. \tag{2.57}$$

Additionally, the costates must satisfy

$$\boldsymbol{\psi}(x_e) = 0 \tag{2.58}$$

in case of Lagrangian objective functionals. The initial condition for the states is

$$\mathbf{y}(x = x_0) = \mathbf{y}_0 \,. \tag{2.59}$$

2.3.4 Short Review of Relevant Optimal Control Applications

In this section, relevant optimal control studies are reviewed. Relevance is understood here with respect to the practical implementation of the corresponding strategies. The studies may differ in their mathematical structure and the applied solution methods. As already mentioned, numerical optimal control methods will be examined in the next chapter. With practical application as the relevance criterion, filtration is relevant because it is exactly the main field considered in this thesis. It is known phenomenologically that filters with spatially varying properties have favorable properties, as discussed in detail in Chapter 4. Such filters are very similar to other porous structures with properties that vary in space. Therefore, optimal control in space is relevant, especially when porous structures are addressed.

As already indicated in Chapter 1, there are very few optimal control approaches in filtration research. All publications known to the author are concerned with some form of membrane filtration and address optimal control in time; these studies are introduced now.

Dynamic programming was used by van Boxtel et al. (1992) to optimize the performance of a one-stage reverse osmosis plant. By applying an overall cost-model, the optimal flow rates and process pressures were determined; membrane fouling was also accounted for. The trajectories in time were compared to optimal constant values of the control variables and benefits were found.

Blankert et al. (2006) presented the optimal control of flow rate for dead-end membrane filtration and found that constant power filtration is optimal, an operational mode that lies between the usual modes of constant-pressure and constant-rate filtration. All computations in this paper were conducted analytically using similar optimality criteria as defined in this chapter. Blankert et al. (2007) extended the previous work and included the effect of compressible cakes build-up on the filter membranes for which the solution is determined numerically. Blankert's work is summed up in his dissertation (Blankert, 2007).

Zondervan and Roffel (2008) optimized the chemical cleaning in dead-end ultra filtration. A bang-bang control of cleaning flow and cleaning agent concentration was found to be optimal. Bang-bang control implies that the control variables switch abruptly between constant values; in this case, they change between zero as the lower bound and some prescribed upper bound. The result of the optimal control approach are optimal switching points. This and further work along similar lines is summed up in Zondervan's dissertation (Zondervan, 2007).

Paulen (2012) applied dynamic programming to optimize batch membrane diafiltration. He determined how an impurity-free diluant should by dosed to the feed solution to minimize separation time or amount of added diluant. Pontryagin's mimimum principle was applied to arrive at analytical solutions, control parametrization was chosen as the numerical method.

In this thesis, mainly optimal control in space is aimed at. This is contrary to most optimal control studies where time is the independent variable, also reflected in the standard terminology for problem classification, e.g., "fixed end time". There are, however, also various studies that determine spatial trajectories of the optimal control variables. Classical works are concerned with plug-flow reactors; those are introduced first.

Horn (1961) computed optimal stationary temperature profiles along the length of tubular reactors. A similar problem was addressed by Chou et al. (1967) where the temperature profile that maximizes yield was determined for tubular reactors including catalyst decay. Ogunye and Ray (1971) determined the optimal catalyst distribution along the length of tubular reactors also in case of decaying catalysts. Besides these early studies, similar problems were also treated in newer publications. Johannessen and Kjelstrup (2004) determined optimal temperature profiles to minimize entropy production in case of SO_2 oxidation in a tubular reactor. They also optimized the reactor length, i.e., they solved a problem variable in the end value of the independent variable.

The main focus of this work is the optimization of filter structures along spatial coordinates. To the knowledge of the author, this has not been addressed so far. There are, however, other applications where similar questions were posed and answered. One example is the determination of spatial configurations to optimize controlled drug delivery. In this manner, Lu et al. (1998) applied optimal control theory to optimize the layered structure of polymer matrices and the embedded amount of drugs therein to control drug release. Similarly, Georgiadis and Kostoglou (2001) used dynamic optimization to determine optimal initial drug profiles for controlled release from multi-layered polymer matrices.

Another area where material structures are directly optimized along spatial coordinates is heat-insulation research. This is a particularly interesting application because porous media, similar to filter structures, are addressed. Venkataraman et al. (2004) and Zhu et al. (2004) determined optimal density and solidosity profiles, respectively, to improve the thermal insulation properties of foam materials. Both works explicitly address functionally graded materials (FGM), i.e., materials that locally vary, for example, in their density, geometry, or material composition. Du et al. (2009) presented profiles for optimal porosity distributions in fibrous insulation layers. However, the resulting curves are rather jagged, a fact that casts doubt on the validity of their numerical approach. Even though the last three studies do not refer explicitly to optimal control theory, they are mentioned here, because in all three cases, spatial trajectories of a control variable that optimize some overall heat-transfer measure were determined. In a new study, Hao et al. (2016) investigated the optimal 1D and 2D porosity distributions in heat insulation layers. Fixed mass and thickness of the material were used as constraints.

Optimal profiles in space are also determined in battery design, an application that again relies heavily on porous material structures. Ramadesigan et al. (2010) optimized the spatial void distribution in electrodes of Li-ion batteries by using a control-parametrization method with six piece-wise constant segments. Ohmic resistance is decreased by distributing the same amount of material with locally varying porosities. Similar results were presented by the same group at a conference (Methekar et al., 2010). Golmon et al. (2014) used a gradient-based method to determine optimal distributions of electrode porosity and radii of particles embedded in the host electrolyte of Li batteries. Their multi-objective optimization of functionally graded electrodes showed benefits for the usable battery capacity over a range of discharge rates while, at the same time, mechanical stresses were limited. However, the study of Daia and Srinivasana (2016) critically examined previous results of electrodes with graded porosity and claimed that some of the found benefits are only due to comparison with unsuitable base cases.

2.3.5 Identifying Optimal Control Problems and Evaluating their Results

After having introduced the basic concepts and some relevant applications, two questions remain:

1) How are worthwhile optimal control problems identified?

2) How are the results of optimal control approaches evaluated?

The hypothetical answers gathered in this section will be further used when the optimal control results of the two case studies in the Chapters 4 and 5 are discussed as well as when the applicability of the strategies of this thesis to other applications is explored in Chapter 6. Optimal control cases which reduce to simple optimization problems and problems in which the optimum is a constant control variable are called trivial. Worthwhile, i.e., non-trivial problems result when the following criteria are fulfilled (1):

a) The optimal control problem conforms to the formal criteria introduced above. Using two examples, it is shown how trivial optimal control problems result, if this is not the case. First, if the control variables $\mathbf{u}$ are not allowed to be functions of the independent variable x, the optimal control problem reduces to an optimization problem. Second, if the current state is not coupled to states at other times or other locations, i.e., if the system equation is no differential equation as shown in Eq. 2.49, the optimal control problem reduces to an optimization problem at each point along the independent variable.

b) Either, the control variables directly contribute to the costs described by the objective functional J, or there are some over-all constraints on the control variables, e.g., that they must have a fixed integral value. If neither is the case, the optimum is simply given by the extrema of the control variables, i.e., by constant values.

These criteria can serve as guidelines to identify worthwhile optimal control solutions prior to the actual computations. Once optimal control solutions are reached, the question remains, how much is gained by them (2). It is common to evaluate to what extent the optimal control trajectories perform better than optimal constant values, as, e.g., done in the study of van Boxtel et al. (1992) introduced in the last section, or how much superior the optimal trajectories are compared to the constant control values indeed used in practice (which often are not the optimal ones).

Also, care must be taken that the optimal control results are indeed juxtaposed with truly comparable scenarios. As shown in Section 2.3.4, a similar point was made by Daia and Srinivasana (2016) by criticizing the use of unsuitable base cases for judging the optimization results in battery design. When judging optimal control outcomes, the only difference between the optimized scenario and the base case should be the paths of the control variables; often, this needs to be assured by additional constraints. If, say, the goal is to maximize the yield of some chemical reaction, it is not enough to compare the increased yield achieved by the optimal control policy, but also the probably higher energy expenditure for the optimal approach needs to be accounted for. In this example, therefore, additional constraints should assure that the energy expenditure is indeed the same in the reference case and the optimally controlled case. Alternatively, energy expenditure can be also included in the performance measure. It will be seen later on in this thesis, however, that it is often impossible to change the control variables alone; this principle, thus, is an idealization. In the case studies of the Chapters 4 and 5 as well as when further applications are discussed in Chapter 6, all process characteristics are depicted by flow charts which are also used to motivate the chosen optimal control approach. Figure 2.7 provides

an illustration of such a flow chart. Overall constraints, important for non-trivial solutions (1, b) as well as for the evaluation of results (2), are shown in green boxes that are connected to the corresponding variables by dashed lines. Control variables are shown in orange. The interdependency between different process variables is shown by solid lines, when an increase in the first leads to an increase in the second, and by dash-dotted lines, when an increase in the first variables causes a decrease in the second variable.

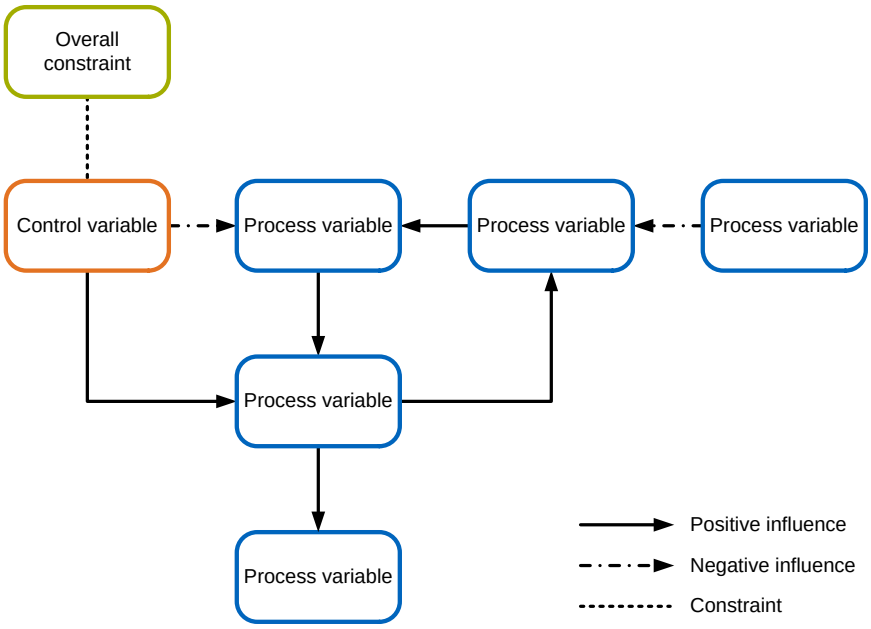

Figure 2.7: Illustration of causality diagrams.

A last remark is made with respect to the evaluation of optimal control results. Based on the above reasoning, a constant value of control variables resulting from optimal control computations has zero benefit because it is the same as the optimal constant value determined from a simple optimization approach. However, prior to the optimal control computation, it might not have been obvious that a constant value is indeed optimal despite the provided guidelines. If this is the case, the optimal control approach indeed had some benefits. Thus, one has to be aware of the psychological effect called **hindsight bias** (Kahneman, 2012, pp. 201-204, 218), sometimes also referred to as **retrospective distortion** (Taleb, 2007, pp. 8, 310), when evaluating optimal control outcomes. Hindsight bias denotes the effect that results, once they are known, often seem completely obvious and it is impossible to imagine not to have known them beforehand; however, it would have been indeed impossible to predict the outcome intuitively in a correct way *ex ante*. In optimal control, this forwards-backwards asymmetry in reasoning is also reflected in computation times: To determine an optimal control solution is much more computationally expensive than to perform forward computations with the optimal trajectories of the control variables. Furthermore, it needs to be remembered that, even though it is sometimes

possible in predict improved control policies intuitively in a qualitative way, the quantitatively optimal trajectories are only obtained by applying optimal control methods.

Chapter 3

Numerical Methods

This chapter introduces the numerical methods that are used throughout this work. It, thus, prevents that the same strategies need to be repeated in the discussion of the different case studies. The presented material is intended as a short toolbox; therefore, the numerical methods and especially the used terminology is briefly summed up so that this thesis remains self-contained. All strategies are discussed in much more detail in the literature to which the corresponding references are made. Computations were performed without exception using MATLAB (version: 2015a, supplier: The MathWorks, Natick/Massachusetts).

3.1 Partial Differential Equations

A differential equation contains derivatives of functions f. If a differential equation contains only one independent variable, such as time or one spatial dimension, it is called an **ordinary differential equation** (ODE); in this case, derivatives are written as df/dx. If a differential equations depends on more than one independent variable, it is called a **partial differential equation** (PDE); the corresponding derivatives are then written as $\partial f/\partial x$, $\partial f/\partial y$, etc. PDEs arise in various disciplines and are therefore of the utmost importance to scientists and engineers. Examples are the Maxwell equations of electrodynamics, the Navier-Stokes equations of fluid mechanics, and Schrödinger's equation of quantum mechanics, in each of which the functional variables depend on space and time and are also derived with respect to these independent variables.

PDEs can be classified according to different criteria which also guide the search for suitable numerical methods to solve the corresponding equations. The **order** of a PDE denotes its highest partial derivative, e.g., an equation containing $\partial^2 f/\partial x^2$ as the highest derivative would be of the second order. PDEs can be **linear** or nonlinear; the former implies that the functional variable f and its derivatives appear only linearly, e.g., not multiplied with each other or squared as f^2. Generally, second order linear PDEs can be written as

$$A \cdot \frac{\partial^2 f}{\partial x^2} + B \cdot \frac{\partial^2 f}{\partial x \partial y} + C \cdot \frac{\partial^2 f}{\partial y^2} + D \cdot \frac{\partial f}{\partial x} + E \cdot \frac{\partial f}{\partial y} + F \cdot f = G. \tag{3.1}$$

A PDE is **homogeneous** if $G(x,y)$ is 0 for all x and y, otherwise it is called inhomogeneous. Another classification is with respect to constant or **variable coefficients** A to G. The same coefficients are also used to group linear PDEs into parabolic, hyperbolic, and elliptic PDEs.

- If $B^2 - 4AC = 0$, the equation is called **parabolic**.
- If $B^2 - 4AC > 0$, the PDE is said to be **hyperbolic**.
- If $B^2 - 4AC < 0$, the equation is classified as **elliptic**[1].

Typical examples for parabolic PDEs are heat and diffusion equations, for hyperbolic PDEs wave and advection equations, and for eliptic PDEs Laplace and Poisson equations (Farlow, 1993, pp. 3-7).

3.1.1 The Method of Lines and Finite Difference Approximations

Among the most popular numerical strategies to solve PDEs is the method of lines (MOL) (Schiesser and Griffiths, 2009). It proceeds by an approximation of the derivatives with respect to all independent variables excluding one. Usually, all spatial derivatives are substituted so that only time derivatives remain. Approximation of derivatives is usually based on finite difference (FDM), finite volume (FVM), or finite element methods (FEM). After applying one of these approximation schemes, the initial PDE problem is reduced to a system of ODEs and can be solved by standard ODE solvers (Schäfer, 2006, pp. 150-151; Wouwer et al., 2014, p. 125).

In this work, MOL is used together with finite difference approximations. FDM are based on the opposite principle as derivations in differential calculus: derivatives are substituted by difference quotients, i.e., df/dx is substituted by $\Delta f/\Delta x$. In case of simple equations, such as the linear advection equation or the one-dimensional diffusion equation, it is still possible to analytically derive quality criteria to be met for the use of approximation schemes. However, for a theoretical discussion of the relation between consistency, stability, and convergence, the reader is referred to the corresponding literature, e.g., Schäfer (2006). Contrary to simple textbook examples for which sometimes, e.g., the stability of numerical methods can be proven theoretically, numerical schemes for more complicated models, such as the Navier-Stokes equations of fluid mechanics, are often chosen based on established heuristics (Ferziger and Perić, 2002, p. 32). Instances for such heuristics that are also used in this dissertation are:

- Spatial derivatives of the first order, i.e., of the advection type, are best approximated by upwind schemes (Carver and Hinds, 1978; Wouwer et al., 2014, pp. 151, 200).
- Derivatives of the second order, i.e., of the diffusion type, are best approximated by central schemes (Wouwer et al., 2014, pp. 151, 200).
- Steep moving fronts can be treated by upwind schemes, adaptive grid methods, or flux limiters (Wouwer et al., 2014, pp. 285-286).

[1] Sometimes, the factor 4 is omitted in these criteria due to a different problem framing; however, the formulation here consistently follows Farlow (1993).

- Problems that are stiff in the time dimension, i.e., that include strongly differing time scales[2], are addressed by implicit ODE solvers (Wouwer et al., 2014, p. 154).

The main equations encountered in the case studies of Chapters 4 and 5 are of the hyperbolic type and are inhomogeneous due to the presence of sink terms. Using the just-mentioned heuristics, the following solution schemes are applied:

- Spatial derivatives of the first order without steep moving fronts are approximated by a five-point upwind scheme (Bickley, 1941).
- Spatial derivatives of the first order with steep moving fronts are approximated by a flux-limiter scheme; more details are provided in the following Section 3.1.2.
- Due to varying time scales, all sets of time-dependent ODEs resulting from the MOL are solved using `ode15s`, a solver for stiff ODEs in MATLAB. `ode15s` is an implicit solver in which the order of the approximation scheme is adapted (Shampine and Reichelt, 1997).

3.1.2 Treating Discontinuities by Flux Limiters

Numerical problems are encountered with most solution strategies for PDEs around discontinuities or sharp changes in the solution. Commonly, the results are spurious oscillations, also referred to as "wiggles". Strategies to address these problems were mentioned in the last section, some of which, such as upwind finite-difference schemes, can handle only mild discontinuities (Wouwer et al., 2014, p. 286); flux limiters, on the contrary, are robust with respect to the changes in the solution. Because large discontinuities are encountered in the case study on filter-aid filtration of Chapter 5, a flux-limter scheme is used. Flux limiters switch between high numerical resolution in regions where the solution is smooth and low resolution around sharp fronts. Detailed information on the theory of flux limiters can be found in LeVeque (1992) and Wouwer et al. (2014).

To solve the system equations of filter-aid filtration, a van-Leer flux limiter is used (van Leer, 1974). Assuming a homogenous grid, the spatial derivative is written as

$$\frac{\partial f}{\partial z} = \frac{f_{i+1/2} - f_{i-1/2}}{\Delta z}, \tag{3.2}$$

with $f_{i+1/2}$ being the flux between node i and $i+1$ and $f_{i-1/2}$ the flux between node $i-1$ and i. The ratio r_i between two consecutive solution derivatives is

$$r_i = \frac{\frac{y_{i+1}-y_i}{\Delta z}}{\frac{y_i-y_{i-1}}{\Delta z}} = \frac{y_{i+1}-y_i}{y_i-y_{i-1}}, \tag{3.3}$$

where y_i is the dependent variable. In case of the van-Leer flux limiter, the limiter function is

[2]Note that this is a simplified notion; the concept of stiffness is more involved and unambiguous definitions are hard to come by (Spijker, 1996).

$$\phi = \frac{r+|r|}{1+r}, \tag{3.4}$$

which adapts the solution accuracy between first and second order according to

$$y_{i+1/2} = y_i + \frac{\phi(r_i)}{2}(y_i - y_{i-1}) \tag{3.5}$$

$$y_{i-1/2} = y_{i-1} + \frac{\phi(r_i)}{2}(y_{i-1} - y_{i-2}). \tag{3.6}$$

Note that here an upwind formulation is presented; the shown equations are only applicable if $df/dy > 0$. The analogue formulations for $df/dy < 0$ are omitted for reasons of brevity and can be found, e.g., in Wouwer et al. (2014, p. 308).

3.1.3 Handling Moving Boundaries by the Front-Fixing Method

Computational domains of PDE problems are often bounded; this is also the case for the method of lines as used in this work. When the domain boundaries are not known, it is distinguished between **free** and **moving boundary problems**. In the former case, boundaries do not move; however, the fixed position of the boundary is not known *ad hoc* but is determined as part of the overall problem solution. On the contrary, in moving boundary problems, the position of the domain boundary changes with time. Due to the growing filter cake height in surface filtration, this process leads to a moving boundary problem. For this reason, this problem-type is relevant for the present work.

Moving boundary problems can be treated by different numerical methods. For example, adaptable grids can be used, i.e., the spatial discretization is adjusted according to the current position of the boundary in each time step. An overview of classical methods is found in Crank (1984). In this work, a coordinate transformation called the front-fixing method is used. It was chosen because it already proved useful in studies of cake filtration (Stamatakis and Tien, 1991; Tien, 2006).

Basic relations are now briefly derived for a 1D problem with the moving boundary $L(t)$. The derivation follows roughly Crank (1984, p. 187) and Nielsen et al. (2002), but is adapted to the form needed in this work. The obtained relations are directly used to treat the system equations of the case study on filter-aid filtration in Chapter 5. To transform the moving boundary problem into a problem with a steady boundary, the new spatial coordinate

$$\eta = \frac{z}{L(t)} \tag{3.7}$$

is introduced, which fixes the boundary at $\eta = 1$. Between an arbitrary space- and time-dependent function $f(z,t)$ in the original coordinate system and the corresponding function $\hat{f}(\eta,t)$ in the transformed coordinate system, the following relationship must hold:

$$f(z,t) = \hat{f}(\eta,t) \tag{3.8}$$

i.e., the function values at z and the corresponding location η must be identical. Functions in the new coordinate system are marked by the hat accent. Deriving Eq. (3.8) with respect to z and t leads to:

$$\frac{\partial f}{\partial z} = \frac{\partial \hat{f}}{\partial \eta} \cdot \frac{\partial \eta}{\partial z} \tag{3.9}$$

$$\frac{\partial f}{\partial t} = \frac{\partial \hat{f}}{\partial t} + \frac{\partial \hat{f}}{\partial \eta} \cdot \frac{\partial \eta}{\partial t}\,. \tag{3.10}$$

If the definition of η from Eq. (3.7) is introduced to the Eqs. (3.9) and (3.10), the final relationships are obtained:

$$\frac{\partial f}{\partial z} = \frac{1}{L} \cdot \frac{\partial \hat{f}}{\partial \eta} \tag{3.11}$$

$$\frac{\partial f}{\partial t} = \frac{\partial \hat{f}}{\partial t} - \frac{\eta}{L} \cdot \frac{dL}{dt} \cdot \frac{\partial \hat{f}}{\partial \eta}\,. \tag{3.12}$$

3.2 Optimization

Numerical strategies to solve optimal control problems often consist in the reduction to conventional optimization problems. For that reason, some optimization basics are introduced before the applied numerical optimal control method is discussed.

3.2.1 Basic Terminology and Algorithms

In computational optimization, a cost function or objective function $J(\mathbf{x})$ is minimized. If no further conditions are imposed, this is an unconstrained optimization task. As long as $J(\mathbf{x})$ linearly depends on the parameters $\mathbf{x}$, this is a **linear** optimization, otherwise it is called **nonlinear**. Additional conditions of the form

$$\mathbf{g}(\mathbf{x}) = 0 \tag{3.13}$$

and

$$\mathbf{h}(\mathbf{x}) \leq 0 \tag{3.14}$$

are called **equality** and **inequality constraints**, respectively. Analogously to the cost function, also the constraints $\mathbf{g}(\mathbf{x})$ and $\mathbf{h}(\mathbf{x})$ are classified according to their dependency on $\mathbf{x}$ in nonlinear and linear.

Similar to the selection of numerical solution methods according to the classification of the system equations, optimization algorithms are chosen based on the categories just introduced. In this manner, MATLAB offers a decision table for algorithm selection (The MathWorks, 2017).

Broadly, these algorithms can be divided into two categories: **gradient-based** and **gradient-free methods**. In the first class of methods, exact or estimated gradients are used to speed up the search for the minimum.

In this work, MATLAB's gradient-based `fmincon` algorithm is used. Using the default settings, gradients are estimated based on a first-order forward finite-difference scheme using external numerical differentiation, i.e.,

$$\frac{dJ(x_i)}{dx_i} \approx \frac{J(x_i + \sqrt{\varepsilon_p}) - J(x_i)}{\sqrt{\varepsilon_p}}, \quad i = 1,2,\ldots n, \tag{3.15}$$

where ε_p is the machine precision and n is the number of parameters. All used cost functions consist of the full model equations and are, therefore, nonlinear. Equality as well as inequality constraints are used.

3.2.2 Numerical Solution Strategy for Optimal Control

Sargent (2000) distinguishes three types of numerical solutions strategies for optimal control problems; these are:

- Solution of the boundary value problem based on the necessary conditions for optimality, as introduced in Section 2.3.3.
- Converting the problem into a finite-dimensional nonlinear program by complete discretization.
- Parameterization of only the control trajectories resulting also in a nonlinear program, however, with the objective and constraint functions still being evaluated by integrating the system equations along the independent variable.

The first strategy is usually referred to as an **indirect method**, the latter two as **direct methods**. In direct optimal control methods, the optimal paths are determined directly from the system equations, i.e., not by using the necessary conditions for optimality.

In this work, a method of the third type is used. This is due to the smaller number of parameters to be determined by optimization compared to complete discretization. The first method is often not suitable for problems based on PDEs, as encountered in this dissertation, because necessary conditions are not always known.

Particularly, the direct method of control parameterization (Goh and Teo, 1988) in combination with a direct single shooting method (Hannemann-Tamas and Marquardt, 2012) is used to numerically solve the optimal control problems based on the full model equations, i.e., as explained, optimal control problems with PDE constraints. The method proceeds as follows: At first, a linear profile is assumed and the two end points are determined optimally, i.e., such that they minimize the given objective functional. In the second step, a new point is introduced in the middle between the start points. The new point is initialized with the mean value of the two

previously optimized points and a new optimization run is conducted. All further iterations consist of analog bisections and initializations. In each optimization step, the points obtained are connected linearly. If enough points are generated, any profile, including strongly non-linear trajectories, can be approximated (Goh and Teo, 1988). Figure 3.1 illustrates the numerical strategy.

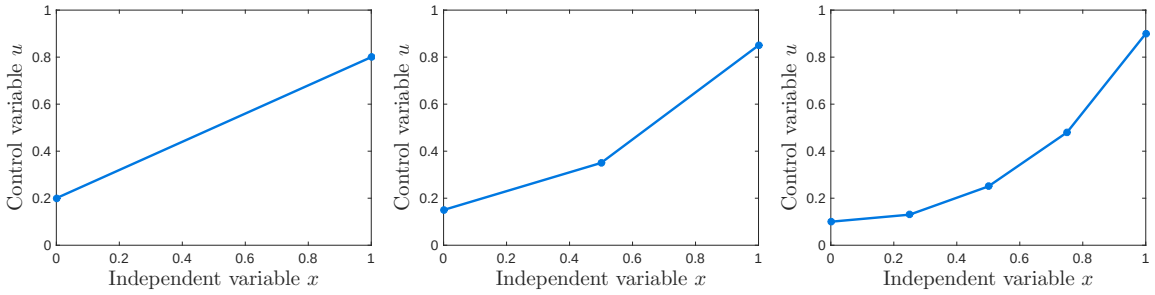

(a) (b) (c)

Figure 3.1: Illustration of numerical optimal control strategy; exemplary trajectory of control variable after first (a), second (b), and third iteration (c).

Chapter 4

Depth Filtration

Depth filters are mostly designed on the basis of trial and error. To address this methodological gap, a new technique to optimize filter design is introduced in this chapter, which is based on the recent publication of Kuhn et al. (2017a). Using optimal control theory, paths of the filter coefficient, a measure for local filtration performance, are determined along the filter depth. An analytical optimal control solution is derived and used to validate the numerical method. Two optimal control scenarios are solved numerically: In the first scenario, local filtration performance is optimized to achieve homogeneous deposition of impurities over the filter depth. The second scenario aims at maximizing the time until some maximal pressure drop is reached. Furthermore, a computational strategy is presented to transform the continuous filter-coefficient trajectories into discrete layers suitable for practical design. All optimized scenarios are compared to a one-layered filter design and significant improvements are found. As this approach is based on strongly validated and widely used filtration models, the presented methods are expected to have broad applicability.

4.1 Introduction

Depth filters come in various designs and are used for a whole range of different purposes. Thin filter media in the form of sheets can be based on the mechanism of depth filtration as well as packed beds of particles or fibers (Sutherland, 2008). Depth filtration is used for many different applications, from the cleaning of gases to the purification of liquids, the latter being the main focus of this chapter. All realizations and applications of depth filters are characterized by the fact that the particles to be separated from the fluid are captured within the filter medium, as contrasted to pure cake filtration, wherefore these particles are usually significantly smaller than the pores of the filter. When depth filtration is used, usually, the cleaned fluid is aimed at in contrast to other solid-liquid separation processes, in which the separated solids are the valuable products.

From the vast literature on depth filtration, two items of phenomenological knowledge are most important for the present chapter: First, separated matter is usually deposited very inhomogeneously over the height of depth filters, with most of the deposit located at the filter inlet;

second, layered filter designs often perform better than homogeneous filters in terms of achievable filtration times or pressure drop. Some of the studies pointing in this direction are reported in the following paragraphs.

Tien et al. (1979) simulated the dynamics of depth filters using continuum models and validated their results via a comparison with experimental data. They found the most pronounced deposit at the fluid inlet and a decreasing profile toward the outlet. Similar results for inhomogeneous deposition of solids obtained from classical continuum models have been reported, e.g., by Bai and Tien (2000); moreover, a summary of continuum approaches is also found in Tien and Ramarao (2007). Burganos et al. (2001) presented deposit curves simulated by network models that show the same inhomogeneous deposition of impurities. Yoon et al. (2006) experimentally determined deposit as a function of filter height by imaging a filter of packed glass beads and also found decreasing deposit along the flow direction. Kandra et al. (2014a) detected a similar inhomogeneous deposit in storm water filters. Mirabolghasemi et al. (2015) conducted micro-scale simulations using real porous media geometries obtained by tomography and found the strongest reduction in porosity due to particle deposition at the fluid inlet.

In the history of filtration, various set-ups have been tried out in which particle size was varied along the filter depth, e.g., to improve filtration performance or make the filter easier to clean (Baker, 1948). Fulton (1981) gave a historical account of filtration in the 20th century and showed that layered depth filters were already used in the pre-World War II period. They were justified by their improved solid-holding capacity. However, in some cases, the realization of filters comprising layers of differently sized particles was prevented owing to the loss of particle-size grading along the bed height during filter cleaning by backwashing. This problem was overcome partly when materials of different densities were used that sustained the particle-size gradient after backwashing due to their differing settling behaviors. Layered filter designs have been also introduced in various current textbooks. Wakeman and Tarleton (1999) mentioned that sand filters are often designed with coarser particles at the fluid inlet. Sutherland (2008, p. 212) referred to multi-media filters for water treatment, i.e., depth filters with coarser particles on top, resulting in larger pores at the water inlet. These stratified designs were justified with a more favorable clogging behavior. In recent studies by Kandra et al. (2012), Kandra et al. (2014b), and Kandra et al. (2014a), it was found that layered storm water filters allow for longer filtration times, compared to homogeneously packed beds.

Based on these two observations, namely inhomogeneous clogging and advantages of layered filter designs, it is hypothesized that homogeneity of the deposit profile within the filter can be increased by varying the local filtration performance. Furthermore, it is assumed that a specifically tailored deposit profile leads to lower pressure drops and, therefore, allows for longer filtration times, given a constant flow rate. The third hypothesis is that layered filters are only an approximation of the true optimum trajectory of filtration performance along the filter depth.

Methods for determining such optimal trajectories are provided by optimal control theory. Thus far, this approach is rarely used in filtration and the few studies on the subject are summed

up in Section 2.3.4. Additionally, Kuhn and Briesen (2015) addressed filter-aid filtration in the case of pure surface filtration by optimal control theory, which will be also considered in the next chapter. To the author's knowledge, the present chapter summarizes the first application of optimal control theory to depth filtration as it was published in Kuhn et al. (2017a). Preliminary work on the topic was presented at a conference (Kuhn and Briesen, 2016b). Contrary to most optimal control studies in which the control variables are determined as functions of time, the method is applied here to a variable in space. Studies from other fields, where also optimal control along spatial coordinates was conducted, were introduced in Section 2.3.4.

As in all optimal control approaches, computational efficiency of the models used is crucial. To find the optimal trajectory of the control variable, the model equations need to be solved many times. Therefore, computation times of the order of seconds are desirable. For that reason, classical continuum models of depth filtration are used instead of the now often-used pore scale models, e.g., Mirabolghasemi et al. (2015). Due to the extensive literature on continuum treatment of depth filtration, the reader is referred to the summaries of Herzig et al. (1970), Tien and Ramarao (2007), Zamani and Maini (2009), and Molnar et al. (2015). Using the classical continuum approach along with some constitutive relationships offers the further advantage that the presented method remains very general. The models used have already been validated for a broad variety of applications, and parametrization strategies are known (Zamani and Maini, 2009).

The goal of this chapter is, therefore, not to optimize a specific case of depth filtration but rather to introduce a general method applicable to many problems. For that reason, all results below are shown in non-dimensional form, and the actual numerical values are not stressed much because they depend strongly on the case at hand. In all shown case studies, the local filtration performance, as expressed by the filter coefficient, is optimized along the filter depth.

Two optimal control scenarios are shown. In the first scenario, the objective is to achieve a completely homogeneous deposition within the filter. For this scenario, also an analytical optimal control solution based on a simplified model is derived which is used to validate the numerical method. Motivation for the first scenario comes from remarks in the literature that consider inhomogeneous clogging of depth filters as disadvantageous (Baker, 1948; Fulton, 1981). Optimizing for homogeneous deposition within the filter offers the additional benefit that validation is very straightforward, meaning that one can observe directly whether the goal was reached. In practice, the objective is often to maximize filtration time, i.e., the time until some maximum differential pressure that can be provided by the system is reached (Sutherland, 2008). However, *ad hoc*, it is not clear whether homogeneous deposition within a filter, as addressed in the first scenario, automatically yields the longest possible filtration times as well. Therefore, filtration time is maximized directly in the second optimal control scenario and the results are compared with those of the first scenario. Given that the optimal trajectories of the filter coefficient are hardly useful for practical filter design , a method for transforming the continuous trajectories into any number of discrete filter layers is introduced. By using this method, layered solutions

are derived for both optimal control scenarios, and the performance of the layered filter designs is compared to those of the optimal configurations.

To pick up the second optimal control scenario, the proposed approach is expected to be beneficial for the following reasons:

- Smaller characteristic length scales of the filter bed, e.g., particle diameters, lead to an increased local filtration performance and, therefore, higher local deposit.
- Smaller characteristic length scales of the filter bed also imply a higher local pressure drop.
- Without any local control of filtration performance, depth filters show the strongest clogging at the inlet.
- Local clogging, increases the local pressure drop.
- Clogging can be made more homogeneous and the increase in overall pressure drop, therefore, smaller by locally varying the characteristic length scale.
- At the inlet, larger characteristic length scales are desirable to counteract the more pronounced clogging there.
- A decrease in characteristic length scale towards the filter outlet is expected to be beneficial.

The mentioned process causalities are also depicted in the flow chart of Figure 4.1. Furthermore, an overall constraint on the local filtration performance is shown in the figure. According to the discussion of Section 2.3.5, the constraint assures that the different scenarios are comparable; this issue will be further discussed when the optimal control strategy is explained. In the next section, the causal relationships of Figure 4.1 are expressed by the corresponding model equations.

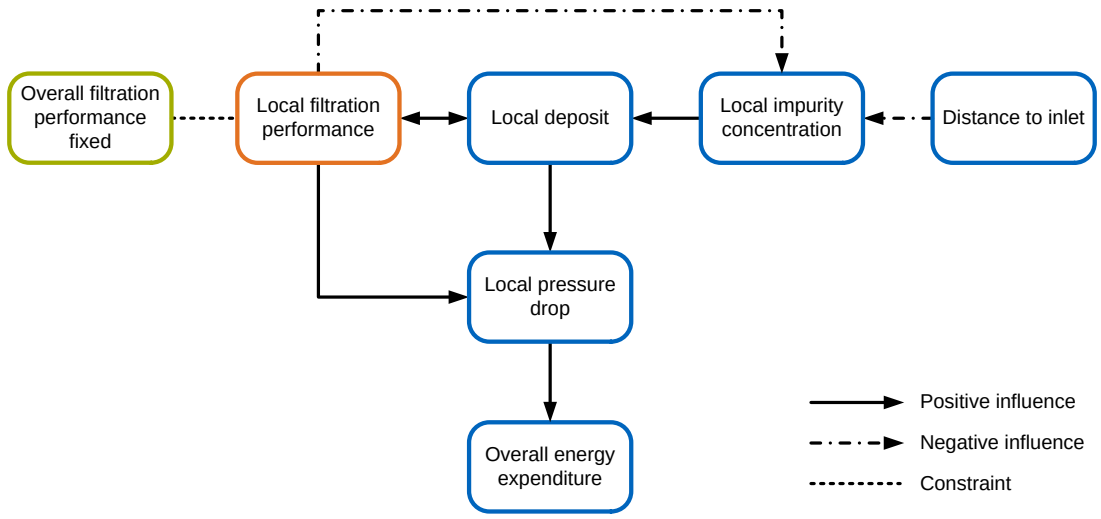

Figure 4.1: Process causalities in depth filtration.

4.2 Model

4.2.1 Model Equations

To model depth filtration, the classical continuum mechanics approach is used, consisting of the mass balance equation

$$\varepsilon \cdot \frac{\partial c}{\partial t} + q \cdot \frac{\partial c}{\partial z} = -\frac{\partial \sigma}{\partial t} \tag{4.1}$$

along with some constitutive relations. ε is the bed porosity; c is the volumetric impurity concentration in the suspension; q is the superficial velocity of the suspension; σ is specific deposit, i.e., deposited volume of impurities per filter bed volume; t and z are the independent variables time and space, respectively. A model sketch, including the coordinate system and important variables, is provided in Figure 4.2.

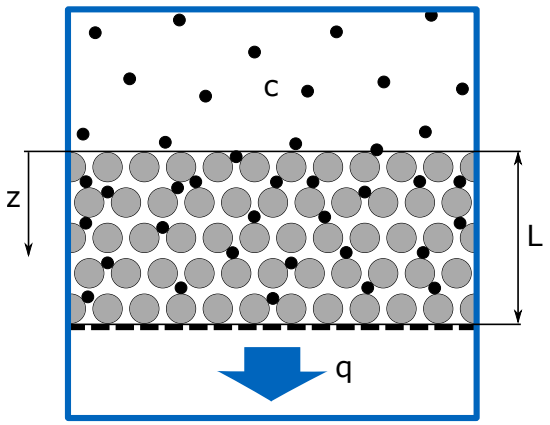

Figure 4.2: Model sketch for depth filtration.

Because only constant-rate filtration is considered, q is constant. The general form of Eq. (4.1) was derived in Section 2.1.2; its application to filtration, including the fact that ε appears outside of the time derivative, was discussed in Section 2.2.3. As shown there, $\partial\sigma/\partial t$ is usually modeled as

$$\frac{\partial \sigma}{\partial t} = \lambda \cdot q \cdot c\,, \tag{4.2}$$

with λ being the filter coefficient, which describes the efficiency of local filtration performance. If λ is assumed to be independent of σ, Eq. (4.2) is introduced into Eq. (4.1), and stationary behavior is considered, Eq. (4.1) reduces to the well-known relationship first formulated by Iwasaki (1937):

$$\frac{dc}{dz} = -\lambda \cdot c\,. \tag{4.3}$$

However, in most cases λ is a function of deposit σ, which is usually formulated as

$$\lambda = F_{\mathrm{DF}}(\sigma, \mathbf{P}) \cdot \lambda_0\,, \tag{4.4}$$

where λ_0 is the filter coefficient of an unclogged bed and $F_{\mathrm{DF}}(\sigma, \mathbf{P})$ is a functional relationship describing the dependency of the filter coefficient on specific deposit σ and a number of parameters collected in the parameter vector $\mathbf{P}$. For the case presented in Eq. (4.3), $F_{\mathrm{DF}} = 1$.

The local drop pressure dp/dz within the filter follows Darcy's law:

$$\frac{dp}{dz} = -\frac{\mu \cdot q}{k}, \tag{4.5}$$

where μ is the dynamic viscosity of the fluid and k the permeability of the solid phase.

The equations presented thus far are generally undisputed and are valid for a broad variety of applications. However, in order to have an applicable model, these equations need to be supplemented by additional constitutive relationships. Before discussing these relationships, some general remarks are in order. Given the wide variety of constitutive relationships in the literature, it is impossible to investigate a representative sample of them in the present chapter or to even focus on typical ones. Therefore, simple and intuitive relationships are used that capture the qualitative behavior of many depth-filtration applications and simultaneously contain only few parameters. So, the focus here is on the method of optimal control; the constitutive relationships can be changed easily enough.

λ_0, the filter coefficient of an unclogged bed, is subject to different influences such as fluid viscosity, flow velocity, and filter characteristics, e.g., bed particle diameter. Because only the latter is of interest for the optimal control problems addressed here, the relationship can be reduced to

$$\lambda_0 = a_{40} \cdot d^{b_{40}}. \tag{4.6}$$

Here, d is the characteristic length of the filter microscale, e.g., the bed particle diameter. a_{40} and b_{40} are model parameters[1]; b_{40} typically ranges between -1.5 and -3, see, e.g., Herzig et al. (1970). The proportionality constant a_{40} captures the remaining effects. This relationship will be employed only for qualitative interpretation of the results and will not be used in actual simulations. For this purpose, only the inverse relationship between λ_0 and d is important. As an illustration, with increasing bed particle size d, the specific surface and, therefore, the capture probability of impurities decreases.

F_{DF}, as defined in Eq. (4.4), is formulated as

$$F_{\mathrm{DF}} = 1 + a_{41} \cdot \sigma, \tag{4.7}$$

i.e., a linear relationship between the filter coefficient λ and specific deposit σ is assumed (Tien and Ramarao, 2007). Reduction of initial porosity ε_0 due to deposit σ is modeled as

$$\varepsilon = \varepsilon_0 - a_{42} \cdot \sigma, \tag{4.8}$$

[1] All parameters in constitutive equations are denoted in their subscripts by first the number of the chapter and then the number of the corresponding parameter. In the case of Eq. (4.6), the numbering starts with 0 because this equation and its parameters are not used for simulations but only for qualitative considerations, as explained subsequently.

where a_{42} is the parameter that accounts for the strength of the effect.

The local permeability of an unclogged bed is a function of the filter coefficient (Herzig et al., 1970):

$$k_0 = a_{43} \cdot \lambda^{b_{41}}, \tag{4.9}$$

where b_{41} has negative values, illustrating that bed properties that guarantee an effective separation of impurities usually also decrease the filter's permeability. For example, large values of λ usually correlate with a high specific surface of the filter bed, which also implies a low permeability. Accordingly, Boccardo et al. (2014) showed that smaller bed particles lead to a higher filtration efficiency, as also given by Zamani and Maini (2009), who mentioned the interplay between separation efficiency and pressure drop.

Clogging of the filter bed leads to a decreasing fluid permeability and therefore an increasing pressure drop, which is described by the following equation (Tien and Ramarao, 2007; Alvarez et al., 2007):

$$k = \frac{k_0}{1 + a_{44} \cdot \sigma^{b_{42}}}. \tag{4.10}$$

Some authors use a linear dependency on σ in the denominator, i.e., $b_{42} = 1$ (Vafai, 2005); also, non-linear relationships, such as polynomials, are often found (Alvarez, 2005).

4.2.2 Preliminary Considerations

For some preliminary considerations, $\lambda(z)$ is taken to be independent of the deposited concentration σ but is allowed to vary along the spatial direction z, which implies that the impurity concentration $c(z)$ exhibits stationary behavior, as is shown in Appendix 4.1. This is a good approximation for the beginning of filtration if the initial penetration of the suspension is neglected. Thus, the result is Eq. (4.3) which is solved by separation of variables and subsequent integration over the filter domain $[0\ L]$:

$$c_L = c_0 \cdot \exp\left(-\int_0^L \lambda(z)\, dz\right) = c_0 \cdot e^{-\overline{\lambda} \cdot L}, \tag{4.11}$$

where c_0 and c_L are the impurity concentrations at the filter inlet and outlet, respectively; $\overline{\lambda}$ is the mean value of the filter coefficient, which is defined as

$$\overline{\lambda} = \frac{1}{L} \int_0^L \lambda(z)\, dz. \tag{4.12}$$

Eq. (4.11) shows that the separation efficiency over a given filter height L, i.e., the reduction in impurity concentration, depends only on the integral value of the filter coefficient $\lambda(z)$ over that same height, implying that only $\overline{\lambda}$ is important, regardless of how $\lambda(z)$ is spatially distributed. This fact will be used to compare different filter designs, because for a meaningful comparison some factors must be kept constant, as discussed in Section 2.3.5, and separation efficiency is one of the most important characteristics of a filter. The choice of $\overline{\lambda}$ for a desired separation

efficiency follows from rearranging Eq. (4.11):

$$\overline{\lambda} = \frac{1}{L} \cdot ln\left(\frac{c_0}{c_L}\right). \tag{4.13}$$

4.3 Analytical Optimal Control Solution for Simplified Model

In this section, an analytical optimal control solution for a simplified model is derived with the goal of achieving homogeneous deposition of impurities within the filter. It is referred to as Scenario DF-A. As in all of the following optimal control cases, $\lambda(z)$ is the control variable. The full model is simplified by assuming that $\lambda(z)$ is not a function of σ, i.e., $a_{41} = 0$, and therefore $F_{\mathrm{DF}} = 1$. Note that porosity, thereby, vanishes from the equations and does not need to be accounted for anymore. A mathematical argument for the stationarity of c as long as λ is not a function of σ is provided in Appendix 4.1. Note that in the entire chapter, $\lambda(z)$ is used instead of λ whenever specific reference is made to the spatial dependency of λ. The objective functional for homogeneous deposit reads

$$J_{\text{DF-A}}(t_h) = \int_0^L \left[\overline{\sigma}(t_h) - \sigma(t_h, z)\right]^2 dz, \tag{4.14}$$

where $\overline{\sigma}(t_h)$ is the mean deposit in the filter, and t_h is the time at which a homogeneous deposit is aimed at which enters here as a parameter. $J_{\text{DF-A}}$, thus, expresses the variance of σ at t_h. From Eq. (4.14), it can be seen that expressions for $\sigma(t_h)$ and $\overline{\sigma}(t_h)$ are needed. Integration of Eq. (4.2) from 0 to t_h yields

$$\sigma(t_h, z) = q \cdot \lambda(z) \cdot c(z) \cdot t_h. \tag{4.15}$$

Substituting $\lambda(z) \cdot c(z)$ using Eq. (4.3) gives

$$\sigma(t_h, z) = -q \cdot t_h \cdot \frac{dc(z)}{dz}. \tag{4.16}$$

$\overline{\sigma}(t_h)$ is obtained by averaging $\sigma(t_h)$ over the filter height L:

$$\overline{\sigma}(t_h) = \frac{1}{L}\int_0^L \sigma(t_h, z)\, dz = -q \cdot t_h \cdot \frac{\Delta c}{L}. \tag{4.17}$$

For the desired goal of achieving homogeneous deposit, it must hold that $\sigma(t_h, z) = \overline{\sigma}(t_h, z)$, which implies that $J_{\text{DF-A}}(t_h)$ of Eq. (4.14) becomes exactly 0. This condition yields

$$\lambda(z) \cdot c(z) = -\frac{\Delta c}{L}. \tag{4.18}$$

For an explicit formulation of $\lambda(z)$, $c(z)$ still needs to be substituted. Using again Eq. (4.3) to substitute $\lambda(z) \cdot c(z)$ gives

$$\frac{dc}{dz} = \frac{\Delta c}{L}, \tag{4.19}$$

which, after integration over the filter depth, results in

$$c(z) = \frac{\Delta c}{L} \cdot z + c_0\,, \tag{4.20}$$

with $\Delta c = c_L - c_0$, where c_0 is the concentration at the filter inlet. Thus, the sought-for spatial trajectory of the filter coefficient $\lambda(z)$ is:

$$\lambda(z) = -\left[L \cdot \left(\frac{c_0}{\Delta c} + \frac{z}{L}\right)\right]^{-1}. \tag{4.21}$$

Note, that t_h completely vanished from the derivation. For the simplified model, the result of Eq. (4.21) therefore yields a homogeneous deposit at any time, which also implies that $J_{\text{DF-A}}(t_h) = J_{\text{DF-A}}$. In the results section, the analytical solution is further interpreted and used to validate the numerical method.

The optimal control solution for $\lambda(z)$, so far obtained by an analysis of the system equations, is now checked against the necessary optimality conditions as introduced in Section 2.3.3. Formulated with the variables of this chapter, the conditions are

$$\frac{\partial H}{\partial \psi} = \frac{dc}{dz} \tag{4.22}$$

$$\frac{\partial H}{\partial \lambda} = 0 \tag{4.23}$$

$$\frac{\partial H}{\partial c} = -\frac{d\psi}{dz} \tag{4.24}$$

$$\psi(L) = 0\,, \tag{4.25}$$

with the Hamiltonian

$$H = (\overline{\sigma} - \sigma)^2 - \psi \cdot \lambda \cdot c\,; \tag{4.26}$$

c is the state variable and λ is the control variable. The first condition

$$\frac{\partial H}{\partial \psi} = -\lambda \cdot c = \frac{dc}{dz} \tag{4.27}$$

is naturally fulfilled. Note that $(\overline{\sigma} - \sigma) = 0$ for the assumed solution, which is already substituted here and in the following equations. The second condition yields

$$\frac{\partial H}{\partial \lambda} = -\psi \cdot c = 0\,. \tag{4.28}$$

In the case of optimality, it follows that ψ is 0 when c is substituted with the proposed solution. From the third condition

$$\frac{\partial H}{\partial c} = -\psi \cdot \lambda \tag{4.29}$$

it follows that $d\psi/dz = 0$ if the assumed solution for $\lambda(z)$ and $\psi = 0$ are substituted. Since ψ is 0 everywhere, it is so also at the final location L, from which it follows that the fourth condition holds as well. Thus, all four necessary conditions are fulfilled. In the case of convex objective functionals and the here given linear system equation, the necessary conditions are also sufficient for optimality (Upreti, 2013). As the objective functional in Eq. (4.14) is of quadratic form and therefore convex, the derived solution is the true optimum.

4.4 Nondimensionalization, Parameter Values, and Initialization

All variables in the numerical part are displayed nondimensionally. This leads to a good problem scaling, advantageous for numerical solution and optimization approaches. Moreover, as it is the primary aim of this chapter to introduce a general method, nondimensional variables make it easier to detect trends. Furthermore, the number of model parameters is reduced. The following nondimensional and scaled variables are introduced:

$$\tilde{c} = \frac{c}{c_0} \tag{4.30}$$

$$\tilde{\sigma} = \frac{\sigma}{c_0} \tag{4.31}$$

$$\tilde{\lambda} = \lambda \cdot L \tag{4.32}$$

$$\tilde{z} = \frac{z}{L} \tag{4.33}$$

$$\tilde{t} = \frac{t \cdot q}{L} \tag{4.34}$$

$$\tilde{p} = \frac{p \cdot L}{\mu \cdot q} \tag{4.35}$$

$$\tilde{k} = \frac{k}{L^2}\,. \tag{4.36}$$

Correspondingly, the nondimensional model parameters are

$$\tilde{a}_{41} = a_{41} \cdot c_0 \tag{4.37}$$

$$\tilde{a}_{42} = a_{42} \cdot c_0 \tag{4.38}$$

$$\tilde{a}_{43} = \frac{a_{43}}{L^{(b_{41}+2)}} \tag{4.39}$$

$$\tilde{a}_{44} = a_{44} \cdot (c_0)^{b_{42}} \tag{4.40}$$

$$\tilde{b}_{41} = b_{41} \tag{4.41}$$

$$\tilde{b}_{42} = b_{42}\,; \tag{4.42}$$

they can be easily checked using Eqs. (4.51) to (4.55) below. A similar scaling was applied by Civan and Rasmussen (2005) and Bedrikovetsky (2008). Owing to the nondimensionalization, c_0, L, q, and μ completely cancel from the equations. Thus, the final equations to be solved become

$$\varepsilon \cdot \frac{\partial \tilde{c}}{\partial \tilde{t}} + \frac{\partial \tilde{c}}{\partial \tilde{z}} = -\frac{\partial \tilde{\sigma}}{\partial \tilde{t}} \tag{4.43}$$

$$\frac{\partial \tilde{\sigma}}{\partial \tilde{t}} = \tilde{\lambda} \cdot \tilde{c} \tag{4.44}$$

$$\frac{d\tilde{p}}{d\tilde{z}} = -\frac{1}{\tilde{k}}. \tag{4.45}$$

In all computed and optimized cases, the following initial conditions are used:

$$\tilde{c}(0,\tilde{z}) = exp\left(-\int_0^{\tilde{z}} \tilde{\lambda}(\tilde{z})\, d\tilde{z}^*\right) \tag{4.46}$$

$$\tilde{\sigma}(0,\tilde{z}) = 0, \tag{4.47}$$

implying that the first layer of fluid has already passed through the filter, see Appendix 4.1, and that the filter is unclogged initially. At the filter inlet, the subsequent boundary conditions are defined:

$$\tilde{c}(\tilde{t},0) = 1 \tag{4.48}$$

$$\tilde{\sigma}(\tilde{t},0) = \tilde{\lambda}(0) \cdot \tilde{t}, \tag{4.49}$$

where the latter condition follows from the time integration of Eq. (4.44); the concentration vanishes, because $\tilde{c}$ is always 1 at the filter inlet. Total, nondimensional pressure drop is obtained from an integration of Eq. (4.45):

$$\Delta\tilde{p} = -\int_0^{\tilde{L}} \frac{1}{\tilde{k}}\, d\tilde{z}. \tag{4.50}$$

As $\Delta\tilde{p}$ is always negative with the coordinate system chosen in this chapter, $|\Delta\tilde{p}|$ is shown in the results section. Note that above no boundary condition was provided for $\tilde{p}$, because none is needed as only the differential pressure $\Delta\tilde{p}$ is evaluated by the definite integral of Eq. (4.50). In nondimensional form, the corresponding constitutive equations are

$$\tilde{\lambda} = \tilde{\lambda}_0 \cdot \tilde{F}_{\mathrm{DF}} \tag{4.51}$$

$$\tilde{F}_{\mathrm{DF}} = 1 + \tilde{a}_{41} \cdot \tilde{\sigma} \tag{4.52}$$

$$\varepsilon = \varepsilon_0 - \tilde{a}_{42} \cdot \tilde{\sigma} \tag{4.53}$$

$$\tilde{k}_0 = \tilde{a}_{43} \cdot \tilde{\lambda}^{\ \tilde{b}_{41}} \tag{4.54}$$

$$\tilde{k} = \frac{\tilde{k}_0}{1 + \tilde{a}_{44} \cdot \tilde{\sigma}^{\ \tilde{b}_{42}}}. \tag{4.55}$$

The filtration quality was specified as a 2/3 reduction in impurities, i.e., $\tilde{c}(\tilde{t},1) = 0.33$. All discussed designs meet this specification exactly at the beginning of filtration and their perfor-

mance improves with clogging according to Eqs. (4.4) and (4.7). All further model parameters are summarized in Table 4.1.

Table 4.1: Model parameters for depth filtration.

Parameter	ε_0	$\tilde{a}_{41}$	$\tilde{a}_{42}$	$\tilde{a}_{43}$	$\tilde{a}_{44}$	$\tilde{b}_{41}$	$\tilde{b}_{42}$
Value	0.40	0.20	0.01	5.0	5.0	-1.0	2.0

4.5 Numerical Methods and Solver Settings

Numerically, the model equations, including their initial and boundary conditions, are solved by the method of lines using a five-point upwind approximation for the spatial derivatives. 150 spatial discretization points are used. For a discussion of these methods, the reader is referred to Chapter 3, especially Section 3.1.1.

Optimal control is approximated numerically by a direct single shooting method, as described in Section 3.2.2. The resulting optimization problem is solved by MATLAB's `fmincon` solver using the default interior-point algorithm and specifying constraint tolerance (`TolCon`), termination tolerance for function values (`TolFun`), and termination tolerance for parameter values all as 10^{-14}. More details on optimization are provided in Section 3.2.2.

To assure a specified filtration quality, i.e., a specified impurity concentration at the filter outlet $\tilde{c}(\tilde{t},1)$, extra conditions must be imposed on the filter coefficient. Eq. (4.11) shows that for a desired separation only the integral value of $\tilde{\lambda}(z)$ over the filter depth matters. Therefore, this integral value is imposed as a constraint in the optimization procedure to guarantee that an unclogged filter always yields the same filtration quality. By this measure, a meaningful comparison of results according to the considerations of Section 2.3.5 is enabled.

Because in many cases a continuous profile of local filtration performance is practically not feasible, discrete layers are derived in the following manner from the computed trajectories. First, the desired number of layers n is specified. Then, the points that bound the layers are initialized for equally thick layers. Obviously, the first and the last point are no free parameters because the total filter height is fixed, i.e., $\tilde{z}_0 = 0$ and $\tilde{z}_L = 1$. So, n layers lead to $n-1$ free parameters to be determined. They are computed by minimizing the objective function

$$J_{\text{Layers}} = \int_0^1 \left[\tilde{\lambda}(\tilde{z}) - f(z)\right] d\tilde{z}, \tag{4.56}$$

with

$$f(z) = \frac{\int_{\tilde{z}_i}^{\tilde{z}_{i+1}} \tilde{\lambda}(\tilde{z}) d\tilde{z}}{\tilde{z}_{i+1} - \tilde{z}_i}, \quad \tilde{z}_i \leq \tilde{z} < 1, \quad i = 1,2,\ldots(n+1), \tag{4.57}$$

yielding the locally constant values of $\tilde{\lambda}$. f is formulated such that the local and, therefore, also the total integral values of the discrete and continuous profiles are the same, which again guar-

antees the specified filtration quality. The discrete filter layers are determined using MATLAB's `fminsearch` solver with its default settings. In the case studies shown below, the number of filter layers n is set to 3.

4.6 Numerical Optimal Control Solutions for Full Model

4.6.1 Numerically Solved Optimal Control Scenarios

In this chapter, two optimal control cases are solved numerically which are referred to as Scenarios DF-OC1 and DF-OC2. Contrary to the simplified model used above, in the Scenarios DF-OC1 and DF-OC2 $\tilde{\lambda}$ changes with deposit according to Eq. (4.52). Therefore, $\tilde{\lambda}_0(z)$, i.e., the filter coefficient prior to deposit, is the control variable, because only $\tilde{\lambda}_0(z)$ can be affected during the design of depth filters. For example, $\tilde{\lambda}_0(z)$ can be influenced by suitably choosing the particle size of the filter bed, see Eq. (4.6). The first numerical optimal control case, Scenario DF-OC1, aims to achieve a homogeneous deposit within the filter at some defined filtration time t_h. The corresponding objective functional is

$$J_{\text{DF-OC1}}(\tilde{t}_h) = \int_0^1 \left[\overline{\tilde{\sigma}}(\tilde{t}_h) - \sigma(\tilde{t}_h, \tilde{z})\right]^2 d\tilde{z}, \tag{4.58}$$

with $\overline{\tilde{\sigma}}(\tilde{t}_h)$ being the mean deposit over the filter depth at time $\tilde{t}_h$, where homogeneous deposit is aimed at. Note that this scenario resembles $J_{\text{DF-A}}$ as formulated in Eq. (4.14). However, it is no longer possible to solve the problem analytically because now $\tilde{a}_{41} \neq 0$ and $\tilde{a}_{42} \neq 0$, wherefore ε and $\tilde{\lambda}$ change with $\tilde{\sigma}$. Thus, the full system of coupled PDEs needs to be considered. Moreover, $J_{\text{DF-OC1}}(\tilde{t}_h)$ truly depends on $\tilde{t}_h$ as a parameter, whereas $\tilde{t}_h$ canceled in the derivation of the analytical solution.

Scenario DF-OC2, the second numerical optimal control case study, aims at maximizing the achievable filtration time. The objective functional is

$$J_{\text{DF-OC2}} = -\tilde{t}_s\,, \tag{4.59}$$

where $\tilde{t}_s$ is the stopping time, i.e., the time where a limit in maximal pressure drop $|\Delta\tilde{p}| = 3$ is reached. $\tilde{t}_s$ is determined by introducing an event function in MATLAB's ODE solver and computing the set of equations only till the event function detects the limiting pressure drop.

4.6.2 Basic Model Results

All optimal control scenarios are compared to a filter configuration with a constant filter coefficient $\tilde{\lambda}_0$, i.e., a homogeneously designed or one-layered filter. This setting is referred to as Scenario DF-0. To illustrate the general model behavior, some basic results for this configuration are shown. At the filter outlet, the impurity concentration $\tilde{c}$ decreases with filtration time, as shown in Figure 4.3a. This reflects the increase of $\tilde{\lambda}$ with deposit $\tilde{\sigma}$, modeled by Eqs. (4.4) and (4.7). Figure 4.3b shows the typical deposit curves, which are also reported in the literature (see

Section 4.1). As usual, the most pronounced deposition is observed at the filter inlet at $\tilde{z} = 0$ and deposit increases with filtration time, i.e., the more solids are retained within the filter.

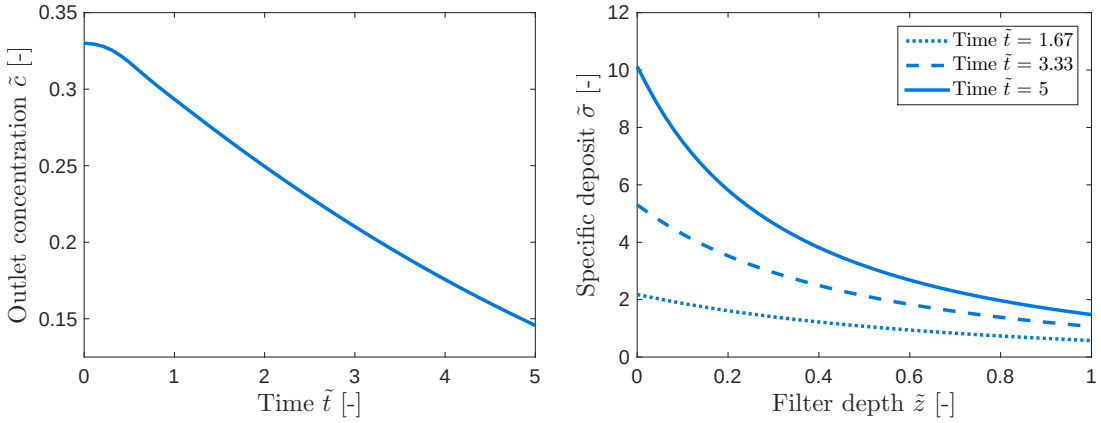

(a) (b)

Figure 4.3: Impurity concentration at filter outlet (a) and specific deposit over filter height at three times for reference Scenario DF-0 (b).

4.6.3 Validation of Numerical Method

To validate the numerical optimal control method, the numerically determined trajectory of $\tilde{\lambda}(z)$ is compared to the analytical solution obtained using Eq. (4.21), which was derived in Section 4.3. For determining the numerical solution, the model was simplified in the same way as it was for determining the analytical solution. It was assumed that $\tilde{\lambda}$ is not a function of $\tilde{\sigma}$, i.e., $\tilde{a}_{41} = 0$, and therefore $\tilde{F}_{\mathrm{DF}} = 1$; $\tilde{\lambda}$ is, thus, equal to $\tilde{\lambda}_0$. In Figure 4.4, the analytical and the numerical optimal control solutions are juxtaposed. A perfect agreement can be observed and, therefore, it is concluded that the numerical method is valid. In this figure and in the following plots of $\lambda(z)$, the points shown on the optimal curves are the discrete points determined by the direct single shooting method as described in Section 3.2.2.

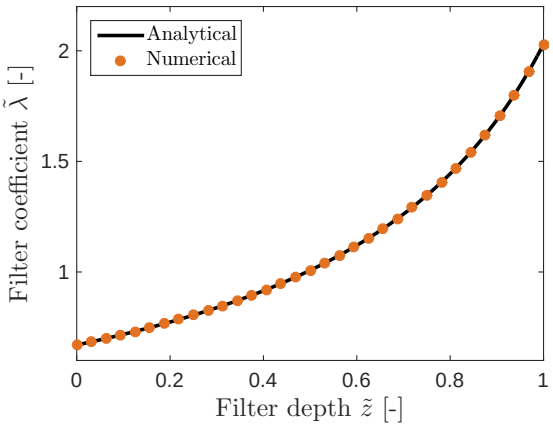

Figure 4.4: Comparison of analytical and numerical optimal control solution for filter coefficient $\tilde{\lambda}(z)$ in case of the simplified model.

Figure 4.5 shows model results computed using the optimized filter coefficient. The impurity concentration in the suspension $\tilde{c}$ decreases linearly along the spatial direction $\tilde{z}$, as compared to the reference scenario with a constant filter coefficient, which shows an exponential decrease. Deposit $\tilde{\sigma}$ has a constant value along the filter depth, which increases with time. The spatially constant value of $\tilde{\sigma}$ shows that the desired goal of a constant deposit is exactly met at each time. The results also precisely confirm the considerations in the derivation of the optimal trajectory of $\tilde{\lambda}(z)$. Mainly, the outcome illustrates that a linear path of $\tilde{c}$ indeed leads to a homogeneous deposit within the filter, as formulated in Eq. (4.19).

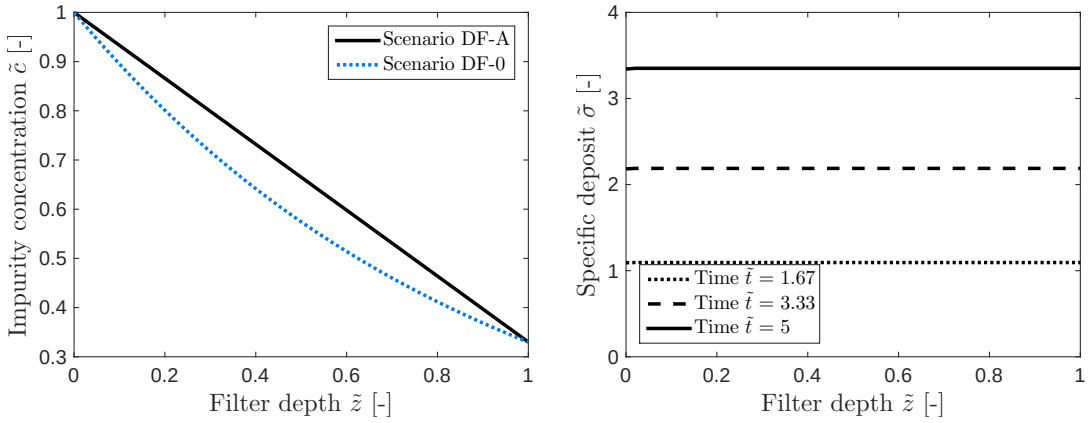

(a) (b)

Figure 4.5: Impurity concentration in suspension at $\tilde{t} = 0$, comparison of analytical optimal control solution of Scenario DF-A and reference Scenario DF-0 (a); specific deposit along the filter depth at three times for Scenario DF-A (b).

4.6.4 Homogeneous Deposit

Now, the results of the first numerical optimal control scenario are shown, where the goal was to achieve a homogenous deposit $\tilde{\sigma}$ at the specified filtration time $\tilde{t} = \tilde{t}_h = 5$, i.e., Scenario DF-OC1. Figure 4.6 shows the results of the trajectory of $\tilde{\lambda}_0(z)$ determined using the cost functional given in Eq. (4.58). In the same figure, the three-layered solution is shown as well, which was determined using the strategy of Eqs. (4.56) and (4.57). For comparison, also the constant $\tilde{\lambda}_0$ value of the reference Scenario DF-0 is plotted.

The temporal development of deposit as well as a comparison of deposit values at $\tilde{t} = \tilde{t}_h = 5$ for the optimal solution of Scenario DF-OC1, the corresponding three-layered solution of Scenario DF-OC1-3L, and the reference Scenario DF-0 are shown in Figure 4.7. First, it can be observed that at $\tilde{t} = 5$, the deposit along the filter height is indeed completely homogeneous, which means that the optimization goal was achieved exactly. Second, in Scenario DF-OC1, the deposit is homogeneous *only* at $\tilde{t} = 5$, compared to the results shown in Figure 4.5, because in this case $\tilde{\lambda}$ is no longer constant but changes with deposit according to Eq. (4.52). Third, the three-layered solution of Scenario DF-OC1-3L still provides a good approximation of the truly

optimal trajectory, because the corresponding deposit curve is still significantly more homogeneous than deposit in the reference Scenario DF-0.

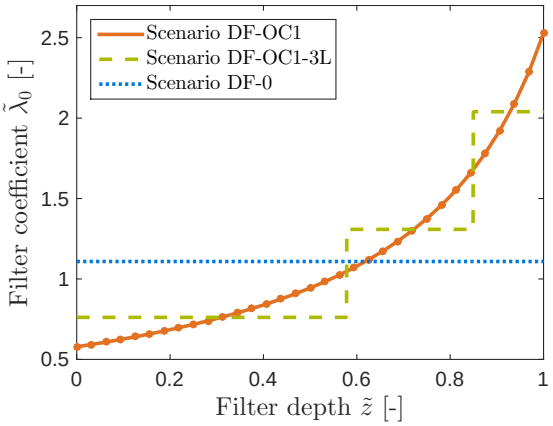

Figure 4.6: Filter coefficient $\tilde{\lambda}_0(z)$ of optimal solution for Scenario DF-OC1, corresponding three-layered solution (Scenario DF-OC1-3L), and reference Scenario DF-0.

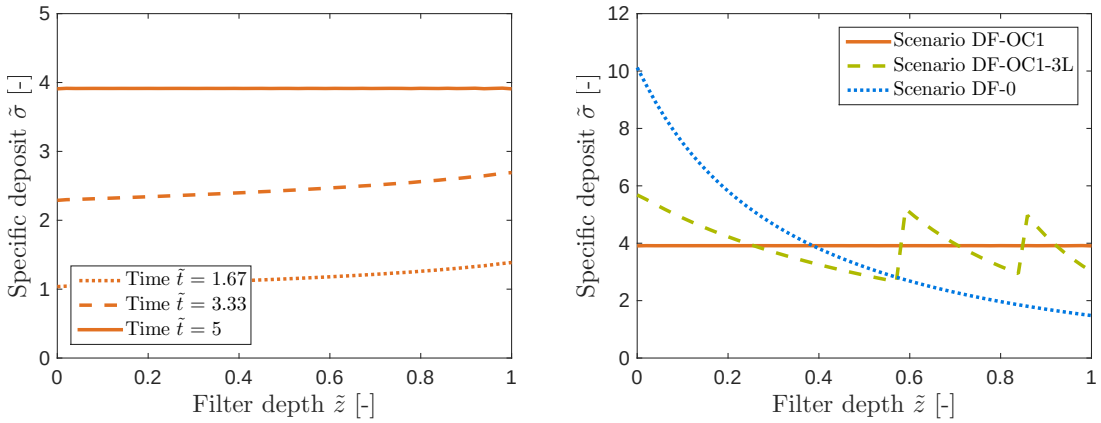

(a) (b)

Figure 4.7: Specific deposit along the filter depth at three times, the final time is $\tilde{t}_h = 5$ (a); comparison of deposit curves for the optimal solution of Scenario DF-OC1, corresponding three-layered solution (Scenario DF-OC1-3L), and reference Scenario DF-0 at $\tilde{t} = \tilde{t}_h = 5$ (b).

4.6.5 Maximization of Filtration Time

Maximization of filtration time according the cost functional $J_{\text{DF-OC2}}$ of Eq. (4.59) leads to the $\tilde{\lambda}_0(z)$ trajectories shown in Figure 4.8. In this case, the optimal trajectory is nearly linear. Therefore, the three layers determined according to Eqs. (4.56) and (4.57) are of approximately equal thickness. The reference Scenario DF-0 is shown again for comparison.

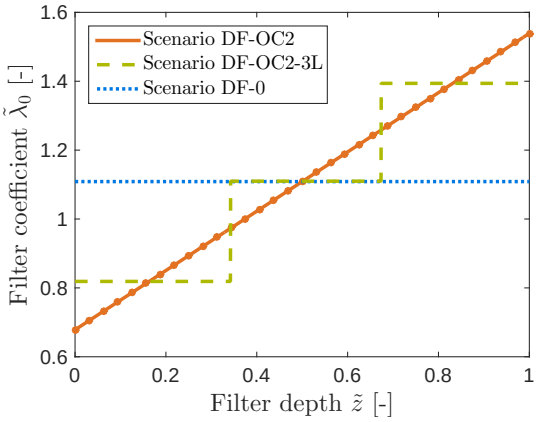

Figure 4.8: Filter coefficient $\tilde{\lambda}_0(z)$ for optimal solution of Scenario DF-OC2, corresponding three-layered solution (Scenario DF-OC2-3L), and reference Scenario DF-0.

Figure 4.9a shows that the deposit profiles within the filter for maximized time differ from the curves determined for homogeneous deposit, as shown in Figure 4.7. Therefore, the two scenarios are not identical. Due to the shorter time span of filtration, also the numerical values of $\tilde{\sigma}$ are smaller in Figure 4.9a compared to the previous scenarios. The trajectories of absolute differential pressure $|\Delta\tilde{p}|$ across the filter are plotted in Figure 4.9b. All curves stop at $|\Delta\tilde{p}| = 3$ because this is the limit defined in the optimal control approach. Already this figure shows that the optimized scenario as well as the three-layered solution derived from it allow longer filtration times compared to the reference scenario with a constant $\tilde{\lambda}$, i.e., $\Delta\tilde{p} = 3$ is reached at later stopping times $\tilde{t}_s$.

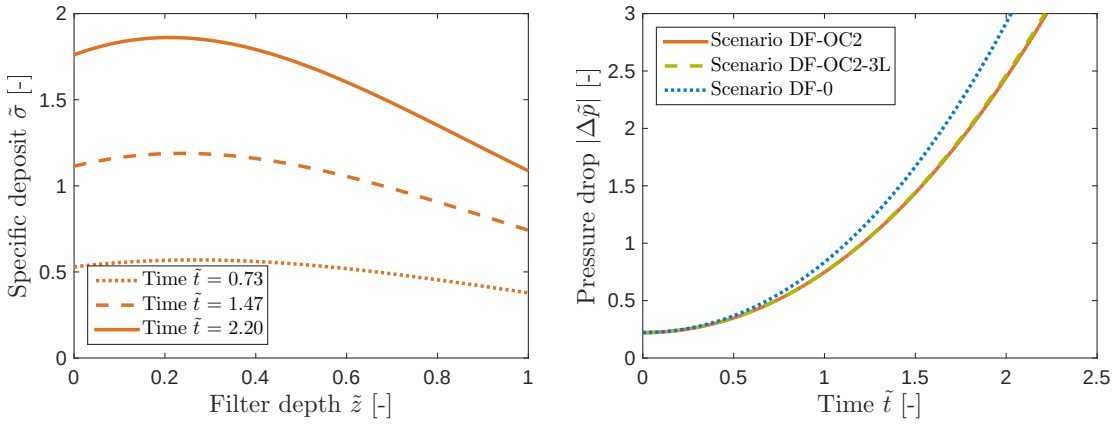

(a) (b)

Figure 4.9: Specific deposit along the filter depth at three times, the stopping time is $\tilde{t}_s = 2.20$ (a); temporal development of absolute differential pressure $|\Delta\tilde{p}|$ for Scenario DF-OC2, corresponding three-layered solution of Scenario DF-OC2-3L, and reference Scenario DF-0 (b).

For quantitative analysis, the corresponding numerical values are given in Table 4.2. It can be observed that stopping time $\tilde{t}_s$ is significantly larger in Scenario DF-OC2, where maximization of time was aimed at, compared to the base case of Scenario DF-0. Moreover, the three-layered solution of Scenario DF-OC2-3L is, again, nearly as good as the continuous trajectory. Further-

more, the concrete values of stopping time confirm that optimizing for maximal filtration time leads to significantly higher values of $\tilde{t}_s$ than in Scenario DF-OC1, in which homogeneous deposit was the goal, even though the latter performs still better than Scenario DF-0. Also, maximizing stopping time leads to a non-homogeneous deposit profile within the filter at $\tilde{t} = \tilde{t}_s$ as can be seen in Figure 4.9a. Thus, the two numerical optimal control scenarios are indeed different and, therefore, cannot be reduced to each other.

Table 4.2: Stopping times $\tilde{t}_s$ when pressure limit $|\Delta\tilde{p}| = 3$ is reached for different scenarios. Increase in $\tilde{t}_s$ denotes the percentage difference between the corresponding optimized scenarios and the reference of Scenario DF-0.

Scenario	DF-0	DF-0C2	DF-0C2-3L	DF-OC1
Stopping time $\tilde{t}_s$ [-]	2.03	2.22	2.21	2.11
Increase in $\tilde{t}_s$ [%]	–	9.36	8.87	3.94

It is important to note, that especially the solution for maximization of filtration time strongly depends on the chosen constitutive equations, including the corresponding parameters. A beneficial optimal control solution is only obtained as long as non-linear clogging behavior is assumed. This is because the overall pressure drop according to Darcy's law, Eq. (4.5), depends on the integral value of inverse permeability. The influence of deposit on permeability is modeled according to Eq. (4.55) with $\tilde{b}_{42} = 2$, i.e., by using a quadratic relationship in the denominator. If deposit linearly affects the denominator, the local distribution of $\tilde{\sigma}$ has no effect on the overall pressure drop and, therefore, a constant filter coefficient $\tilde{\lambda}_0$ leads to the same result as a locally-variable $\tilde{\lambda}_0(z)$.

Moreover, it is highlighted that all optimal control cases resulted in an increasing value of filter coefficient $\tilde{\lambda}_0$ along the filter depth. Because $\tilde{\lambda}_0$ and the characteristic length of the filter microscale d are usually inversely proportional, compare Eq. (4.6), larger values of d are desirable at the filter inlet and smaller values at the outlet. This agrees exactly with the phenomenological evidence gathered in the literature review of this chapter and the systematic reasoning provided also in Section 4.1.

4.7 Conclusions from Optimally Controlled Depth Filtration

In this chapter, a new model-based method for improving the design of depth filters was introduced. From an analysis of the system equations and by using optimal control theory, an analytical solution of local filtration performance, as expressed by the filter coefficient, was derived to achieve homogeneous deposit along the filter depth. This solution is based on a simplified model assuming a filter coefficient that is independent of deposit. Using this analytical solution,

the numerical optimal control algorithm, a direct single shooting approach, was validated. It could be shown that under the assumption of the simplified model, a linear decrease in impurity concentration in the suspension while passing through the filter leads to homogeneous deposit along the filter depth.

Using the full model, the targeted optimal control scenarios could only be solved numerically. If the filter coefficient functionally depends on deposit, also homogeneous deposit along the filter depth can be achieved by optimally controlling the initial filter coefficient, but in this way, the desired homogeneous deposit is now achieved only at one specific time. The second numerically-solved optimal control scenario addressed the maximization of filtration time, i.e., of the time until a specific overall pressure drop is reached. A significant increase in filtration time could be achieved with a solution that differs from the scenario of homogeneous deposit. It follows that homogeneous deposit is not generally the same as maximization of filtration time. However, it was also highlighted that especially the maximization of filtration time depends strongly on the constitutive equations describing the influence of deposit on permeability.

Due to the difficulties in realizing continuous variation of the filter coefficient practically, layered solutions were computed. For both numerical optimal control scenarios, three discrete filter layers were derived from the continuous solutions by using a newly developed optimization approach. In both cases, the three layers well approximated the continuous optimal control solutions. However, the layered solutions showed some local discontinuities at the boundaries of the discrete layers.

In future work, the effect of these discontinuities should be observed by pore-scale simulations because it can be hypothesized that local effects play a role at that scale that are not captured by the present continuum mechanical treatment. The main purpose of the present chapter was to introduce the general optimization method; however, application of this strategy to practical cases of depth filtration is needed to finally test its usefulness. It is asserted that methods, as the one developed in the this chapter, will gain increasing importance in the future. Even though layered filter configurations continue to be the state of the art, continuous design of filters is within reach due to the advent of the 3D printer. For example, 3D-printing of particle agglomerates was conducted by Ge et al. (2017). Perspectives for 3D printing of filter membranes were discussed by Low et al. (2017). The possibility of locally tailored filters within the micro-manipulative paradigm (see Section 1.2.1) will, therefore, increasingly demand quantitative methods to determine the desired spatial distributions. The short outlook provided here will be broadened and generalized in Chapter 7.

Appendix 4.1

In this appendix[2], an analytical solution is derived for the main depth filtration model under the assumption that the filter coefficient $\lambda(z)$ is not a function of the deposited solids' concentration σ. The derivation follows the strategy used by Civan and Rasmussen (2005), except that these authors assumed a constant λ. The solution is derived using the method of characteristics, which is based on the definition of the total differential, given as

$$\frac{dc}{ds} = \frac{\partial c}{\partial t} \cdot \frac{dt}{ds} + \frac{\partial c}{\partial z} \cdot \frac{dz}{ds}, \tag{4.60}$$

where s is the characteristic variable. If the coefficients and terms of this definition are compared with the basic depth filtration equation

$$\varepsilon \cdot \frac{\partial c}{\partial t} + q \cdot \frac{\partial c}{\partial z} = -q \cdot \lambda \cdot c, \tag{4.61}$$

the following three equations are obtained:

$$\frac{dc}{ds} = -q \cdot \lambda \cdot c, \tag{4.62}$$

$$\frac{dt}{ds} = \varepsilon, \tag{4.63}$$

and

$$\frac{dz}{ds} = q. \tag{4.64}$$

According to the optimal control approach presented in this chapter, λ is a function of the spatial variable z. Therefore, the solution of the first ODE presented above is:

$$c = K \cdot \exp\left(-q \cdot \int_0^s \lambda \, d\hat{s}\right). \tag{4.65}$$

It is demanded that at $t = 0$ also $s = 0$; thus

$$t = s \cdot \varepsilon. \tag{4.66}$$

From the third ODE, it follows that

$$z = q \cdot s + z_0. \tag{4.67}$$

The initial condition for $s = 0$ is given by

$$c(0, z_0) = c_0 \cdot [1 - H(z_0)], \tag{4.68}$$

[2]As this appendix exclusively refers to Chapter 4, it is included directly after the chapter rather than at the end of the thesis, because it is deemed that this aids the reading flow.

which implies that the initial impurity concentration inside the filter is 0 and it has the value c_0 in the suspension outside of the filter, i.e., for $z < 0$. Further, it is required that at $z = 0$, the impurity concentration should remain at c_0, i.e.

$$c(t,0) = c_0\,. \tag{4.69}$$

Enforcing both conditions leads to an integration constant of

$$K = c_0 \cdot [1 - H(z_0)] \cdot \exp\left(-\int_0^{z_0} \lambda\, dz\right) = c_0 \cdot [1 - H(z - q/\varepsilon \cdot t)] \cdot \exp\left(-\int_0^{z_0} \lambda\, dz\right). \tag{4.70}$$

Turning back to Eq. (4.65) and substituting the integral to the z coordinate gives

$$c = K \cdot \exp\left(-\int_{z_0}^{z} \lambda\, d\hat{z}\right). \tag{4.71}$$

If K is substituted with the above expression, one gets

$$c = c_0 \cdot [1 - H(z - q/\varepsilon \cdot t)] \cdot \exp\left(-\int_0^{z_0} \lambda\, d\hat{z}\right) \cdot \exp\left(-\int_{z_0}^{z} \lambda\, d\hat{z}\right), \tag{4.72}$$

respectively

$$c = c_0 \cdot [1 - H(z - q/\varepsilon \cdot t)] \cdot \exp\left(-\int_0^{z} \lambda\, d\hat{z}\right). \tag{4.73}$$

Thus, it follows that after the initial disturbance, represented by the Heaviside function, has passed through the filter, a stationary solution is reached, as expressed by the last term. This solution is similar to the one derived by Civan and Rasmussen (2005) for a constant λ. Therefore, the assumption of a time-independent solution of c is justified, as long as the initial disturbance is neglected.

Chapter 5

Filter-Aid Filtration

Based on Kuhn and Briesen (2016a), a new mechanistic model for filter-aid filtration with incompressible cakes is presented in this chapter. The model considers surface- and depth-filtration effects and leads to a moving boundary problem with sharp moving fronts. Proper mathematical and numerical methods for its solution are identified which allow fully transient simulations concerning all process variables and parameters. All relevant physical phenomena known from experimental studies are captured by the model, some of them for the first time. An analytical optimal control solution is derived for a simplified model in which only surface filtration is regarded; the control variable is the filter-aid concentration and the goal is to minimize energy consumption. Subsequently, the properties of the full model are explored in two case studies. First, the effects of changing the filter-aid particle diameter at a discrete time point are observed. Second, a continuous variation of the amount of filter aid dosed to the suspension is considered. Significant influences on the separation efficiency, the local deposit profile within the filter cake, and the overall energy consumption are found. Lastly, a numerical optimal control scenario based on the full model is shown in which again the filter-aid concentration is the control variable and the objective is to minimize energy consumption. The main outcome can be summarized as follows: As long as only surface filtration is encountered, a constant filter-aid dosage is truly optimal. When depth filtration is present, a time-variable dosage offers benefits for the energy consumption; however, the effect is so small that it is deemed insignificant.

5.1 Introduction

Filter aids are used for systems that prove hard to filter. Such systems often contain impurities that differ widely in their properties or gelatinous particles which tend to block the filter medium. In these cases, the use of filter aids assures increased filtration times and lower energy expenditure due to higher filter-cake permeabilities. This technique is applied in many areas, such as chemistry and biotechnology (Hunt, 2009), water filtration (Bhardwaj and Mirliss, 2005), and filtration of beverages (Annemüller and Manger, 2011).

There are different modes of filter-aid use. If a layer of filter aid is only added to the filter medium in the beginning of a process cycle, one speaks of precoat filtration. The filter aid

constantly dosed to the suspension is referred to as body feed and the corresponding operational mode is called body or filter-aid filtration (Sutherland and Hidi, 1966). Often, in body filtration a precoat is used as well. The remaining chapter addresses filter-aid filtration including a precoat layer, but focuses especially on the body feed.

The selection and dosage of filter aids in industrial practice is mostly based on experience. It is, however, very unlikely that the optimal operation strategy is thus found, because the process at hand is rather complex and comprises many free variables, such as filter-aid material, size distribution, and concentration. For many decades, the role of the right amount of body feed for successful filtration was emphasized (Carman, 1938, 1939; Babbitt and Baumann, 1954; Sutherland and Hidi, 1966; Haba and Koch, 1978; Heertjes and Zuideveld, 1978a,c). Some of these classical works presented simple models that relate the cake resistance to the ratio of impurity and filter-aid concentration. They assumed that separation only takes place by pure cake filtration, i.e., directly at the surface of the cake (Sutherland and Hidi, 1966; Haba and Koch, 1978). However, in the meantime, the importance of depth-filtration effects has been shown experimentally (Heertjes and Zuideveld, 1978a,b; Husemann et al., 2003; Hebmüller, 2003).

A series of PhD theses, conducted in the 1980s at TU Dresden under the supervision of Professor Heidenreich, presented and validated models of filter-aid filtration that combine surface and depth filtration (Berndt, 1981; Wegner, 1985; Blobel, 1985; Tittel, 1987). However, due to computational limitations, these models were simplified to analytical equations and can only consider scenarios with constant impurity concentrations and a constant dosage of filter aids which is clearly a disadvantage because the beneficial effects of a time-varying dosage of filter aids were shown experimentally (Coote, 1999).

A general approach for describing growing, compressible filter cakes which are also blocked on the inside is provided by Tien et al. (1997). But neither does this study focus on time-varying process conditions nor are the applied numerical methods able to handle sharp moving fronts, as they are encountered when filter-aid filtration is modeled. Therefore, a new mechanistic model that combines surface and depth filtration and allows considering fully transient conditions concerning all process variables and parameters is presented. The focus is laid on the effects of filter-aid particle diameter and volume concentration in the body feed. Mathematical and numerical methods to solve the resulting set of partial differential equations (PDEs) are identified.

Despite some evidence on the benefits of a time-variable dosage of filter aids, a constant body-feed concentration is still common industrial practice. One possibility of improving the constant body-feeding strategy by a rigorous application of optimal control theory is explored in this chapter. As shown in Section 2.3.4, optimal control has only scarcely been used in the field of filtration so far; and, to the knowledge of the author, optimal control theory has never been applied to filter-aid filtration before. Using filter-aid concentration as the control variable, the body-feeding strategy is optimized in this chapter with the goal to minimize the overall energy consumption of one filtration cycle, i.e., within a given time interval. An analytical

control solution is provided for pure surface filtration and numerical results are shown for the full model, comprising contributions of surface and depth filtration. Alternative optimal control scenarios are discussed in the outlook at the end of the chapter. For the following reasons, optimally controlling the filter-aid dosage is expected to be beneficial:

- Dosage of filter aids leads to cake growth.
- Filter cake growth increases the overall pressure drop and, therefore, the energy consumption.
- Clogging of the filter cake increases local pressure drop and, therefore, energy consumption.
- Filter-aid dosage decreases clogging of the filter cake.
- So far, an optimal trade-off between cake growth and cake clogging seems expectable.
- Additionally, when depth filtration takes place, the existing cake is continuously penetrated by impurities from the suspension. Clogging, therefore, continuously takes place not only at the cake surface but also in deeper layers of the filter cake.
- In case of occurring depth filtration, it is, therefore, likely that more body feed is to be supplied at the beginning of filtration and filter-aid concentration is to be decreased over the course of one filtration cycle.
- Thus, it is guaranteed that earlier on in the process a less clogged filter cake is created that is able to accommodate impurities later separated by depth filtration.

The reasoning is also reflected in the process causalities depicted in Figure 5.1. A fixed overall amount of filter aids is shown in the figure as a constraint on the control variable. Analogous to Chapter 4 and according to the principles discussed in Section 2.3.5, the constraint guarantees that the different scenarios are comparable; it will be further discussed when the optimal control strategy is explained.

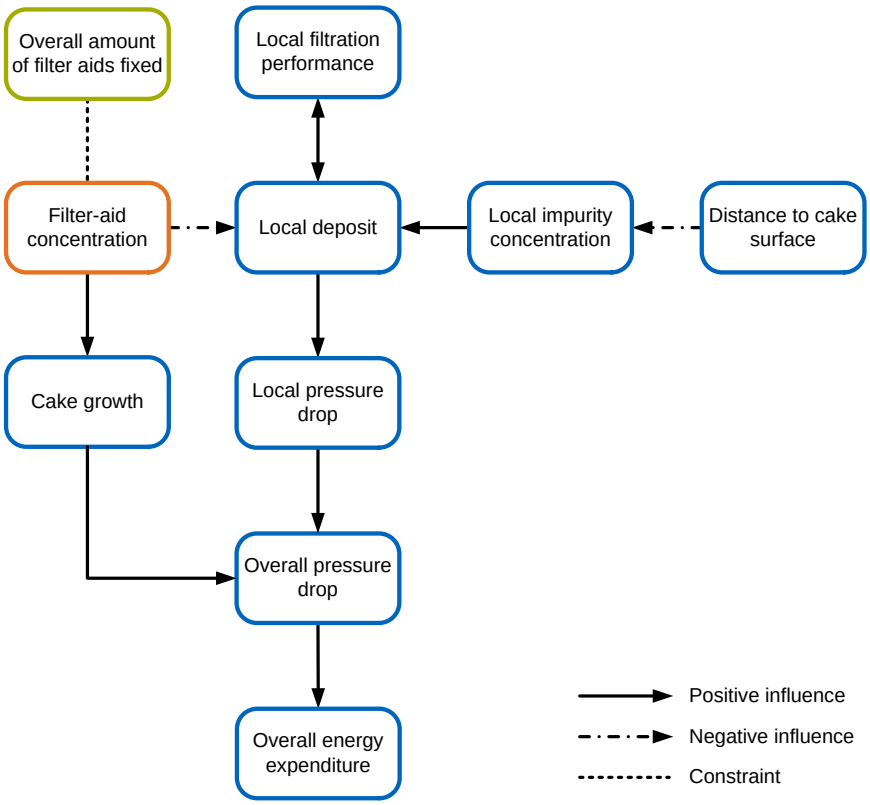

Figure 5.1: Process causalities in filter-aid filtration.

5.2 Model Derivation

Before approaching the optimal problems discussed in the introduction, the new model for filter-aid filtration is introduced. It is based on the following assumptions:

- **A1**: The filter cake is treated as incompressible.
- **A2**: All filter aids are deposited at the cake surface.
- **A3**: A constant share of impurities is deposited at the cake surface, but does not contribute to cake growth.
- **A4**: The rest of the impurities passes on to deeper cake layers and is subject to depth filtration.
- **A5**: Sedimentation is not taken into account.
- **A6**: The filter medium is neglected.

A1 is a safe assumption for all traditionally used filter aids, such as kieselguhr or perlite, and also holds true for alternative ones, such as cellulose, at moderate pressures. **A2** implies that the filter aids do not contain fine enough particles able to penetrate the already existing filter

cake. **A3** is commonly assumed in filter-aid filtration (Tittel, 1987; Hebmüller, 2003). Ideally, impurity particles are properly embedded within the porous filter-aid layer and do, therefore, not contribute to cake growth. If they do, this usually leads to unpredictably compressible cakes and means that too little filter aid was added. **A3** and **A4** can be interpreted in terms of the impurity particle sizes. Larger impurity particles are completely deposited at the surface; smaller particles penetrate the cake and are separated to a certain degree by depth filtration. **A5** is reasonable because in filtration practice the suspension's velocity is high enough for sedimentation not to take place (Annemüller and Manger, 2011, p. 222). **A6** is also a standard assumption (Heertjes and Zuideveld, 1978a) which is not essential here but simply reduces the number of model parameters. Further, in the following only constant rate filtration is addressed because this is the most common mode in industrial practice. However, mathematically, the model readily allows for a time-variable flow rate. From **A2** and **A3** follows that only filter aid contributes to cake growth. Thus, the velocity of the cake surface can be derived by a mass balance directly at the suspension-cake boundary, leading to

$$\frac{dL}{dt} = -\frac{c_{\mathrm{FA}}}{\varepsilon_s} \cdot q\,, \tag{5.1}$$

assuming that $c_{\mathrm{FA}} \ll \varepsilon_s$, compare Section 2.2.3. L is the cake height, t the time, q the superficial velocity of the liquid, c_{FA} the volume concentration of filter aids in the liquid phase, and ε_s the solidosity of the resulting, unclogged cake. Solidosity is defined as volume solid per total volume. As explained in Section 2.2.3, ε_s is the complement to porosity; nevertheless, both are used to keep the nomenclature in agreement with literature. The minus sign in Eq. (5.1) is due to the fact that q and dL/dt have opposing directions, compare Figure 5.2 below.

Analogous to Chapter 4, depth filtration is modeled by a mass balance along the flow direction within the cake and a corresponding constitutive equation characterizing the separation, thus defining the sink term in the balance equation. The mass balance is given as

$$\varepsilon \cdot \frac{\partial c}{\partial t} + q \cdot \frac{\partial c}{\partial z} = -\frac{\partial \sigma}{\partial t}\,. \tag{5.2}$$

The constitutive equation for the separation is

$$\frac{\partial \sigma}{\partial t} = -\lambda \cdot q \cdot c\,; \tag{5.3}$$

σ is the specific deposit, i.e., the volume of deposited matter per unit filter volume, z is the spatial coordinate, and λ is the filter coefficient. Note that the minus sign on the right-hand side of Eq. (5.3) arises from the fact that the flow direction here is opposed to the positive spatial coordinate direction; this is contrary to most depth-filtration models and, therefore, also to the model presented in Chapter 4. A schematic of the problem setup including the coordinate system and important variables is given in Figure 5.2.

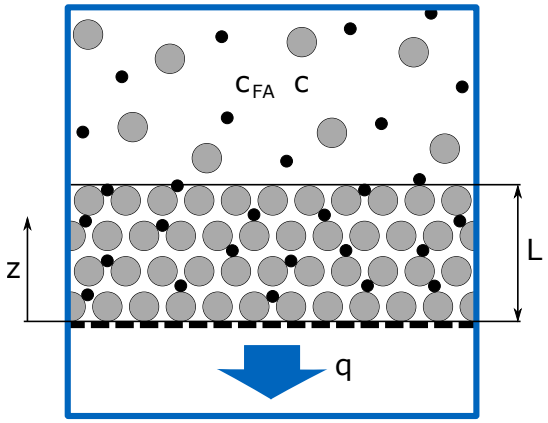

Figure 5.2: Model sketch for filter-aid filtration; gray circles symbolize filter-aid particles, black circles stand for impurities.

The sink model goes back to Iwasaki (1937) and is by now well established for a broad variety of applications. A rigorous derivation of the depth filtration model can be found, e.g., in Civan and Rasmussen (2005); compare also Sections 2.1.2 and 2.2.3 for a derivation of the transport equation and further explanations on the separation model. In the mass balance of Eq. (5.2), the first term is often neglected in filtration research, because it is claimed that it only contributes significantly at the beginning of the filtration process (Herzig et al., 1970; Zamani and Maini, 2009). Here, however, the full equations need to be used as the depth filtration within an unloaded, newly formed filter layer is always present due to the constantly growing cake. The local drop pressure dp/dz within the filter cake is modeled by Darcy's law:

$$\frac{dp}{dz} = -\frac{\mu \cdot q}{k}; \tag{5.4}$$

μ is the dynamic viscosity of the fluid and k the permeability of the solid phase. Energy consumption is expressed as energy per filter area e and is given as

$$e = -\int q \cdot \Delta p \, dt \,. \tag{5.5}$$

The overall pressure difference Δp follows from an integration of Darcy's law. Note that q and Δp always have opposing directions, i.e., in a 1D formulation one of them is negative. Therefore, the minus sign in Eq. (5.5) always leads to positive values of e.

Additionally to the basic relationships of the last equations, some additional constitutive equations are needed for a closed problem description. Depth-filtration performance, expressed by the filter coefficient λ, depends on the diameter of the particles composing the packed bed, which here is the filter-aid diameter d_{FA}. This relationship can be generalized to

$$\lambda_0 = a_{51} \cdot d_{\mathrm{FA}}^{b_{51}} \,, \tag{5.6}$$

where λ_0 denotes the filter coefficient of the unclogged bed. Parameter a_{51} summarizes other influences such as the fluid's viscosity and flow velocity, which are not the focus of attention in

this work. The model parameter b_{51} has negative values, meaning that the separation improves with smaller filter-aid particles (Herzig et al., 1970). Usually, Eqs. (5.2) and (5.3) cannot be reduced to one equation because λ is also a function of σ in the following way (Tien and Ramarao, 2007; Zamani and Maini, 2009):

$$\lambda = F_{\mathrm{FA}}(\sigma, \mathbf{P}) \cdot \lambda_0 \,; \tag{5.7}$$

F_{FA} contains constitutive relationships (Tien and Ramarao, 2007; Zamani and Maini, 2009) of which the following is used here:

$$F_{\mathrm{FA}} = 1 + a_{52} \cdot \sigma \,, \tag{5.8}$$

implying that the separation improves as the filter cake gets clogged, because the parameter a_{52} has positive values. Eq. (5.8) can be interpreted in terms of the capture probability of impurity particles. This probability increases as the pores get smaller due to deposited impurities. Therefore, deposit also reduces the overall cake porosity, which is modeled as

$$\varepsilon = \varepsilon_0 - a_{53} \cdot \sigma \,, \tag{5.9}$$

with ε_0 being the porosity of the unclogged cake and a_{53} a parameter describing the internal porosity of the deposited material (Herzig et al., 1970; Tien and Ramarao, 2007; Zamani and Maini, 2009). The permeability in the unclogged cake k_0 is described by a Kozeny-Carman-type equation (Kozeny, 1927; Carman, 1997):

$$k_0 = a_{54} \cdot d_{\mathrm{FA}}^{b_{52}} \,. \tag{5.10}$$

The influences of porosity, tortuosity, and shape of the pores of the full Kozeny-Carman model as introduced in Section 2.2.3 are summarized here in the parameter a_{54}. This is justified because only the effects of particle size and clogging on the overall pressure drop are studied. Eq. (5.10) shows that smaller particles lead to higher pressure drops and *vice versa*. Because real filter aids do not consist of monodisperse spherical particles, d_{FA} is interpreted as a representative particle diameter.

To account for the change in pressure drop due to clogging by directly modeling the influence on structural filter cake parameters, such as porosity and tortuosity, was shown to be generally not reliable. Instead, a number of constitutive relationships were proposed in literature (Herzig et al., 1970; Tien and Ramarao, 2007; Zamani and Maini, 2009). Here, the Sutherland equation, as introduced and explained in Section 2.2.3, is used because it is widely applied and validated in filter-aid filtration; it reads

$$k = k_0 \cdot \exp\left(-a_{55} \cdot \sigma\right) \,, \tag{5.11}$$

and includes the model parameter a_{55}. As a_{55} has positive values, deposit σ decreases the permeability compared to the unclogged cake. Note that this form of the Sutherland equation

differs from the one introduced in Section 2.2.3, namely that Eq. (5.11) contains only σ in the exponent whereas Eq. (2.47) was formulated in terms of the c/c_{FA} ratio. The difference is due to the fact that Eq. (2.47) holds true as long as only surface filtration is considered; the relation between both formulations is further explained in Appendix 5.1.

Thus, the overall model derived in this chapter comprises many submodels which reflect the current state of the art. Although, these submodels were all separately validated in the literature, a model for the dynamic behavior of the fully coupled problem has been lacking so far. On the one hand, the new coupled model appears to yield particular numerical challenges, but, on the other hand, it allows for a mechanistic explanation of previously unexplained experimental observations. Before analyzing the full model, a simplified model is used in the next section to derive an analytical optimal control solution. This analytical solution will be used to shed more light on the numerical model and optimal control results presented subsequently.

5.3 Analytical Optimal Control Solution for Simplified Model

Based on the assumption that depth filtration is negligible and separation of solids, therefore, occurs by pure surface filtration, an analytical optimal control solution is derived in this section; it is referred to as Scenario FA-A. These considerations build on the work of Heertjes and Zuideveld (1978c). In their study, an optimal body-feed concentration c_{FA} was derived; however, it was assumed that the impurity concentration c as well as the filter-aid concentration c_{FA} are constant over time. At first glance, it may be surprising that there is an optimal body-feed concentration at all because the Sutherland equation, Eq. (2.46), appears to suggest that with respect to cake resistance it is desirable to add as much filter aid as possible. But there are two mechanisms at work at the same time: On the one hand, a higher body-feed concentration leads to a lower local cake resistance; on the other hand, an increased body-feed concentration leads to a more pronounced cake growth, as seen from Eq. (5.1). The found optimum is the trade-off between these two effects.

Contrary to the study by Heertjes and Zuideveld (1978c), here both c and c_{FA} are understood as functions of time. The results of this section are, thus, generalizations of their findings. The derivation below is modified from Kuhn and Briesen (2015). Goal of the optimal control approach is to minimize energy consumption, filter-aid concentration c_{FA} is the control variable.

The system state is described by the total cake resistance R according to

$$R = \int_0^{t_e} \left(\frac{dL}{dt} \cdot r \right) dt = \int_0^{t_e} \left(-\frac{c_{\mathrm{FA}}}{\varepsilon_s} \cdot q \cdot r \right) dt \,. \tag{5.12}$$

dL/dt follows from Eq. (5.1); r is the specific cake resistance which is modeled by the resistance-form of the Sutherland equation according to

$$r = r_0 \cdot \exp\left(a'_{55} \cdot \frac{c}{c_{\mathrm{FA}}} \right) . \tag{5.13}$$

Eq. (5.13) shows that the resistance r decreases at a constant level of impurities c when the amount of filter aids c_{FA} dosed to the suspension is increased. As already mentioned, the different variants of the Sutherland equation, i.e., formulations that account only for surface filtration as opposed to versions that can also consider depth filtration effects are explained in detail in Appendix 5.1. For now, it is only important to note that Eq. (5.13) is valid under the assumption of pure surface filtration, i.e., exactly the simplified scenario studied in this section. Time derivation of Eq. (5.12) yields

$$\frac{dR}{dt} = \frac{dL}{dt} \cdot r = -\frac{c_{\mathrm{FA}}}{\varepsilon_s} \cdot q \cdot r \,. \tag{5.14}$$

The corresponding initial condition is $R(0) = 0$, i.e., initially, the cake has no resistance. Note that this implies that the resistance of the filter medium is neglected, as already discussed at the beginning of Section 5.2. Furthermore, the precoat layer is not taken into account because its effect on the overall resistance is relatively small and it contributes nothing to the optimal control problem that is addressed here. Energy per filter area e is used as the performance index:

$$J_{\text{FA-A}} = e = -\int_0^{t_e} q \cdot \Delta p \, dt \,. \tag{5.15}$$

Using Darcy's law in it resistance form (Blankert et al., 2006)

$$q = -\frac{\Delta p}{\mu \cdot R} \tag{5.16}$$

to substitute Δp, one gets

$$e = q^2 \cdot \mu \cdot \int_0^{t_e} R \, dt \,. \tag{5.17}$$

Due to the form of e, this problem can be classified as being of the Lagrangian type with a fixed final time t_e and a free final state $R(t_e)$, according to the optimal control framework presented in Section 2.3. The corresponding Hamiltonian reads as follows:

$$H = q^2 \cdot \mu \cdot R - \psi \cdot \frac{c_{\mathrm{FA}}}{\varepsilon_s} \cdot q \cdot r_0 \cdot \exp\left(a'_{55} \cdot \frac{c}{c_{\mathrm{FA}}}\right) ; \tag{5.18}$$

ψ is the costate. The three necessary conditions for an extremal solution, as introduced in Section 2.3, when formulated with the present variables are the state equation

$$\frac{dR}{dt} = \frac{\partial H}{\partial \psi} , \tag{5.19}$$

the control condition

$$\frac{\partial H}{\partial c_{\mathrm{FA}}} = 0 , \tag{5.20}$$

and the costate equation

$$\frac{d\psi}{dt} = -\frac{\partial H}{\partial R} . \tag{5.21}$$

Furthermore, it is required that

$$\psi(t_e) = 0\,. \tag{5.22}$$

It can be easily checked that the first of the conditions above is naturally fulfilled. The control condition leads to

$$\psi \cdot \left(\frac{a'_{55} \cdot c}{c_{\mathrm{FA}}} - 1 \right) \cdot r_0 \cdot \exp\left(a'_{55} \cdot \frac{c}{c_{\mathrm{FA}}} \right) = 0\,. \tag{5.23}$$

An evaluation of the third condition, i.e., the costate equation, shows that

$$\frac{d\psi}{dt} = q^2 \cdot \mu\,. \tag{5.24}$$

As the term $q^2 \cdot \mu$ is constant, separation of variables and integration yields

$$\psi = q^2 \cdot \mu \cdot t + a\,, \tag{5.25}$$

with the integration constant a. Thus, ψ follows a linear profile which is non-zero except at the final time t_e, as follows from Eq. (5.22). Turning back to Eq. (5.23), only the second term on the left-hand side can guarantee that the equation yields zero over the whole time span. Thus, it must hold that at each time t

$$\left(\frac{a'_{55} \cdot c}{c_{\mathrm{FA}}} - 1 \right) = 0\,, \tag{5.26}$$

and, therefore,

$$c_{\mathrm{FA}} = a'_{55} \cdot c\,. \tag{5.27}$$

That Eq. (5.27) is the best and not the worst extremum is shown in Kuhn and Briesen (2015) by a comparison to other constructed trajectories which are found to perform worse. In that same publication, the identical result was arrived at by way of a different derivation. Interestingly, also Heertjes and Zuideveld (1978c) obtained the result of Eq. (5.27), only under the restrictions that c and c_{FA} are no functions of time.

To summarize the main findings of this section again: Allowing c, c_{FA}, and, therefore, also r to be functions of time, energy consumption of filter-aid filtration based purely on surface filtration is minimal if impurity concentration c and filter-aid concentration c_{FA} follow Eq. (5.27) at each point in time. Thus, in case of a constant impurity concentration, a constant dosage of filter aids is optimal.

According to the nomenclature of Section 2.3.5, the obtained solution is trivial in that a constant control is optimal for the simplified model. As can be seen from Eq. (5.14), the system state R is not coupled to states at other times, i.e., R does not appear at the right-hand side of the differential equation. For that reason, a trivial solution could have been expected according to the considerations of Section 2.3.5; see especially 1, a). However, as also discussed there, one

has to be aware of hindsight bias when judging optimal control results. Before a close analysis of the problem, the obtained solution, most likely, would have been impossible to predict.

5.4 Nondimensionalization, Parameter Values, and Initialization

After the analysis of the simplified model in the last section, the full model equations as introduced in Section 5.2 are considered again. Similar to Chapter 4, all basic considerations, including the derivations in the appendices of this chapter, rely on the dimensional equations to ease comparison with literature. All numerical solutions, on the contrary, are based on the nondimensionalized equations of the full model, as this yields a good problem scaling. Furthermore, the nondimensional variables aid interpretation of the results and additionally reduce the number of model parameters. The following nondimensional variables are introduced:

$$\tilde{c}_{\mathrm{FA}} = \frac{c_{\mathrm{FA}}}{\varepsilon_s} \tag{5.28}$$

$$\tilde{c} = \frac{c}{c_0} \tag{5.29}$$

$$\tilde{\sigma} = \frac{\sigma}{c_0} \tag{5.30}$$

$$\tilde{d}_{\mathrm{FA}} = \frac{d_{\mathrm{FA}}}{d_{\mathrm{FA,PC}}} \tag{5.31}$$

$$\tilde{\lambda} = \lambda \cdot L_0 \tag{5.32}$$

$$\tilde{L} = \frac{L}{L_0} \tag{5.33}$$

$$\tilde{z} = \frac{z}{L_0} \tag{5.34}$$

$$\tilde{t} = \frac{t \cdot |q|}{L_0} \tag{5.35}$$

$$\tilde{p} = \frac{p \cdot L_0}{\mu \cdot |q|} \tag{5.36}$$

$$\tilde{k} = \frac{k}{L_0^2} \tag{5.37}$$

$$\tilde{e} = \frac{e}{\mu \cdot |q|}\,. \tag{5.38}$$

Correspondingly, the nondimensional model parameters are:

$$\tilde{a}_{51} = a_{51} \cdot L_0 \cdot (d_{\mathrm{FA,PC}})^{b_{51}} \tag{5.39}$$

$$\tilde{a}_{52} = a_{52} \cdot c_0 \tag{5.40}$$

$$\tilde{a}_{53} = a_{53} \cdot c_0 \tag{5.41}$$

$$\tilde{a}_{54} = \frac{a_{54}}{L_0^{(b_{52}-2)}} \tag{5.42}$$

$$\tilde{a}_{55} = a_{55} \cdot c_0 \tag{5.43}$$

$$\tilde{b}_{51} = b_{41} \tag{5.44}$$

$$\tilde{b}_{52} = b_{42}\,; \tag{5.45}$$

these relationships can be easily checked using Eqs. (5.60) to (5.65) below. L_0 is the height of the precoat layer. $|q|$ is used here for nondimensionalization, because in the case study of this chapter, contrary to Chapter 4, superficial velocity q is negative due to the chosen coordinate system as depicted in Figure 5.2. $d_{\mathrm{FA,PC}}$ is the diameter of filter-aid particles in the precoat layer. In nondimensional form, cake growth velocity is formulated as

$$\frac{d\tilde{L}}{d\tilde{t}} = -\tilde{c}_{\mathrm{FA}} \cdot \mathrm{sgn}(q)\,. \tag{5.46}$$

Note that the signum function $\mathrm{sgn}(q)$ arises due to the chosen nondimensional variables, because it holds that $q/|q| = \mathrm{sgn}(q)$. q is always negative in this chapter, i.e., $\mathrm{sgn}(q) = -1$. If the remaining system equations are treated by the front-fixing method, as explained in Section 3.1.3, and nondimensionalized, the resulting relationships are

$$\varepsilon \frac{\partial \tilde{c}}{\partial \tilde{t}} + \frac{\partial \tilde{\sigma}}{\partial \tilde{t}} = \left(\varepsilon \frac{\eta}{\tilde{L}} \frac{d\tilde{L}}{d\tilde{t}} \frac{\partial \tilde{c}}{\partial \eta} - \frac{\mathrm{sgn}(q)}{\tilde{L}} \right) \frac{\partial \tilde{c}}{\partial \eta} + \left(\frac{\eta}{\tilde{L}} \frac{d\tilde{L}}{d\tilde{t}} \right) \frac{\partial \tilde{\sigma}}{\partial \eta} \tag{5.47}$$

$$\frac{\partial \tilde{\sigma}}{\partial \tilde{t}} = \left(\frac{\eta}{\tilde{L}} \frac{d\tilde{L}}{d\tilde{t}} \right) \frac{\partial \tilde{\sigma}}{\partial \eta} - \mathrm{sgn}(q) \tilde{\lambda} \tilde{c} \tag{5.48}$$

$$\frac{\partial \tilde{d}_{\mathrm{FA}}}{\partial \tilde{t}} = \left(\frac{\eta}{\tilde{L}} \frac{d\tilde{L}}{d\tilde{t}} \right) \frac{\partial \tilde{d}_{\mathrm{FA}}}{\partial \eta} \tag{5.49}$$

$$\frac{d\tilde{p}}{d\tilde{z}} = -\frac{\mathrm{sgn}(q)}{\tilde{k}}\,. \tag{5.50}$$

More details on applying the front-fixing method are provided in Appendix 5.2. In particular, the origin of the new Eq. (5.49) is explained in this appendix. Next, the initial conditions are introduced. At the beginning, the cake height is equal to the precoat layer height L_0 which yields

$$\tilde{L}(0) = 1 \tag{5.51}$$

in nondimensional form. Neglecting, as usual, the first flooding of the cake, it holds that

$$\tilde{c}(0,\eta) = (1 - \tilde{c}_{\Delta}) \cdot \exp\left[-\tilde{\lambda}_0 \cdot \tilde{L}_0 \cdot (1-\eta) \right], \tag{5.52}$$

i.e., the impurity concentration is initialized with the stationary solution. $\tilde{c}_{\Delta}$ is the concentration of impurities which is completely deposited at the cake surface (compare assumption **A3**). At the beginning of filtration, the cake is unclogged, i.e.,

$$\tilde{\sigma}(0,\eta) = 0\,. \tag{5.53}$$

As initially only the precoat layer is given, $\tilde{d}_{\mathrm{FA}}$ is expressed as

$$\tilde{d}_{\mathrm{FA}}(0,\eta) = 1\,. \tag{5.54}$$

The boundary conditions are

$$\tilde{c}(\tilde{t},1) = (1-\tilde{c}_\Delta) \tag{5.55}$$

$$\tilde{\sigma}(\tilde{t},1) = \frac{\tilde{c}_\Delta}{\tilde{c}_{\mathrm{FA}}} \tag{5.56}$$

$$\tilde{d}_{\mathrm{FA}}(\tilde{t},1) = \tilde{d}_{\mathrm{FA}}(1,\tilde{t})\,. \tag{5.57}$$

When $\tilde{c}_\Delta = 1$, i.e., $c_\Delta = c_0$, the resulting process is completely governed by surface filtration as can be seen from Eqs. (5.52), (5.55), and (5.56); this was assumed when deriving the analytical optimal control solution in Section 5.3. Eq. (5.56) results from a mass balance at the cake surface and is derived in Appendix 5.3. As seen from Eq. (5.56), the cake surface clogs more with higher cake solidosities ε_s, higher impurity concentrations separated at the surface $\tilde{c}_\Delta$, and lower filter-aid concentrations in the suspension $\tilde{c}_{\mathrm{FA}}$.

Total, nondimensional pressure drop is obtained from an integration of Eq. (5.50) as

$$\Delta\tilde{p} = -\int_0^{\tilde{L}} \frac{\mathrm{sgn}(q)}{\tilde{k}}\, d\tilde{z}. \tag{5.58}$$

As in Chapter 4, no boundary condition was provided for $\tilde{p}$, because none is needed as only the differential pressure $\Delta\tilde{p}$ is evaluated by the definite integral of Eq. (5.58). Using $\Delta\tilde{p}$ and Eq. (5.5) in its nondimentional form, specific energy consumption is obtained from

$$\tilde{e} = -\mathrm{sgn}(q)\int_0^{\tilde{t}_e} \Delta\tilde{p}\, d\tilde{t}\,. \tag{5.59}$$

Due to the fact that q is always negative, $\Delta\tilde{p}$ is, therefore, positive, and $\tilde{e}$ is positive as well. The constitutive relationships in nondimensional form read:

$$\tilde{\lambda}_0 = \tilde{a}_{51}\cdot \tilde{d}_{\mathrm{FA}}^{\tilde{b}_{51}} \tag{5.60}$$

$$\tilde{\lambda} = \tilde{\lambda}_0 \cdot \tilde{F}_{\mathrm{FA}} \tag{5.61}$$

$$\tilde{F}_{\mathrm{FA}} = 1 + \tilde{a}_{52}\cdot\tilde{\sigma} \tag{5.62}$$

$$\varepsilon = \varepsilon_0 - \tilde{a}_{53}\cdot\tilde{\sigma} \tag{5.63}$$

$$\tilde{k}_0 = \tilde{a}_{54}\cdot\tilde{\lambda}^{\tilde{b}_{52}} \tag{5.64}$$

$$\tilde{k} = \tilde{k}_0 \cdot \exp\left(-\tilde{a}_{55}\cdot\tilde{\sigma}\right). \tag{5.65}$$

All model parameters, expressed nondimensionally, are summarized in Table 5.1. $\tilde{c}_\Delta = c_\Delta/c_0 = 0.5$, as shown in the table, means that half of the impurity concentration in the suspension is separated by surface filtration.

Table 5.1: Model parameters for filter-aid filtration.

Parameter	ε_0	$\tilde{c}_\Delta$	$\tilde{a}_{51}$	$\tilde{a}_{52}$	$\tilde{a}_{53}$	$\tilde{a}_{54}$	$\tilde{a}_{55}$	$\tilde{b}_{51}$	$\tilde{b}_{52}$
Value	0.50	0.50	1.0	0.005	0.005	1.0	0.015	-2.0	2.0

Note that ε_s is not shown separately in Table 5.1, because it is simply defined as $\varepsilon_s = 1 - \varepsilon$, as explained in Section 2.2.3. For the numerical computations of Section 5.6, a filter-aid concentration $\tilde{c}_{\mathrm{FA}}$ of 0.006 is used; this value is not shown in Table 5.1 because it is not a fixed parameter but will be changed for the optimization and optimal control approaches presented in Section 5.7.

5.5 Numerical Methods and Solver Settings

Numerically, the above equations, including their initial and boundary conditions, are solved by the method of lines using a van-Leer flux limiter scheme with 100 spatial discretization points. For a discussion of the numerical methods, the reader is referred to Chapter 3, especially Sections 3.1.1 and 3.1.2.

As described in Section 3.2.2, optimal control is approximated numerically by a direct single shooting method. The resulting optimization problem is solved by MATLAB's `fmincon` solver using the default interior-point algorithm and specifying constraint tolerance (`TolCon`), termination tolerance for function values (`TolFun`), and termination tolerance for parameter values all as 10^{-7}. Tolerances were relaxed compared to the values reported in Chapter 4 to reduce the computational time; it was assured that the chosen tolerance values do not affect the results significantly.

5.6 Numerical Model Results

To understand the basic properties of the model, a simulation with a constant dosage of filter aids and a constant filter-aid particle diameter is shown first. This setting will be further on used for comparison and is referred to as Scenario FA-0. Figure 5.3 shows the impurity concentration in the suspension while passing through the growing cake at three different times. The step of 0.5 in $\tilde{c}$ is the constant fraction which is separated at the cake surface, i.e., $\tilde{c}_\Delta$, and therefore also marks the current cake height $\tilde{L}$. It can be seen that the filtration quality improves with time, i.e., the outlet concentration at $\tilde{z} = 0$ decreases, due to the growing filter cake and the thus increased cake volume available for depth filtration. This agrees exactly with measurement data (Blobel, 1985; Tittel, 1987; Hackl et al., 1993).

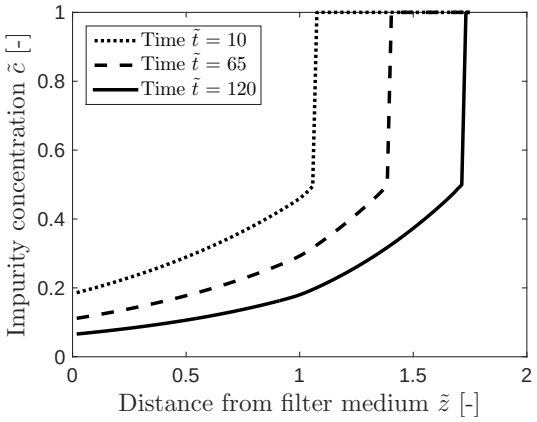

Figure 5.3: Impurity concentration within the filter cake at three different times for the reference Scenario FA-0.

Specific deposit within the filter cake at three different times is shown in Figure 5.4. The offset in specific deposit of about 85 units, present from the precoat layer height at $\tilde{z} = 1$ to the final value of $\tilde{z} = \tilde{L}$, can be attributed to surface filtration. It is nonexistent in the precoat cake, because from the beginning matter is separated only by depth filtration for $\tilde{z} < 1$. This offset, together with the fact that in depth filtration most matter is accumulated at the filter inlet (Bai and Tien, 2000; Burganos et al., 2001), leads to a pronounced peak in local deposit at the boundary from the precoat cake to the body-feed cake ($\tilde{z} = 1$). The same behavior was measured by Heertjes and Zuideveld (1978a) and is also observed in Annemüller and Manger (2011) as well as Hebmüller (2003). It is mechanistically modeled here for the first time. Figure 5.4 shows, furthermore, that deposit within the precoat layer ($\tilde{z} < 1$) decreases towards the filter medium whereas the curve inclines in the opposite direction within the filter-aid layer, i.e., for $\tilde{z} > 1$, because in the precoat cake the usual deposition profile due to depth filtration, as also encountered in Chapter 4, is still retained. In the body-feed cake, on the contrary, less material is deposited in newer cake layers because newer layers of filter aid have less time to accumulate impurities separated by depth filtration.

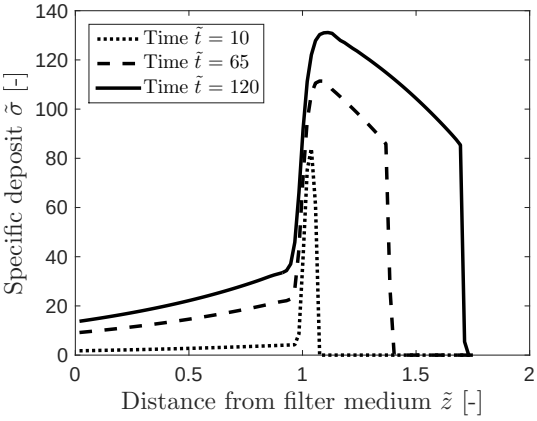

Figure 5.4: Specific deposit within the filter cake at three different times for the reference Scenario FA-0.

Next, two case studies are discussed to illustrate the model's transient capabilities and to better understand the physical mechanisms at work. Further, both scenarios also serve the purpose of exploring advanced process control scenarios that will be discussed later. In Scenario FA-1, the filter-aid particle diameter $\tilde{d}_{\mathrm{FA}}$ is abruptly increased by 50% at $\tilde{t} = 65$ compared to its initial value. This time point corresponds to $\tilde{z} = 1.4$, meaning that the cake had a height of $\tilde{L} = 1.4$ when the particle diameter was changed. The scenario shows that the numerical strategy can handle sharp changes in model variables without instabilities. Also concerning process control in filtration practice, it is more realistic to switch particle diameter discretely instead of continuously varying it. The physical motivation is: If depth filtration contributes ever more strongly to the overall separation (as seen in Scenario FA-0), it makes sense to switch at some point to a larger filter-aid particle size, as long as the desired surface filtration, described by $\tilde{c}_{\Delta}$, is still guaranteed. The larger particles increase the permeability in the newly grown cake, as seen from Eq. (5.10), which in turn reduces energy consumption. Figure 5.5a shows a smaller slope in $\tilde{c}$ for values of $\tilde{z} > 1.4$, i.e., from the point onwards where the changed filter aid was used, which can be attributed to the reduced separation efficiency of the larger particles, as modeled by Eq. (5.6). However, it can be seen that the outlet concentration does not increase significantly due to the stronger clogging of the filter cake for $\tilde{z} < 1.4$ and the thus increased filter coefficient, as described by Eq. (5.8). Note that cake growth according to Eq. (5.1) is not affected because, for reasons of simplicity, the filter-aid concentration remained unchanged while it was assumed that the larger particles form a cake of the same packing density as the smaller ones.

In Figure 5.5b, it can be seen that increasing the filter-aid particle diameter leads to less deposition in the top filter layers. Instead, a more pronounced deposit peak around the precoat layer height at $\tilde{z} = 1$ is found compared to Scenario FA-0, because the top cake layers capture a lower share of impurities in Scenario FA-1 and, therefore, more is deposited in the lower layers.

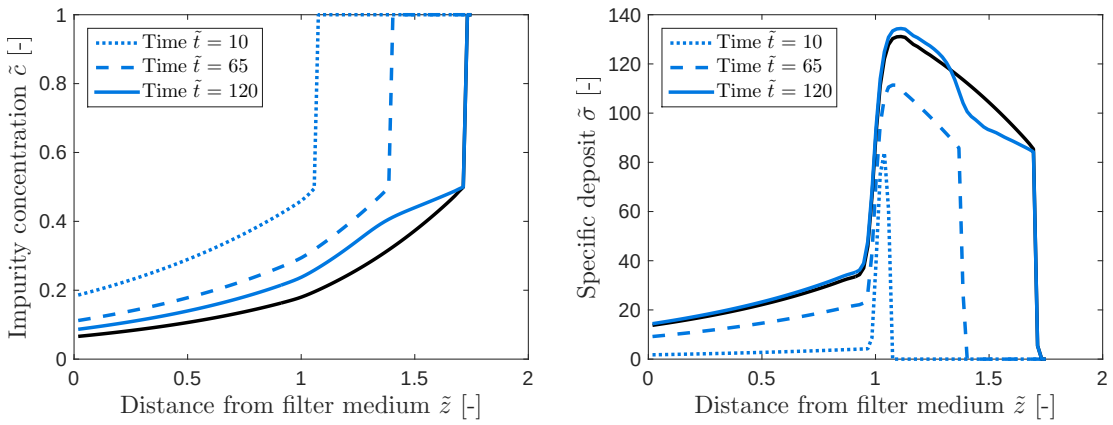

(a) (b)

Figure 5.5: Impurity concentration (a) and specific deposit (b) within the filter cake at three different times for Scenario FA-1 in which the filter-aid particle diameter was increased by 50 % at $\tilde{t} = 65$. A comparison to Scenario FA-0 is shown at $\tilde{t} = 120$ (black line).

In Scenario FA-2, the amount of body feed is linearly decreased in the time span $\tilde{t} = [0\ 125]$. The corresponding profile is depicted in Figure 5.6. Note that the mean value of c_{FA} is 0.006, i.e., the same value that was previously used as a constant; therefore, the overall amount of filter aids stayed the same.

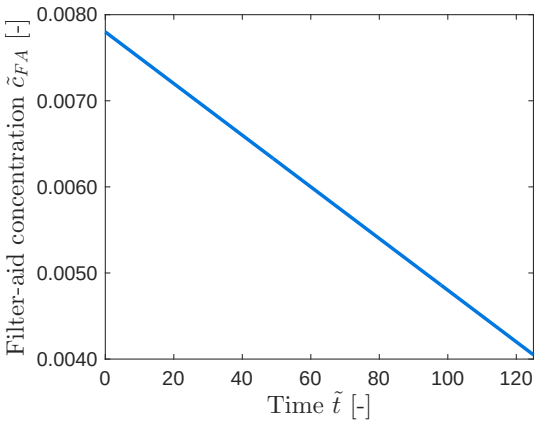

Figure 5.6: Profile of body-feed concentration $\tilde{c}_{\mathrm{FA}}$ as used in Scenario FA-2.

Scenario FA-2 illustrates the physical effects of changing the filter-aid concentration over time. It is already a step in the direction of the numerical optimal control approach presented below in Section 5.7. A justification for varying $\tilde{c}_{\mathrm{FA}}$ was also given in the bullet-point list at the end of Section 5.1. Figure 5.7a shows the effect of a varied filter-aid dosage on impurity concentration within the cake. The nonuniform cake growth is reflected by the fact that the filter cake grew more from $\tilde{t} = 10$ to $\tilde{t} = 65$ than from $\tilde{t} = 65$ to $\tilde{t} = 120$. The concentration profile at $\tilde{t} = 120$, however, is nearly identical to those of Scenario FA-0 which can be attributed to the fact the same amount of filter aids is used in both scenarios.

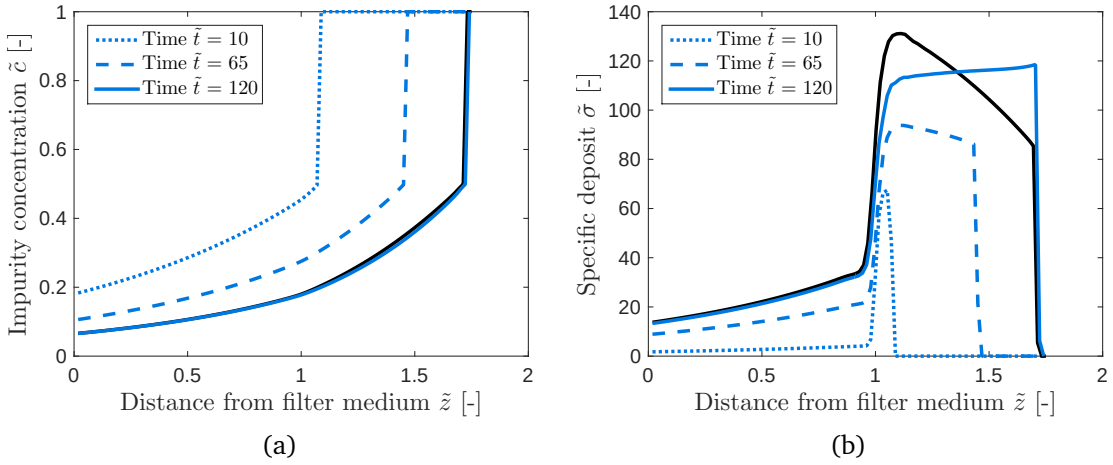

(a) (b)

Figure 5.7: Impurity concentration (a) and specific deposit (b) within the filter cake at three different times for Scenario FA-2 in which the filter-aid concentration c_{FA} was linearly decreased. A comparison to Scenario FA-0 is shown at $\tilde{t} = 120$ (black line).

The effect of the decreased dosage on the deposit profile within the filter cake is also shown in Figure 5.7b. Whereas varying $\tilde{c}_{\mathrm{FA}}$ had only a small influence on the impurity concentration in the cake, the effect on the deposit profile is significant. The higher body-feed concentration in the beginning leads to a less pronounced clogging of the cake surface, as described by Eq. (5.56), and, therefore, to a decreasing step on the right-hand side of the deposit curves for small values of $\tilde{t}$; as $\tilde{c}_{\mathrm{FA}}$ is decreased over time, surface clogging increases. Note again that despite the sharp moving fronts in various variables, smooth solutions could be achieved for all analyzed cases with the selected numerical methods.

A comparison of all three scenarios by looking at global performance values is given in Figures 5.8 and 5.9. The first plot shows the scaled impurity concentration at the filter outlet. Increasing the filter-aid particle diameter in Scenario FA-1 leads, as already discussed, to a lower separation efficiency and, therefore, a higher outlet concentration. Scenarios FA-0 and FA-1 are identical up to the point where the filter-aid diameter is increased (indicated by the arrow in the figure); after that point, Scenario FA-1 shows a smaller slope of the impurity concentration due to the reduced separation efficiency of the larger particles, as modeled by Eq. (5.6). Scenario FA-2 diverges from Scenario FA-0 over time but ends at the same point at $\tilde{t} = 125$ because the same amount of filter aid is used in both scenarios.

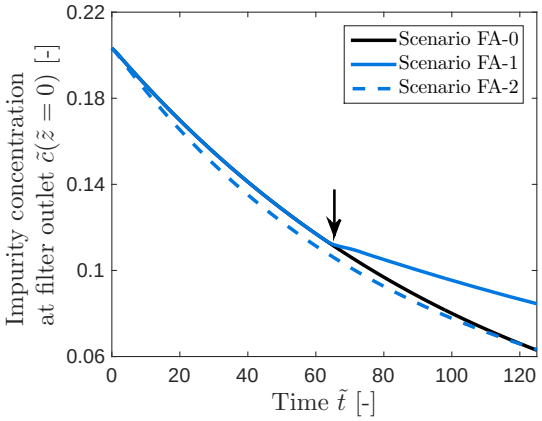

Figure 5.8: Development of the impurity concentration at the filter outlet for the Scenarios FA-0, FA-1, and FA-2. The arrow indicates the point where in Scenario FA-1 the filter-aid particle diameter was increased by 50 %.

In Figure 5.9, the scenarios are compared with respect to the total differential pressure across the filter. As in Scenario FA-0, also experimental studies found non-linear differential pressure curves for cases of incompressible filter-aid filtration with a constant dosage (Heertjes and Zuideveld, 1978a; Kain, 2004). This shows that depth filtration cannot be neglected and also indicates a nonlinear clogging behavior which further warrants the use of Sutherland's model, as shown in Eq. (5.11). In Scenario FA-1, the slope of the differential pressure becomes smaller from the point onwards where the coarser filter aids were used (indicated by the arrow), as was to be expected from Eq. (5.10). In general, pressure drop increases due to two competitive factors: cake growth and clogging of the cake, i.e., higher cake growth rates lead to lower cake clogging and *vice versa*. In Scenario FA-2, a case is presented where the influence

of cake clogging steadily increases due to the decreasing amount of filter aids used, as shown in Figure 5.6. Therefore, one can observe first a lower increase in pressure drop and subsequently and higher $\Delta\tilde{p}$ gradient compared to Scenario FA-0. However, it must be mentioned that the characteristics of the pressure-drop curves depend on the value of a_{55}.

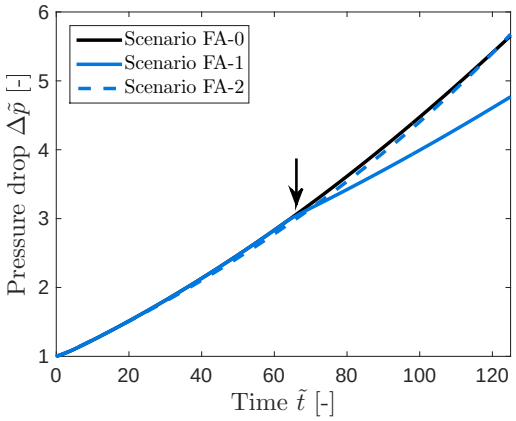

Figure 5.9: Pressure drop across the filter for the Scenarios FA-0, FA-1, and FA-2. The arrow indicates the point where in Scenario FA-1 the filter-aid particle diameter was increased by 50 %.

Last, the energy consumption according to Eq. (5.59) of the different scenarios is compared. In case of Scenario FA-0, $\tilde{e} = 382.2$; for Scenarios FA-1 and FA-2, the values are $\tilde{e} = 357.1$ and $\tilde{e} = 377.4$, respectively. Scenario FA-0, therefore, has the highest energy consumption. It is no surprise that Scenario FA-1 consumes less energy, because, as already discussed, the larger particles used for $\tilde{t} > 65$ create a more permeable filter cake and, thereby, $\tilde{e}$ is reduced. However, it is surprising that Scenario FA-2 leads to a decreased energy consumption even though over the time span of $t = [0\ 125]$ the same amount of filter aids was used. This finding gives further warrant to the argumentation in Section 5.1 for the benefits of a time-variable filter-aid dosage. In the next section, the time variation of $\tilde{c}_{\mathrm{FA}}$ is addressed by an numerical optimal control approach.

5.7 Numerical Optimization and Optimal Control Solutions for Full Model

As explained in Section 2.3.5, it is important to compare optimal control results with suitable base cases. In this section, the common option of juxtaposing optimal control outcomes with optimal constant values of the control variables is chosen. Therefore, an optimization is conducted first to find the optimal constant value of $\tilde{c}_{\mathrm{FA}}$; the case is referred to as Scenario FA-Opt. The objective function is given by the energy consumption, as defined in Eq. (5.59), i.e.,

$$J_{\text{FA-Opt}} = \tilde{e}(\tilde{c}_{\mathrm{FA}})\,. \tag{5.66}$$

$\tilde{c}_{\mathrm{FA,Opt}}$, the optimal constant value, is found to be 0.0089. The corresponding energy consumption of Scenario FA-Opt is $\tilde{e} = 365.9$, a value that is significantly smaller than for all tested scenarios of the last section. This finding provides a valuable hint on the importance of the body-feed concentration and confirms the phenomenological knowledge gathered in the literature review at the beginning of this section.

$\tilde{c}_{\mathrm{FA,Opt}}$, obtained from the full model by numerical optimization, is now compared to approximate solutions determined from the analytical optimal control solution of Eq. (5.27). In its nondimensional form, the condition is

$$\tilde{c}_{\mathrm{FA}} = \tilde{a}'_{55} \cdot \tilde{c} = \tilde{a}_{55} \cdot \tilde{c}\,. \tag{5.67}$$

Compare Appendix 5.1 for the relation between $\tilde{a}'_{55}$ and $\tilde{a}_{55}$; note that the factor ε_s, relating a'_{55} and a_{55} in the appendix cancels due to the scaling of the parameters. As Eq. (5.67) was derived in Section 5.3 under the assumption of pure surface filtration, it is unclear what value of $\tilde{c}$ is to be used in the present case where also depth filtration is considered. If $\tilde{c}$ is interpreted as $\tilde{c}_{\Delta}$, i.e., if only surface filtration is taken into account, $\tilde{c}_{\mathrm{FA}}$ is 0.0075. Alternatively, $\tilde{c}$ can be interpreted as the total reduction in impurities, including surface and depth filtration. As this value changes over time and is dependent on the scenario, it is roughly approximated by 0.9; compare, e.g., Figure 5.8. In this case, $\tilde{c}_{\mathrm{FA}}$ is obtained from Eq. (5.67) as 0.0135. The numerically found $\tilde{c}_{\mathrm{FA,Opt}} = 0.0089$ is, thus, different from both values and is located between the two analytically calculated extremes.

Using the single-shooting method described in Sections 3.2.2 and 5.5, the optimal trajectory of $\tilde{c}_{\mathrm{FA}}(\tilde{z})$ is approximated. The scenario is abbreviated as FA-OC. Goal is again to minimize energy consumption according to Eq. (5.59), i.e., the objective functional is

$$J_{\text{FA-OC}} = \tilde{e}(\tilde{c}_{\mathrm{FA}}(\tilde{t}))\,. \tag{5.68}$$

In the numerical optimization, it is enforced by constraints that the integral value of $\tilde{c}_{\mathrm{FA}}(\tilde{z})$ over the whole time span is the same as the time integral of $\tilde{c}_{\mathrm{FA,Opt}}$. Note that this condition implies that the same amount of filter aids is used in both cases, only in Scenario FA-OC the given amount is dosed unevenly over the time of one process cycle, i.e., here $\tilde{t} = [0\ 125]$. The approximation of the optimal trajectory together with $\tilde{c}_{\mathrm{FA,Opt}}$ is shown in Figure 5.10. As can be seen in the figure, the optimally controlled profile is approximated by only five points and is non-smooth; the latter observation points to numerical instabilities of the optimal control approach in this case. More jagged curves result, if the profile is approximated by an increased number of points. However, the present five-point profile of Scenario FA-OC still performs better than a corresponding curve which is only approximated by two points, i.e., an optimal linear profile. Having noted this here, these points will be picked up and explained in more detail a little later.

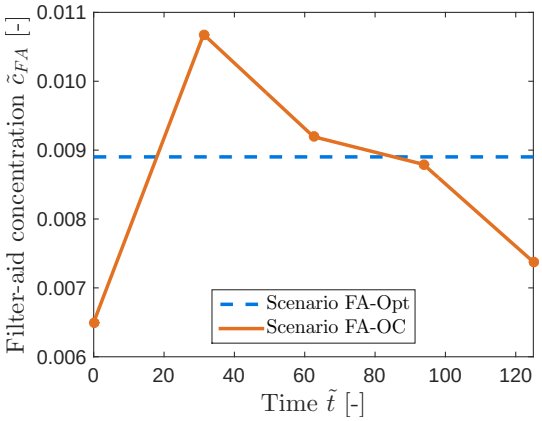

Figure 5.10: Approximation of optimal dosage trajectory $\tilde{c}_{\mathrm{FA}}(\tilde{t})$ and comparison to optimal constant body-feed concentration $\tilde{c}_{\mathrm{FA,Opt}}$.

The effects on impurity concentration and deposit within the filter cake are shown in Figure 5.11 and compared to Scenario FA-0 of the last section as well as to the optimal constant filter-aid dosage of Scenario FA-Opt. In terms of $\tilde{c}$, the Scenarios FA-Opt and FA-OC show no significant differences; FA-0 results in a smaller cake height but results in a qualitatively similar profile. On the contrary, the deposit curves show significant differences between all three scenarios. Both for FA-Opt and FA-OC, the peak values of $\tilde{\sigma}$ are smaller, because a higher filter-aid dosage leads to less surface clogging according to Eq. (5.56). The resulting smaller peak values of $\tilde{\sigma}$ in turn influence cake permeability and energy consumption, compare Eqs. (5.5) and (5.11).

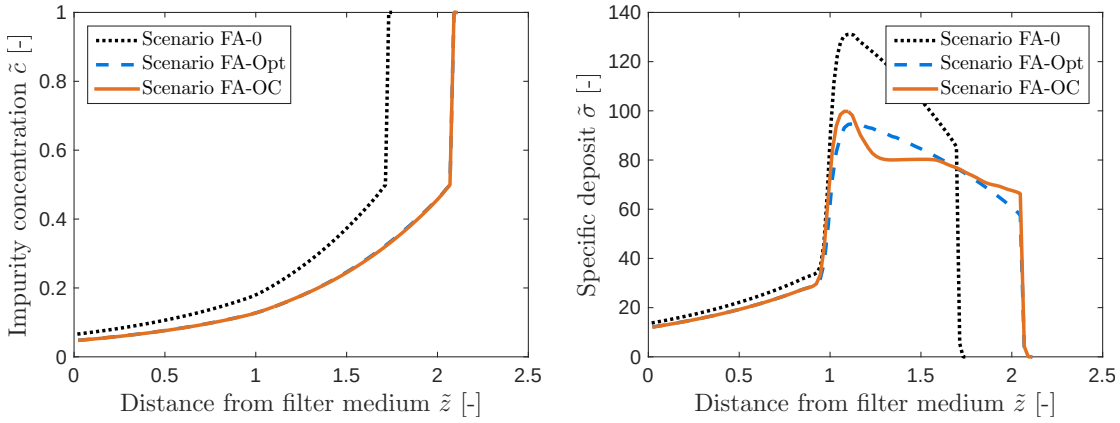

(a) (b)

Figure 5.11: Impurity concentrations within the filter cake for the Scenarios FA-0, FA-Opt, and FA-OC at $\tilde{t} = 120$ (a); specific deposit within the filter cake at $\tilde{t} = 120$ for the Scenarios FA-0, FA-Opt, and FA-OC (b).

Scenario FA-OC leads to an energy consumption of $\tilde{e} = 365.2$, as compared to $\tilde{e} = 365.9$ in case of Scenario FA-Opt. For the chosen setup, optimally controlling the body-feed concentration, thus, results in a benefit of only 0.2%. As the comparison of Scenario FA-0 of the last section with Scenario FA-Opt showed a much larger improvement, the effect of the constant body-

feed concentration on energy consumption was investigated and the outcomes are shown in Figure 5.12.

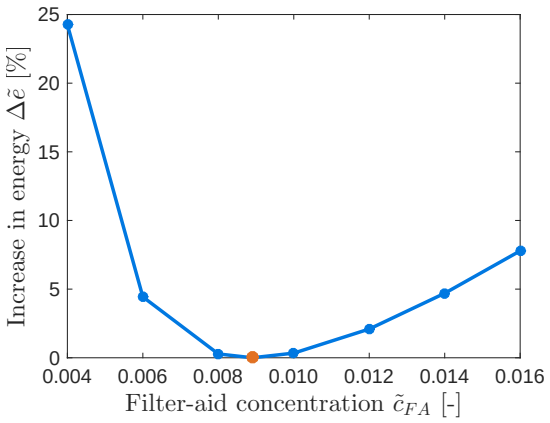

Figure 5.12: Influence of constant body-feed concentration on energy consumption. The optimal concentration $\tilde{c}_{\mathrm{FA,Opt}}$ is marked by the orange point and all values of $\tilde{e}$ are normalized by $\tilde{c}_{\mathrm{FA,Opt}}$.

It can be seen that the constant body-feed concentration has a large influence on $\tilde{e}$. Due to this finding and the very small effect of optimally controlling the body feed, the optimal control approach is not further pursued here. Note that even though the share of depth filtration on the overall separation was chosen to be rather large in that only 50 % of impurities were separated by surface filtration, the benefits of Scenario FA-OC are still small. Also, it is unlikely that the numerical instabilities alone led to this outcome, because optimally controlling $\tilde{c}_{\mathrm{FA}}$ did decrease energy consumption.

Two further points are worth mentioning: First, the general reasoning for the benefits of an optimal control approach, provided at the beginning of this chapter in Section 5.1, remains valid; only the quantitative benefits are small for the investigated case. This finding does, however, not exclude benefits for other scenarios, some of which will be discussed in the next section. Second, it is important to note that also the optimal constant body-feed concentration could only be determined by numerical optimization. This was underlined by contrasting $\tilde{c}_{\mathrm{FA,Opt}}$ with values obtained from the analytical optimal control solution that was derived in Section 5.3. The newly developed model is, thus, indispensable for calculating the optimal body-feed concentration.

5.8 Conclusions from Optimally Controlled Filter-Aid Filtration

Whereas the focus of Chapter 4 was clearly on the optimal control approach, the focus of this chapter lies primarily on model development and analysis. A new mechanistic model for filter-aid filtration with incompressible cakes that considers the contributions of surface and depth filtration was introduced. The problem was identified as of the moving-boundary type and treated by the front-fixing method. Van Leer's flux-limiter scheme was found suitable to yield smooth results, despite sharp moving fronts in the solution. To the knowledge of the author, this is the first model capable of handling transient process conditions concerning all variables and

parameters. It was shown that the growing filter cake leads to a decreasing impurity concentration at the filter outlet due to the increasing influence of depth filtration. The interplay between surface and depth filtration resulted in a pronounced deposit peak at the boundary between the precoat and the body-feed cake. The model successfully reproduced these effects which were by now known only from experimental studies.

Based on a simplified model where the contribution of depth filtration was neglected, an analytical optimal control solution was derived. It was shown that filter-aid concentration should be proportional at each time to the concentration of impurities in the suspension. This result is a generalization of the findings by Heertjes and Zuideveld (1978c). As one important consequence, the generalized relation offers benefits for process control. Online measurements of impurity mass concentration in the suspension, e.g., by a calibrated turbidity sensor, can be used to determine the optimal body-feed concentration at each time. But it also follows from the derived analytical optimal control solution that, in case of a constant impurity concentration, a constant dosage of filter aids is optimal.

The full model's capabilities were explored in two case studies where filter-aid dosage was changed dynamically. Increasing the filter-aid particle diameter at a discrete point in time led to a decreased separation efficiency in the following coarser cake layers. However, due to the more pronounced clogging in the finer layers, the effect on the overall separation efficiency was moderated. Continuously varying the amount of body feed caused a variable cake growth velocity and a strongly changed deposit profile within the filter cake. A decreased energy consumption was found in case of time-variable dosage, even though the same amount of filter aids was used. This last finding motivated an optimal control approach.

However, it was discovered that varying the optimal constant amount of filter aids over the time of one process cycle, as determined by an numerical optimal control approach, showed only small benefits for the energy consumption. It appeared that the decisive factor is the amount of filter aids used per filtration cycle, with a significantly lower energy consumption in case of the optimal quantity. Dosing this given optimal amount in turn unevenly over the time of one process cycle led to a slightly lower energy consumption, an effect that was deemed insignificant compared to the influence of the overall amount of filter aids.

In general, the simulation results showed that the complex interplay between the various process variables and parameters is hard to predict intuitively. The given model can, therefore, significantly aid a mechanistic process understanding and allows to study the effects of different control strategies. Due to the high efficiency of the numerical approach, it could be also used for computational optimization. Additionally, the model might also be applied for model-predictive control where real-time capabilities are a prerequisite. For all practical purposes, the model equations have to be parameterized. Due to the fact that this approach is a combination of already established surface and depth filtration models, the corresponding parameterization methods can be adapted directly if the two phenomena are separated experimentally. The feasibility of this strategy was already shown by Heertjes and Zuideveld (1978b,c). Parameterization methods can be, e.g., found in Tien (2006) for cake filtration and Tien and Ramarao (2007) as

well as Zamani and Maini (2009) for depth filtration. In future work, the model can be further developed to cover cake compression as well. This becomes especially important when filter aids are used that are themselves compressible, as encountered in fibers (Braun, 2012).

Even though the conducted optimization and optimal control approaches provided important insights, many questions remain to be investigated. In the first place, it needs to be mentioned that the results are only optimal with respect to energy consumption; however, minimal energy consumption is not necessarily the economic optimum in every case. For example, the used amount of filter aids could be taken into account by an overall cost model because filter aids need to be bought and might cause disposal costs as well. After all, it seems likely that the identified optimal filter-aid concentrations can be interpreted as upper bounds that should not be exceeded because, in that case, both filter-aid consumption and energy expenditure would be overly large. Besides the mentioned case of multi-objective optimization, i.e., optimizing with respect to energy consumption and filter-aid usage, other scenarios are possible. To name just three further examples: The amount of filter aids could be minimized under the constraint that some filtration quality is still guaranteed; the time until some maximal pressure drop is reached could be maximized, as done in Chapter 4 for the case of depth filtration; besides controlling filter-aid concentration, also filter-aid particle size might be varied in time even though this is more challenging to implement practically. Obviously, all optimization and optimal control results strongly depend on the chosen constitutive equations and the used model parameters. For that reason, optimization should be conducted in the future for practical problems of filter-aid filtration using a fully parameterized model. In that case, the quantitative effects of implementing an optimal control strategy must be evaluated again. If optimal control seems a promising strategy, the numerical stability of the used algorithm needs to be checked again and, if necessary, the algorithms have to be further developed, an outcome that is made likely by the numerical instabilities encountered in Section 5.7.

Appendix 5.1

Two forms of the Sutherland equation, that are both found in the literature, are related in this Appendix[1]. As introduced in Section 2.2.3, Eq. (2.46), the Sutherland equation in one formulation reads

$$k = k_0 \cdot \exp\left(-a'_{55} \cdot \frac{c}{c_{\mathrm{FA}}}\right). \tag{5.69}$$

In this case, the model is based on the assumption that separation takes places solely due to surface filtration, i.e., all impurities $c = c_\Delta$ are deposited on top of the cake. The c/c_{FA} ratio, when expressed in terms of volume concentrations, is simply a measure for specific deposit:

$$\frac{c}{c_{\mathrm{FA}}} = \frac{\sigma}{\varepsilon_s}, \tag{5.70}$$

as obtained when using the relation

$$\sigma = \frac{\varepsilon_s \cdot c_\Delta}{c_{\mathrm{FA}}} \tag{5.71}$$

that is derived below in Appendix 5.3; ε_s again is the solidosity. Thus, the Sutherland equation can be also expressed as

$$k = k_0 \cdot \exp\left(-a_{55} \cdot \sigma\right), \tag{5.72}$$

if ε_s is included in the new constant a_{55}, i.e.

$$a_{55} = \frac{a'_{55}}{\varepsilon_s}. \tag{5.73}$$

In this more general form, the equation can be also used if, additionally to surface filtration, depth filtration occurs for which case deposit σ is caused by both mechanisms. An analogous formulation, based on mass concentrations instead of volume concentration and resistances instead of permeabilites, is derived and used in Hackl et al. (1993, p. 29); similar formulations were used by Berndt (1981, p. 83) and Tittel (1987, p. 55).

Appendix 5.2

In this Appendix, the front-fixing method is applied to the main system equations. Using the dimensionless height coordinate

$$\eta = \frac{z}{L(t)} \tag{5.74}$$

and applying the transformation rules that were derived in Section 3.1.3, namely

[1] Analogously to Chapter 4, the appendices are again directly included after the main chapter to which they exclusively refer.

$$\frac{\partial f}{\partial z} = \frac{1}{L} \cdot \frac{\partial \hat{f}}{\partial \eta} \tag{5.75}$$

$$\frac{\partial f}{\partial t} = \frac{\partial \hat{f}}{\partial t} - \frac{\eta}{L} \cdot \frac{dL}{dt} \cdot \frac{\partial \hat{f}}{\partial \eta}, \tag{5.76}$$

to the main model equations, i.e., substituting f with c and σ, respectively, yields:

$$\varepsilon \left(\frac{\partial \hat{c}}{\partial t} - \frac{\eta}{L} \frac{dL}{dt} \frac{\partial \hat{c}}{\partial \eta} \right) + \frac{q}{L} \frac{\partial \hat{c}}{\partial \eta} = - \left(\frac{\partial \hat{\sigma}}{\partial t} - \frac{\eta}{L} \frac{dL}{dt} \frac{\partial \hat{\sigma}}{\partial \eta} \right) \tag{5.77}$$

$$\frac{\partial \hat{\sigma}}{\partial t} - \frac{\eta}{L} \frac{dL}{dt} \frac{\partial \hat{\sigma}}{\partial \eta} = -\hat{\lambda} q \hat{c}. \tag{5.78}$$

Minor rearrangements and nondimensionalization lead to the Eqs. (5.47) and (5.48) of the main text of this chapter. A side effect of the front-fixing method is that a fixed spatial point in the original coordinate system (z) moves in the new coordinate system (η). Because incompressible cake filtration is considered, the filter-aid particle diameter d_{FA} at a given spatial location stays constant with time in the original coordinate system, i.e.,

$$\frac{\partial d_{\mathrm{FA}}}{\partial t} = 0. \tag{5.79}$$

However, applying Eq. (5.76) results in an additional transport equation that needs to be considered in the transformed coordinate system:

$$\frac{\partial \hat{d}_{\mathrm{FA}}}{\partial t} - \frac{\eta}{L} \frac{dL}{dt} \frac{\partial \hat{d}_{\mathrm{FA}}}{\partial \eta} = 0. \tag{5.80}$$

Eq. (5.80) in its nondimensional form corresponds to Eq. (5.49) of the main text of this chapter. The hat signs are omitted in the equations of the main text to improve readability. Wherever η is encountered as the spatial variable, the transformed coordinate system is used; all numerical results where obtained by the transformed equations, i.e., with a fixed front.

Appendix 5.3

For the PDE system, the specific deposit at the cake surface, i.e., at $z = L$, is needed as a boundary condition. Since Eq. (5.56) of the main text is not found in the literature, its derivation is shown in this appendix. Specific deposit is defined as volume of deposited impurities V_d per total volume V. This can also be written differentially as

$$\sigma(t, L) = \frac{dV_d}{dV}. \tag{5.81}$$

Because a time-dependent process is considered, rates are used instead, i.e., the last equation is expanded by dt, giving

$$\sigma(t,L) = \frac{dV_d/dt}{dV/dt}\,. \tag{5.82}$$

dV/dt is the cake growth velocity of Eq. (5.1) multiplied with the total area A:

$$\frac{dV}{dt} = -\frac{c_{\mathrm{FA}}}{\varepsilon_s}\cdot q\cdot A\,. \tag{5.83}$$

dV_d/dt describes the rate with which impurities are supplied. It can be expressed as:

$$\frac{dV_d}{dt} = -c_\Delta\cdot q\cdot A\,, \tag{5.84}$$

where c_Δ is the volume concentration of impurities in the suspension deposited at the surface, q is the suspension's superficial velocity, and dL/dt the cake growth velocity. As q is negative in the present coordinate system, the last two equations contain minus signs. Note that Eq. (5.84) depends only on q and cake growth velocity is neglected here. This is justified because cake growth is much slower than fluid transport. However, the same final result is arrived at when the effect of cake growth is included in Eq. (5.84) and the full equation for dL/dt is used, as shown in Eq. (2.43); this was demonstrated in Kuhn and Briesen (2016a). Under the present assumptions, the final relationship is obtained when Eqs. (5.83) and (5.84) are introduced into Eq. (5.81):

$$\sigma(t,L) = \frac{\varepsilon_s\cdot c_\Delta}{c_{\mathrm{FA}}}\,. \tag{5.85}$$

Chapter 6

Further Applications

Some new paths within filtration research may also open up new ways outside of this field. A few examples where this might be the case are introduced in this chapter. Only a simplified mathematical treatment is presented and no optimization results are shown. However, it is argued on systematic grounds that the methods used in the previous case studies might also be beneficial for the applications presented here. The systematic argumentation hinges on the principles presented in Section 2.3.5 to identify worthwhile optimal control problems and to judge their outcomes. Flow charts in the form of causality graphs are used to further illustrate analogies between the different applications. The material of this chapter, therefore, falls under the category of "bold conjectures" as discussed in Section 1.3; future research may build on it and judge its validity. The discussed applications are broadly divided into two subcategories, namely flow through compressible porous media and processes based on intra-particle diffusion. As can be seen, both categories are still closely related to the previous investigations on filtration as they also belong to the fields of transport in porous media as well as particle technology.

6.1 Flow Through Compressible Porous Media

Compressible porous media are encountered in various different fields and applications. In many cases, soils are characterized by compressible behavior (Bear, 1988, p. 52); the same holds true for biological tissues (Khaled and Vafai, 2003). Filter cakes are often compressible (Sorensen and Sorensen, 1997; Alles, 2000) and columns for preparative chromatography are packed frequently with compressible media (Carta and Jungbauer, 2010, pp. 119-121, 317-326). It is generally distinguished between mechanical compression and flow compression. The first leads to a homogeneous compression within the medium, the latter causes an increasing compression along the flow direction (Parker et al., 1987). In this section, only flow compression is considered. Phenomenologically, compression reduces the fluid permeability and, therefore, leads to an increasing differential pressure across the porous medium if a constant flow rate is enforced.

For the following considerations, a cylindrical geometry is investigated and treated as one-dimensional with the spatial dimension z being the axis of the cylinder. A model sketch including the main variables is provided in Figure 6.1.

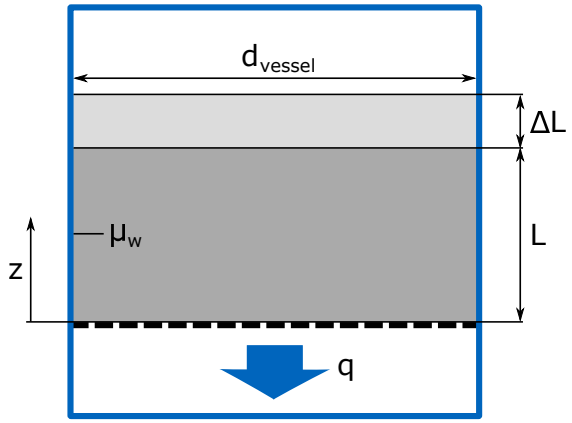

Figure 6.1: Model sketch for stationary flow through compressible porous media.

Only a stationary process is considered. In this case, a force balance on an infinitesimal 1D element leads to

$$\frac{d\sigma_c}{dz} = -\frac{dp}{dz} - \frac{4}{d_{\text{vessel}}}\mu_w \frac{\nu}{1-\nu}\sigma_c\,, \tag{6.1}$$

where σ_c is the compressive or tensile stress, p is the fluid pressure, z is the height coordinate, d_{vessel} is the diameter, μ_w is the coefficient of wall friction, and ν is Poisson's ratio (Hekmat et al., 2013). The right term accounts for wall support, i.e., the fact that the vessel wall counteracts compression. Note that wall support is negligible for large containers, i.e., $d_{\text{vessel}} \to \infty$. If the pressure gradient is substituted by Darcy's law, one gets:

$$\frac{d\sigma_c}{dz} = \frac{q \cdot \mu}{k} - \frac{4}{d_{\text{vessel}}}\mu_w \frac{\nu}{1-\nu}\sigma_c\,, \tag{6.2}$$

where permeability k is a function of the characteristic length scale d of the pore space, as previously discussed. The equation is solved within the domain $[0\ L]$ using the initial condition

$$\sigma_c(L) = 0\,. \tag{6.3}$$

However, the initial height L_0 is reduced to L due to compression. Local uniaxial compression is defined as

$$e_c = \frac{du_d}{dz}\,, \tag{6.4}$$

with the local displacement u_d (Gross et al., 2011, pp. 14, 20). Assuming zero displacement at $z = 0$, i.e., at the fluid outlet, the global change in length results from an integration of e_c as

$$\Delta L = u(L) = \int_0^L e_c \, dz. \tag{6.5}$$

In implicit form, L can be expressed as

$$L = L_0 \left(1 - \frac{\Delta L}{L}\right), \tag{6.6}$$

e is coupled to compressive stress via Hooke's law, if linear elastic behavior is assumed for reasons of simplicity:

$$e_c = E \cdot \sigma_c, \tag{6.7}$$

where E is Young's modulus which describes the stiffness of the packed bed, i.e., it is an effective or macroscopic elastic modulus. Based on these equations, the compressive stress σ_c is lowest at the flow inlet, namely 0, and increases steadily towards the flow outlet.

Two further causalities need to be mentioned, namely, how the characteristic length scale of the micro scale d influences the permeability k and the compressibility described by E. On the one hand, k increases with d, as, e.g., modeled by the Kozeny-Carman equation (Section 2.2.3). Therefore, larger particles lead to a more permeable packed bed. On the other hand, packings of larger particles are also often more compressible, i.e., E of the packed bed increases with d. For fibers, the van-Wyk equation implies that larger, i.e., longer, fibers lead to a higher bed compressibility. This behavior was attributed to a more pronounced bending of larger single fibers (Van Wyk, 1946). If single spherical particles are considered, their stiffness increases with increasing particle size, as described, e.g., by Hertz' law (Flores and Lankarani, 2016, pp. 19-21). This is contrary to the just discussed behavior of fibers. However, deformation of single particles is not the only mechanism for macroscopic bed compression. Other effects, like rearrangement of particles or breakage of agglomerates, can also be important (Alles, 2000). Therefore, the macroscopic bed behavior can differ from the compression behavior of single particles. For example, a direct proportionality between particle size and effective elastic modulus of the bed was also reported for nearly incompressible sand particles (Brzesowsky et al., 2014). The reasoning in the next section is based exemplarily on the same phenomenological behavior, namely that bed compressibility increases with particle size.

In all of the following considerations about process optimization, a minimal overall pressure drop Δp is aimed at. The corresponding objective functional is:

$$J = \int_0^L \left(\frac{dp}{dz}\right) dz = \Delta p. \tag{6.8}$$

In case of processes with a constant flow rate, minimal pressure drop also leads to the smallest energy consumption. Now that the performance index is defined, suitable control variables still need to be identified. Hypothetically, the characteristic length scale d of the pore space as well

as the vessel diameter d_{vessel} are chosen as promising candidates for control variables. These two options are explored in the following two sections.

6.1.1 Using Stratified Packings

Using the characteristic length scale d of the pore space as the control variable and varying it along the independent variable z leads to stratified packings. Stratified packings denotes packings of particulate materials that vary in their properties along the height. In this first consideration, the wall support is neglected, i.e., vessels with large diameters d_{vessel} are considered. The characteristic length scale d is interpreted as the particle size, where particles are understood in a broad sense, comprising, for example, also fibers. It can be observed that the underlying logic here is similar to the one applied in the previous case studies, especially in Chapter 4 where the packing properties of depth filters were varied along the filter depth.

Process causalities for flow through compressible porous media using local particle size as the control variable are depicted in Figure 6.2. As indicated in the figure, it is assumed that the overall size distribution of the particles is constant, i.e., that a given batch of particles is used that are distributed along the bed height according to their sizes. This is true to the principle discussed in Section 2.3.5 that for a meaningful comparison of standard and optimized process configurations, ideally all properties except for the control variables need to be kept constant.

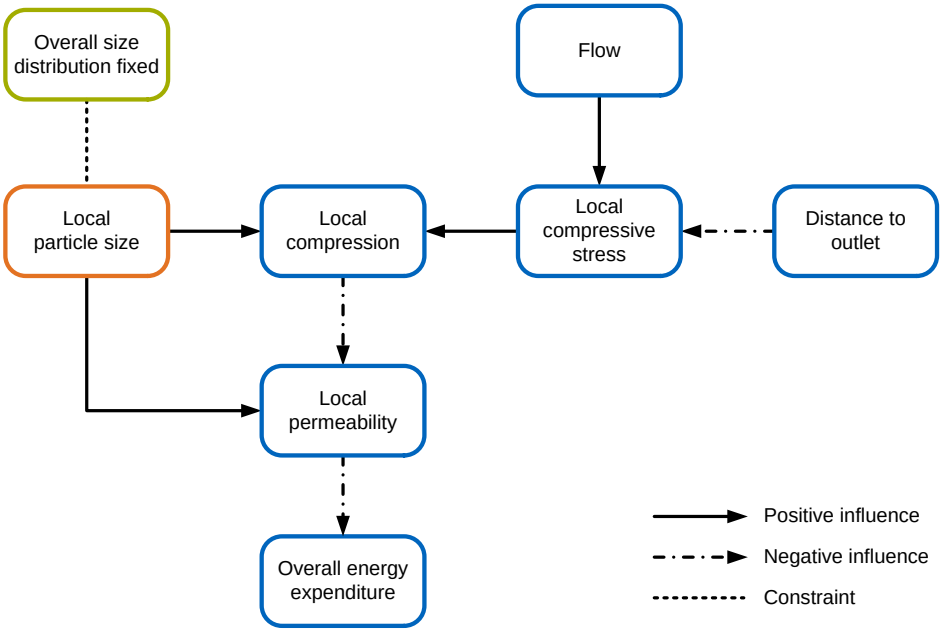

Figure 6.2: Process causalities in flow through compressible porous media including the influence of the local particle size.

However, an important assumption is implied here, namely that the packing porosity is not affected by spatially rearranging the particles according to their sizes. Contrary to that assump-

tion, packing porosity is indeed affected by the size distribution of particles. Consider as an example particles of two sizes: Each particle fraction alone will have a higher packing porosity than the homogeneous particle mixture (Mota et al., 2001; Dias et al., 2004; Brouwers, 2013), as discussed in Section 2.2.3. Thus, a stratified packing configuration with two layers composed each of mono-sized particles will have a higher porosity than a bed of mixed particles; also the overall bed height will be affected. Usually, the effect will be less pronounced in case of broad particle size distributions, instead of two mono-sized particle fractions. However, as the effect of a broader size distribution is not easy to generalize, further research is necessary to investigate the quantitative influence on the packing properties for given cases. For now, only the simplification is noted and it is assumed that variations in packing porosity will not eliminate the benefits of the proposed optimal control approach. Based on Figure 6.2 and the introduced equations, an optimal control approach is expected to reduce the overall energy expenditure for the following reasons:

- Larger particles result in an higher permeability k in an uncompressed state, i.e., $d \uparrow \longrightarrow k \uparrow$.
- However, larger particles are also more compressible than smaller ones, i.e., $d \uparrow \longrightarrow E \downarrow$.
- The compressive stress is lowest at the flow inlet and increases steadily towards the flow outlet.
- It is assumed that a certain particle size spectrum is available.
- Therefore, larger particles out of the available size spectrum should be used at the inlet and their size should be decreased toward the fluid outlet.

Whereas the basic idea of local particle size variation to counteract increased energy expenditure due to flow compression was illustrated so far in a general manner, this principle can be used for process optimization in different fields. Examples are provided now by picking up some applications mentioned at the beginning of Section 6.1.

One mode of precoat filtration is based on a constant precoat layer height (Hackl et al., 1993, pp. 7-9). Often, compressible fibers are used as a precoating material. In this case, grading of fiber length along the layer height with the shortest fibers closest to the fluid outlet might decrease energy consumption. However, care must be taken that the separation properties of the graded or stratified precoat layer are still within a tolerable margin, i.e., comparable to a homogeneous layer.

Particle sizes in preparative chromatography columns could, analogously, be varied along the column height. Again, it is desirable that the particles which form the stiffest packing are located at the fluid outlet where the compressive stress is highest. Similar to the last example, care must be taken that the chromatographic operation is still guaranteed to a sufficient degree by this modified packing configuration. Li and Liapis (2012) showed evidence that for some chromatographic operations stratified beds are directly beneficial; however, no optimal control

approach is used. Fee et al. (2014) and Nawada et al. (2017) did experiments on 3D printing of chromatography columns and packing materials, respectively. Even though not mentioned in these studies, both techniques are usable for the fabrication of locally optimized chromatography packings, a strategy which is directly related to the micro-manipulative paradigm in filtration research as identified in Section 1.2.1.

Another application is the washing of compressible particulate materials. For some uses, fibers or particles are washed in packed beds before they are further used (Noerpel et al., 2012). For example, this is the case in the fabrication of chromatographic media. In contrast to pre-coat filtration or chromatography where a particle-size gradient might affect the function of the process, particle washing should not be impaired by stratified particle-packing configurations.

Whereas the previous examples can be and often are described by the modeling approach sketched in this section, also further applications that go beyond this model can be optimized along similar lines. Compressible cake filtration is mentioned as an instance (Tien, 2006, pp. 51-89). The growing cakes are no longer stationary, as assumed in the model equations above. On the contrary, a moving-boundary problem is encountered. Nevertheless, the highest compressive stress occurs at the filter medium. Therefore, it may be beneficial to filter the smallest particles first and the largest last. This particle size grading is contrary to the natural sedimentation layering of size-distributed particles where the largest particles sink fastest and are, therefore, encountered at the bottom. For this reason, a combination of cake filtration with some pre-treatment steps, e.g., centrifugation, may be advantageous. It is suggested that particles are subsequently filtered in different size classes, starting with the smallest ones.

6.1.2 Using Wall Support

So far, wall support was neglected, i.e., $d_{\text{vessel}} \to \infty$. On the contrary, now not only vessels with a finite diameter are considered but d_{vessel} is actively used as the control variable. The process follows the causalities depicted in Figure 6.3.

In this case, the total bed height is imposed as a constraint so that only the distribution of vessel diameters within that height is considered. Otherwise, the given particle volume could be accommodated within a vessel of the smallest possible diameter so that the wall support is maximal everywhere. Distributing d_{vessel} along the height might be beneficial for the following reasons:

- The compressive stress is lowest at the flow inlet and increases steadily towards the fluid outlet.
- A certain amount of particles need to be accommodated within a given height L which is imposed as an additional constraint.
- The column diameter, therefore, should be smallest at the fluid outlet to offer the highest wall support where it is needed most.

The general idea of varying the diameter distribution might be beneficial for different applications. In preparative chromatography, ever higher flow rates are desired for economical reasons. Therefore, bed stability is an issue, e.g., due to channel formation at the column wall or within the bed (Hekmat et al., 2011).

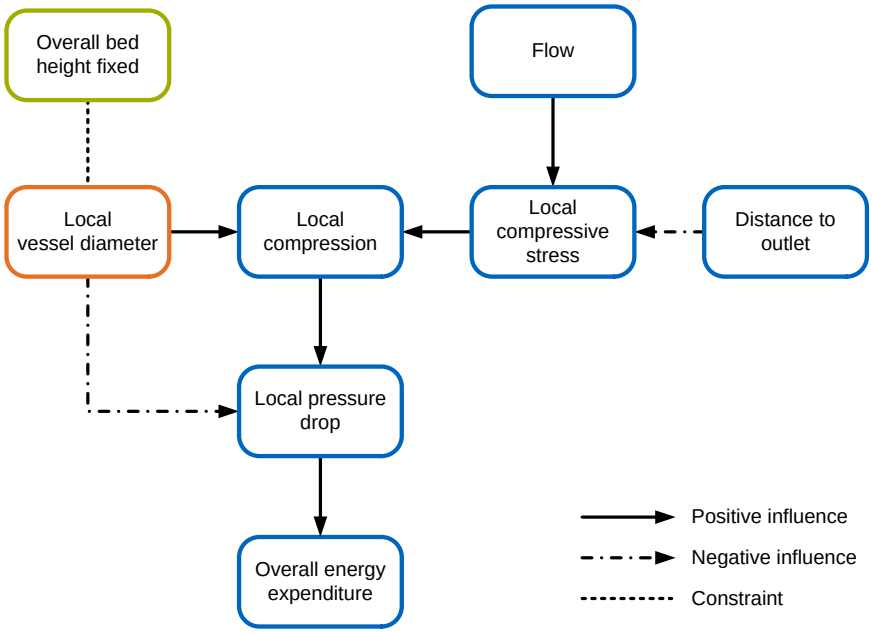

Figure 6.3: Process causalities in flow through compressible porous media including the influence of the local vessel diameter.

Gerontas et al. (2015) investigated the effect of mechanical inserts, i.e., concentric metal rings, in chromatography packings to increase wall support and by that achieve higher bed stability. However, rings of constant diameter were used and the diameters seem to have been selected by trial and error. Using an optimal control approach, in contrast, offers the possibility to determine not only improved wall support but the optimal wall support according to the chosen model and cost functional – an argument that hinges on the discussion of Section 2.3.5 where improvement based on intuition was contrasted with mathematical optimization.

Once the optimal vessel geometry is known, also additional overall process improvements can be addressed. An example of how to move from a single vessel geometry to a new process design, in this case a counter-flow arrangement, is shown in Figure 6.4. The figure illustrates that also more complicated geometries of single vessels can be accommodated effectively by using advanced overall designs. Even though preparative chromatography was used as an example so far, similar approaches can, of course, be also beneficial for filtration. In this respect, advanced geometries become ever more attractive, the higher the compressibility of the corresponding materials and the more, therefore, is gained by counteracting local compression. A further, related idea is worth mentioning that arose in discussions with Jörg Engstle, former employer at the Chair of Process Systems Engineering. Local wall support cannot only be increased by ac-

tually changing the overall vessel geometry, but also by inserts in a given vessel; the concentric rings used by Gerontas et al. (2015) to achieve higher wall support in chromatography columns were already mentioned. In contrast, the idea of Jörg Engstle and the author of this thesis was to use random packing rings[1], normally applied, e.g., in fractionating columns (Raschig, 2017), to locally increase wall support. The idealized concept is that the random packing rings create internal confinements of small dimensions that offer high local wall support to the compressible particle packing. In this mode of usage, random packing rings can also be conceived as macroscopic filter aids, because the random packing rings enable the build-up of stable filter cakes just as conventional filter aids do, only their geometrical dimensions are orders of magnitudes larger than the substances to be separated, which distinguishes them from conventional filter aids.

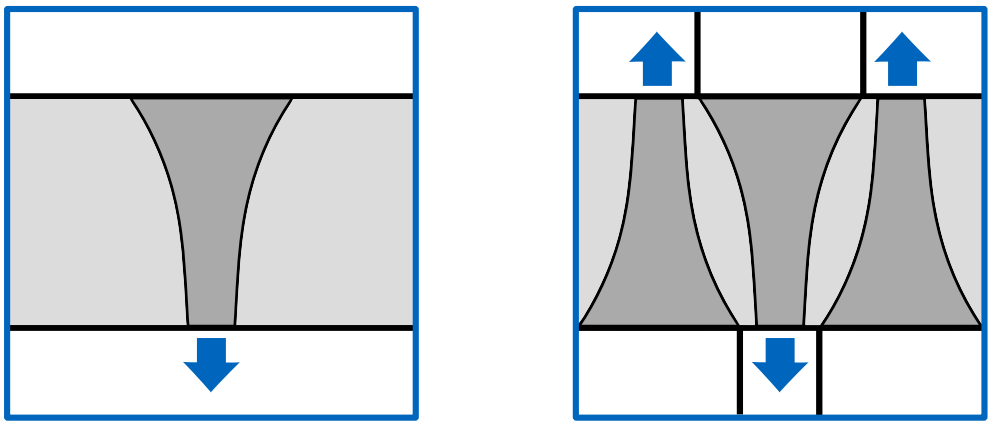

(a) (b)

Figure 6.4: Illustration of optimally controlled vessel diameter: single narrowing vessel (a) and three narrowing vessels in counter-flow arrangement (b); the blue arrows indicate the flow direction.

Preliminary experiments by Jörg Engstle for lautering, a solid-liquid separation step in the beer brewing process that comprises highly compressible filter cakes, showed promising results, i.e., increased flow rates at a still acceptable separation efficiency. Currently, further experiments with compressible fibrous materials are being conducted. Using optimal control methods, the local packing configuration of the random packing rings can be optimized. However, especially when small geometrical confinements are encountered, the effect of confinement diameter on pressure drop also needs to be taken into account (Cheng, 2011). This effect is also marked in Figure 6.3 as the relationship between local vessel diameter and local pressure drop. Whether the strategy described is beneficial for filtration practice depends on the actual financial savings. Different scenarios are conceivable: For example, either the random packing rings are regenerated, i.e., cleaned, and used repeatedly or they are discarded with the filter cake. In addition to their use in filtration, random packing rings can also be used to decrease packing compressibility in a row of other applications where flow through compressible porous media is encountered.

[1] Often, random packing rings are also simply called random packings or they are referred to by their commercial names, e.g., Raschig rings or Pall rings.

6.2 Processes Based on Intra-Particle Diffusion

As a second broad field of applications, processes based on intra-particle diffusion are considered. To name a few examples, intra-particle diffusion is decisive in various extraction processes, e.g., of coffee. Furthermore, intra-particle diffusion plays an important role during washing of porous particles as well as for many chromatographic applications.

In this section, a case is considered where solids are laden with the substance of interest which is transported within the solid particles by diffusion and within the fluid phase by convection. All considerations analogously hold for the converse case where solids are increasingly enriched with the component of interest by transport from the fluid phase. Note that, phenomenologically, such extraction-like processes are opposed to filtration: During the first, a clear fluid enters a particle packing and gets enriched with substances; during the second, a fluid laden with substances passes a filter medium and, thereby, gets clarified.

According to the phenomenological description provided so far, processes based on intra-particle diffusion can be modeled by a diffusion equation in the solid phase that is coupled to a convection equation in the fluid phase. The following model was developed for coffee extraction in Kuhn et al. (2017b). A model sketch is provided in Figure 6.5.

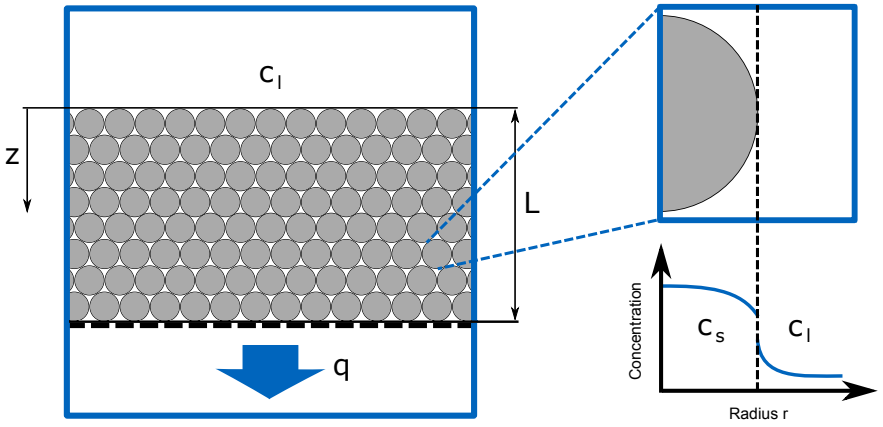

Figure 6.5: Model sketch for diffusive mass transport from particles to fluid flow.

As derived in Section 2.1.2, convective transport is described by

$$\varepsilon \cdot \frac{\partial c_l}{\partial t} + q \cdot \frac{\partial c_l}{\partial z} = s, \tag{6.9}$$

with c_l being the component's mass concentration[2] in the liquid phase and s as a source term which can be formulated as

$$s = S_v \cdot k_l \cdot (c_l^* - c_l)\,, \tag{6.10}$$

[2]In this section, mass concentrations are used as is customary in mass transfer studies. Note that this is contrary to the volume concentration used when filtration was treated in the previous chapters. A justification for the use of volume concentrations in filtration was given at the end of Section 2.2.3.

where k_l is the mass transfer coefficient on the liquid side and c_l^* is the concentration in the liquid at the phase boundary. S_v, the specific surface of the bed, can be expressed in terms of the specific particle surface $S_{v,p}$ and the bed porosity ε (Bear, 1988, p. 51) as

$$S_v = (1-\varepsilon)\cdot S_{v,p} = (1-\varepsilon)\cdot \frac{3}{R}, \tag{6.11}$$

with the particle radius R, if spherical particles are considered. Phase equilibrium at the boundary between the solid and the liquid phase is described by

$$c_l^* = K \cdot c_s^*, \tag{6.12}$$

with the equilibrium constant K and the solid concentration at the phase boundary c_s^*. Mass transfer in the solid phase is modeled as Fickian diffusion according to

$$\frac{\partial c_s}{\partial t} = \frac{1}{r^2}\frac{\partial}{\partial r}\left(-r^2 \cdot j\right) = D\left(\frac{\partial^2 c_s}{\partial r^2} + \frac{2}{r}\frac{\partial c_s}{\partial r}\right), \tag{6.13}$$

i.e., in spherical coordinates with symmetry assumed along both angular directions. c_s is the concentration in the solid phase, j is the diffusive flux, r is the particle radius, and D the diffusivity of the solid particles. Note that D needs to be interpreted as an effective diffusivity when porous particles are encountered, as is the case for coffee extraction (Moroney et al., 2015) as well as in many chromatography applications (Carta and Jungbauer, 2010, p. 70). The boundary conditions are

$$c_l(z=0) = 0 \tag{6.14}$$

$$j(r=0) = 0 \tag{6.15}$$

$$j(r=R) = -k_l \cdot (c_l^* - c_l)\,. \tag{6.16}$$

Initially it holds that

$$c_s = c_{s,0}\,; \tag{6.17}$$

c_l can be initialized with a stationary profile if the initial flooding of the porous material is neglected. An analysis of these system equations shows that the strongest gradient and, therefore, the largest driving force for extraction is given at the flow inlet. This driving force decreases towards the fluid outlet because ever more of the considered substance is enriched in the fluid phase. Hubbuch et al. (2003a) and Hubbuch et al. (2003b) showed that the local concentrations can be studied experimentally by CLSM using a small model chromatography column. The same studies illustrate how diffusive transport is dependent on the particle radius. As can be seen also by the system equations, especially Eq. (6.11), smaller particles release their content of the considered component faster than larger ones. Based on these observations, the process causalities are depicted in Figure 6.6.

The control variable is again the particle size, meaning the radius R here, and its distribution along the bed height is to be determined. Assuming that the extraction shall be conducted as fast as possible, the task turns into an optimal control problem with a free final time. The objective functional, therefore, is

$$J = t_e \,, \tag{6.18}$$

where t_e is the end time at which some cumulative extracted amount of the considered component m_c shall be achieved. To assure this, the following stopping criterion can be used

$$m_c = \int_0^{t_e} \left[c_l(t, z = L) \cdot q \cdot A \right] dt \,, \tag{6.19}$$

where m_c is the cumulative component mass and A is the cross-sectional area. Alternatively, one could set the goal also to maximize the yield m_c, respectively to minimize $(-m_c)$ within a fixed time period $[0\ t_e]$.

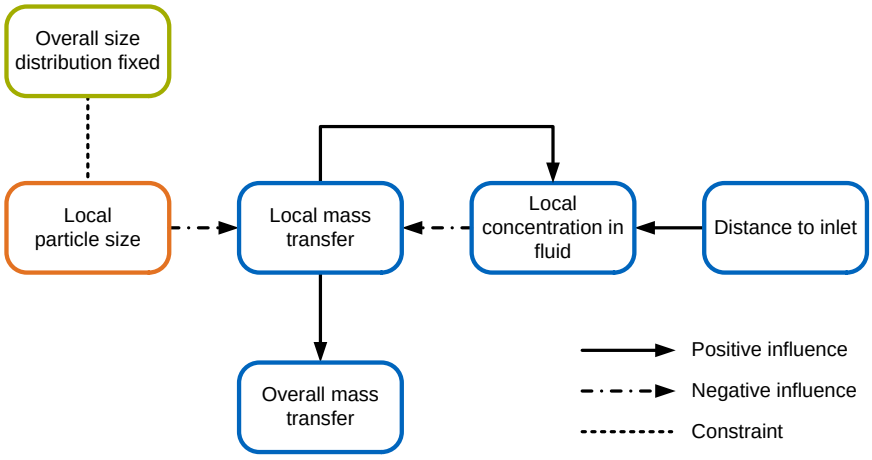

Figure 6.6: Causalities for processes based on intra-particle diffusion including the influence of the local particle size.

As supported by Figure 6.6, the reasoning for the benefits of such an optimal control approach is as follows:

- The driving force for extraction is highest at the flow inlet and decreases towards the outlet.
- It is assumed that a certain particle size spectrum is available.
- Therefore, larger particles out of the available size spectrum should be used at the fluid inlet where the driving gradient is largest and smaller particles at the fluid outlet to compensate for the smaller gradient there.

However, as already discussed in Section 2.3.5, for a meaningful comparison of standard and optimized process configurations, all properties except for the control variables need to be

kept constant. In this case, this is particularly important for the particle size distribution. In an ideal case, the particle diameter is as small as possible; thus, extraction is maximal everywhere. If, however, a certain amount of size distributed particles need to be accommodated within a given height L, i.e., additional constraints are imposed, then the distribution of diameters along the height offers benefits.

As quickly mentioned at the beginning of this section, the washing of porous particles could be optimized by the described approach. Particles with an internal or intra-particle porosity are used in areas such as catalysis, chromatography, or pharmaceutics. After manufacturing, porous particles usually still contain unwanted impurities from their synthesis within the inner pore system (Noerpel et al., 2012). Due to the small size of the inner pores, usually only diffusive transport takes place within the particles. Based on the above reasoning, the washing process could be optimized by arranging them in stratified packings with the largest particles at the flow inlet and the smallest at the outlet.

Using the same strategy, extraction from coffee particles can be improved. This becomes especially attractive when only the overall yield matters as is the case, for example, during decaffeination where as much caffeine as possible is to be extracted in the shortest possible time. Note that usually whole beans are decaffeinated, i.e., the particles are understood here as whole coffee beans. As the beans are distributed in their size, they can be arranged in stratified packings too. With a modified objective functional and kinetics for different key aroma components, also the aroma profile of coffee could be optimized by a spatial arrangement of milled coffee grains according to their sizes.

As a last example, mass transport in chromatography could be optimized. As already mentioned above, Li and Liapis (2012) reported benefits of stratified beds for the chromatographic operation based on a continuum modeling approach. However, they used no optimal control method to determine their optimal particle-packing configuration as is suggested here. It is important to emphasize that they set larger particles at the flow inlet and smaller ones at the outlet, i.e., the identical strategy suggested in this section. It is noted in passing that the same authors found benefits of stratified particle packings for freeze drying of particulate substances a few years later (Bruttini and Liapis, 2015). Even though they conducted a model-based study, again no optimization or optimal control approach was used.

6.3 Conclusions from the Considered Further Applications

In this chapter, it was argued on systematic grounds that the methods used in the case studies of Chapters 4 and 5 might also be beneficial for different other applications. Two process classes that are closely related to these earlier investigations on filtration were discussed: flow through compressible porous media and processes based on intra-particle diffusion.

In case of flow through compressible porous media, two strategies were proposed to counteract media compression and, therefore, reduce energy consumption of the corresponding processes. First, it was suggested to make the particle diameter the control variable and vary the

particle size along the bed height. It was argued that larger particles should be used at the flow inlet and smaller particles at the fluid outlet. However, it is important to note that this strategy is only valid if bed compressibility increases with particle size, as is the case, e.g., for fibers. As a second option, it was proposed to use the local vessel diameter as the control variable. Larger diameters are desirable at the fluid inlet and smaller vessel diameters at the outlet. Some suggestions for practical realization were made. It was also highlighted that the effective vessel diameter can be modified as well by mechanical inserts into some given overall geometry.

Maximization of extraction yield was the goal defined for processes based on intra-particle diffusion. The local particle size was again chosen as the control variable. It was argued that a particle size gradient leading from larger particles at the flow inlet to smaller ones at the outlet increases extraction yield.

In all cases that were discussed, some principles of Section 2.3.5 were applied and, thereby, illustrated. It was repeatedly shown that it is important to keep all variables except for the control variables constant in order to evaluate the benefits of the optimal control approach in a meaningful way. Furthermore, overall constraints on the control variables are often one important prerequisite for non-trivial, i.e., non-constant, optimal control solutions; otherwise, the optimal trajectory is simply given by one of the bounds of the control variables.

Hopefully, the hypotheses for process improvement and beneficial optimal control approaches are picked up in future work. Only fully conducted optimal control computations, ideally together with an experimental validation, can judge the proposed strategies. Note that also many suggestions can be interpreted as micro-manipulative strategies, according to the label introduced in Section 1.2.1, notably where the particle packing is optimized locally or when mechanical inserts are used to increase local wall support.

Chapter 7

Conclusions and Outlook

Different optimal control problems in the field of filtration and related areas were considered in this dissertation. Throughout the work, a few central motifs, explicitly introduced in Chapter 1, were present in the background. Arranged by increasing abstractness, these central motifs are:

1) In many cases, variable control functions, i.e., the paths determined by optimal control methods, offer benefits over constant values of control variables.

2) The continuum models, used in this thesis because of their computational efficiency, are to be considered as part of a larger framework for multiscale design and control of filtration and similar processes.

3) Results from one area of science and engineering can offer benefits for other areas.

4) Engineering, like natural science, advances by trial and error. On the one hand, therefore, all results have to be seen as hypothetical; on the other, bold conjectures can help to advance the knowledge in a field.

Motifs 1) to 4) are also used to organize this conclusion and give some outlook. Note that the detailed and topic-specific summaries, provided at the end of Chapters 4 to 6, are not repeated here. Only those points most important for the central storyline are included in this chapter. Motif 1), the hypothetical benefits of variable control paths, was a central guideline in the two case studies of Chapters 4 and 5, the main findings of which are summed-up first. The other motifs will be picked up subsequently.

In Chapter 4, a new model-based design method for depth filters was developed. Using the filter coefficient, a measure for local filtration performance, as the control variable which is varied along the filter depth, two scenarios were investigated: First, the filter-coefficient path was optimized in order to achieve a constant deposition of impurities along the filter depth; second, the time until some maximal pressure drop is reached was maximized. The numerical algorithm was also validated for the first scenario using a newly-derived analytical optimal control solution based on a simplified model. Discrete filter layers, usable for practical filter design, were subsequently derived from the optimal trajectories for both scenarios.

A new mechanistic model for filter-aid filtration was introduced in Chapter 5. The model's properties were explored and it was used for optimization and optimal control computations. The chosen mathematical and numerical methods were shown to be able to handle the moving boundary problem including its sharp moving fronts. A front-fixing method was used to transform the problem into one with a fixed computational domain; a flux-limiter scheme assured a numerically stable solution despite strong discontinuities in the solution. Optimization and optimal control showed that the optimal constant filter-aid concentration offers large benefits for energy consumption compared to deviating concentrations; optimally controlling the filter-aid dosage, on the contrary, led only to insignificant improvements.

According to Motif 4), technological and scientific knowledge is always fallible and incomplete. The incompleteness is addressed now by summing-up some open points. The studies on depth filtration, presented in Chapter 4, need to be applied to practical cases of filtration using a fully parameterized model in order to judge the benefits of the proposed design method. To put it briefly: Only the actual use in design can finally judge the value of a design method. The same holds true for the case of filter-aid filtration as discussed in Chapter 5. Even though the new model was qualitatively compared to literature results, a detailed empirical validation is still necessary. Also, the optimization and optimal control results need to be tested empirically. In a nutshell: Only its use for actual process control can finally judge the value of a control method. Additionally, it was found that the chosen numerical optimal control method, a direct single-shooting algorithm, showed some numerical instabilities when computing the optimal filter-aid dosage trajectories. This provided no problem in the context of Chapter 5 because optimal control was found to offer little benefits. If the method is to be applied to analogous cases, however, it is likely that the algorithm needs to be further developed.

One of the common themes in the case studies on depth filtration and filter-aid filtration was the creation of structures with spatially varying characteristics. Note that also the time-variable dosage of filter-aids finally leads to a filter cake with spatially varying properties. According to Motif 3), the transfer of this principle to related areas was explored in Chapter 6. These areas were divided into flow through compressible porous media and processes based on intra-particle diffusion. In the first case, it was suggested that compression and, therefore, energy consumption can be reduced by varying the particle size along the whole packing height or by providing locally varying wall support. In case of diffusion-limited processes, also benefits of varying the particle size along the flow direction were asserted. As all proposed measures were neither developed theoretically in great detail nor tested empirically, the material of Chapter 6 consists of many "bold conjectures". According to Motif 4), it is hoped that they might benefit future research. In this respect, it is important to remark that even when no actual optimal control computations are performed, the proposed strategies might be beneficial. Simply the idea of varying certain process variables along spatial dimensions may open up room for experimental investigations and practical process improvement.

Last, a multiscale approach to porous-media design is outlined for which the present work is an important building block; this paragraph, thus, picks up Motif 2). The multiscale approach to

be described is depicted in Figure 7.1; it is based on a row of observations: First, the important mechanisms in porous media transport often take place on the microscale; e.g., in filtration, impurities are separated on the pore level. Second, in recent times it is possible to a previously unimaginable degree to tailor microstructures after given specifications; this was called the micro-manipulative paradigm in Section 1.2.1. Third, what is needed, therefore, are precise criteria stating what microstructural properties are actually desirable. Fourth, optimal control is a suitable tool to determine optimal profiles of continuum-scale properties, as was shown in this thesis. Fifth, a method is required to bridge the gap between the microscale and the continuum scale.

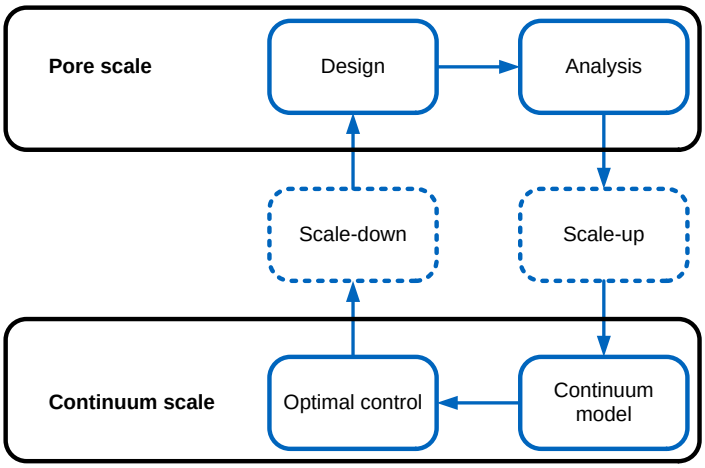

Figure 7.1: Schematic of multi-scale approach to porous-media design.

To flesh-out the sketched multiscale approach, the manufacturing of microstructures as well as the bridging of scales is addressed next. From the different possibilities within the micro-manipulative paradigm, 3D-printing and selective-manufacturing technologies are of great importance. To provide a few examples: Fee et al. (2014) reported on their use of 3D printing to create porous media with precisely defined packing morphologies. Ge et al. (2017) produced particle agglomerates with defined properties by 3D printing. Low et al. (2017) provided a review of 3D printing technologies and their possible application for the fabrication of separation membranes. In the context of chromatography, Nawada et al. (2017) used additive manufacturing to produce columns with defined microstructures and characterized their transport properties. In none of these studies, however, structures with spatially varying properties were addressed, even though their manufacturing clearly is technologically possible.

Bridging of scales is an important ingredient in all multiscale approaches (Horstemeyer, 2010). In the context of porous media research, spatial averaging is a known method to derive macroscopic information from micro-scale properties. Due to its importance in the present context, it was introduced in some detail in Chapter 2. Using spatial averaging, the continuum equations of this work can be derived from pore-scale descriptions. Therefore, all the needed ingredients for the sketched multiscale approach are given. Pore geometries can be manufac-

tured and analyzed on the microscale. Spatial averaging can be used to derived continuum models from microscale mechanisms. Optimal control can be used to optimize spatial profiles on the continuum scale. The known correlations between the continuum equations and the microscale properties can, in turn, be used to translate the continuum results back to the pore scale. Spatially-variable microstructures can be manufactured by 3D printing; thus, the predictions can be validated and the benefits of the optimal control approach can be evaluated.

It is hoped that some of the new paths that were explored in this thesis will be used, extended, and improved upon by others. Science and engineering are open-ended endeavors; thus, there is much to do.

Bibliography

K. G. Allen, T. W. von Backström, and D. G. Kröger. Packed bed pressure drop dependence on particle shape, size distribution, packing arrangement and roughness. *Powder Technology*, 246:590–600, 2013.

C. M. Alles. *Prozeßstrategien für die Filtration mit kompressiblen Kuchen*. Ph.D. thesis, Universität Fridericiana Karlsruhe (TH), Fakultät für Chemieingenieurwesen und Verfahrenstechnik, 2000.

A. C. Alvarez. *Inverse problems for deep bed filtration in porous media*. Ph.D. thesis, Instituto Nacional de Matemática Pura e Aplicada, Rio de Janeiro, Brasil, 2005.

A. C. Alvarez, G. Hime, D. Marchesin, and P. G. Bedrikovetsky. The inverse problem of determining the filtration function and permeability reduction in flow of water with particles in porous media. *Transport in Porous Media*, 70 (1):43–62, 2007.

H. Anlauf. Mechanische Fest/Flüssig-Trennung im Wandel der Zeit. *Chemie Ingenieur Technik*, 75 (10):1460–1463, 2003.

G. Annemüller and H.-J. Manger. *Klärung und Stabilisierung des Bieres*. VLB Berlin, Berlin, 2011.

W. B. Arthur. *The nature of technology – What it is and how it evolves*. Free Press, New York, 2009.

H. E. Babbitt and E. R. Baumann. Effect of body feed on the filtration of water through diatomite. *University of Illinois Bulletin*, 51 (81):1–40, 1954.

R. Bai and C. Tien. Transient behavior of particle deposition in granular media under various surface interactions. *Colloids and Surfaces A: Physicochemical and Engineering Aspects*, 165 (1-3):95–114, 2000.

R. B. Bai and C. Tien. Particle detachment in deep bed filtration. *Journal of Colloid and Interface Science*, 186 (2):307–317, 1997.

M. N. Baker. *The quest for pure water*, vol. I. American Water Works Association, Denver, 1948.

J. Bear. *Dynamics of fluids in porous media*. Dover Publications, New York, 1988. Original Edition: 1972, Elsevier.

P. Bedrikovetsky. Upscaling of stochastic micro model for suspension transport in porous media. *Transport in Porous Media*, 75 (3):335–369, 2008.

S. Bennett. A brief history of automatic control. *IEEE Control Systems*, 16 (3):17–25, 1996.

R. Berndt. *Zur Prozessmodellierung der Filtration von Suspensionen unter besonderer Berücksichtigung der Anschwemmfiltration*. Ph.D. thesis, Technische Universität Dresden, Dresden, 1981.

V. Bhardwaj and M. J. Mirliss. *Water Encyclopedia*, chap. Diatomaceous earth filtration for drinking water. John Wiley & Sons, 2005.

W. G. Bickley. Formulae for numerical differentiation. *The Mathematical Gazette*, 25 (263):19–27, 1941.

C. Bissell. A history of automatic control. In: S. Y. Nof (Ed.), *Springer handbook of automation*, chap. A history of automatic control, pp. 53–69. Springer, Berlin, 2009.

B. Blankert. *Short to Medium Term Optimization of Dead-End Ultrafiltration*. Ph.D. thesis, University of Groningen, 2007.

B. Blankert, B. H. L. Betlem, and B. Roffel. Dynamic optimization of a dead-end filtration trajectory: Blocking filtration laws. *Journal of Membrane Science*, 285 (1-2):90–95, 2006.

B. Blankert, C. Kattenbelt, B. H. L. Betlem, and B. Roffel. Dynamic optimization of a dead-end filtration trajectory: Non-ideal cake filtration. *Journal of Membrane Science*, 290 (1-2):114–124, 2007.

H.-J. Blobel. *Theoretische und experimentelle Untersuchungen zur Trennwirkung bei der Anschwemmfiltration mit Schichtzunahme*. Ph.D. thesis, Technische Universität Dresden, Fakultät für Maschinenwesen, 1985.

G. Boccardo, D. L. Marchisio, and R. Sethi. Microscale simulation of particle deposition in porous media. *Journal of Colloid and Interface Science*, 417:227–237, 2014.

F. H. Braun. *Auswirkungen des Einsatzes von Zellulose als Filterhilfsmittel in der Bierfiltration*. Ph.D. thesis, Technische Universität München, Fakultät Wissenschaftszentrum Weihenstephan für Ernährung, Landnutzung und Umwelt, 2012.

H. J. H. Brouwers. Random packing fraction of bimodal spheres: An analytical expression. *Physical Review E*, 87 (3):032202–1–032202–8, 2013.

H. J. H. Brouwers. Packing fraction of particles with lognormal size distribution. *Physical Review E*, 89 (5):052211–1–052211–12, 2014.

G. Brown. Henry Darcy and the making of a law. *Water Resources Research*, 38 (7):11–1–11–12, 2002.

E. Brun, J. Vicente, F. Topin, R. Occelli, and M. J. Clifton. Microstructure and transport properties of cellular materials: Representative volume element. *Advanced Engineering Materials*, 11 (10):805–810, 2009.

R. Bruttini and A. Liapis. The drying rates of spray freeze drying systems increase through the use of stratified packed bed structures. *International Journal of Heat and Mass Transfer*, 90:515–522, 2015.

A. E. Bryson Jr. and Y.-C. Ho. *Applied optimal control*. Taylor & Francis, New York, 1975.

R. H. Brzesowsky, C. J. Spiers, C. J. Peach, and S. J. T. Hangx. Time-independent compaction behavior of quartz sands. *Journal of Geophysical Research: Solid Earth*, 119 (2):936–956, 2014.

V. N. Burganos, E. D. Skouras, C. A. Paraskeva, and A. C. Payatakes. Simulation of the dynamics of depth filtration of non-Brownian particles. *AIChE Journal*, 47 (4):880–894, 2001.

P. Carman. Fluid flow through granular beds. *Chemical Engineering Research and Design*, 75 (S):S32–S48, 1997. First published 1937.

P. C. Carman. The action of filter aids. *Industrial & Engineering Chemistry*, 30 (10):1163–1167, 1938.

P. C. Carman. The action of filter aids. *Industrial & Engineering Chemistry*, 31 (8):1047–1050, 1939.

G. Carta and A. Jungbauer. *Protein chromatography: Process development and scale-up*. Wiley-VCH, Weinheim, 2010.

M. B. Carver and H. W. Hinds. The method of lines and the advective equation. *Simulation*, 31 (2):59–69, 1978.

N.-S. Cheng. Wall effect on pressure drop in packed beds. *Powder Technology*, 210 (3):261–266, 2011.

A. Chou, W. H. Ray, and R. Aris. Simple control policies for reactors with catalyst decay. *Transactions of the Institution of Chemical Engineers*, 45 (4):153–159, 1967.

F. Civan. Incompressive cake filtration: Mechanism, parameters, and modeling. *AIChE Journal*, 44 (11):2379–2387, 1998.

F. Civan. *Porous media transport phenomena*. John Wiley & Sons, Hoboken, 2011.

F. Civan. Modified formulations of particle deposition and removal kinetics in saturated porous media. *Transport in Porous Media*, 111 (2):381–410, 2015.

F. Civan and M. L. Rasmussen. Analytical models for porous media impairment by particles in rectilinear and radial flows. In: K. Vafai (Ed.), *Handbook of Porous Media*, pp. 485–542. CRC Press, Boca Raton, 2nd ed., 2005.

N. Coote. Turning the art of filter-aid filtration into a science. In: W. Höflinger (Ed.), *International Symposium: Filtration and Separation of Fine Particle Suspensions, Proceedings*, vol. 10-12 November, pp. 315–328. Austrian Chemical Society, Vienna, 1999.

J. Crank. *Free and moving boundary problems*. Oxford University Press, Oxford, 1984.

Y. Daia and V. Srinivasana. On graded electrode porosity as a design tool for improving the energy density of batteries. *Journal of The Electrochemical Society*, 163 (3):A406–A416, 2016.

H. Darcy. *Les fontaines publiques de la ville de Dijon*. Dalmont, Paris, 1856.

R. De Boer. Development of porous media theories – A brief historical review. *Transport in Porous Media*, 9 (1-2):155–164, 1992.

R. Dias, J. Teixeira, M. Mota, and A. Yelshin. Particulate binary mixtures: Dependence of packing porosity on particle size ratio. *Industrial & Engineering Chemistry Research*, 43 (24):7912–7919, 2004.

R. P. Dias, M. Mota, J. A. Teixeira, and A. Yelshin. Study of ternary glass spherical particle beds: Porosity, tortuosity, and permeability. *Filtration*, 5 (1):68–75, 2005.

K. J. Dong, R. Y. Yang, R. P. Zou, and A. B. Yu. Settling of particles in liquids: Effects of material properties. *AIChE Journal*, 58 (5):1409–1421, 2012.

D. A. Drew. Mathematical modeling of two-phase flow. *Annual Review of Fluid Mechanics*, 15 (1):261–291, 1983.

N. Du, J. Fan, H. Wu, and W. Sun. Optimal porosity distribution of fibrous insulation. *International Journal of Heat and Mass Transfer*, 52 (19-20):4350–4357, 2009.

A. Dunne and F. Raby. *Speculative everything: Design, fiction, and social dreaming*. The Mit Press, Cambridge, 2014.

M. Eberhard. *Optimisation of filtration by application of data mining methods*. Ph.D. thesis, Technische Universität München, Fakultät Wissenschaftszentrum Weihenstephan für Ernährung, Landnutzung und Umwelt, 2006.

N. Epstein. On tortuosity and the tortuosity factor in flow and diffusion through porous media. *Chemical Engineering Science*, 44 (3):777–779, 1989.

S. J. Farlow. *Partial differential equations for scientists and engineers*. Dover Publications, New York, 1993.

C. Fee, S. Nawada, and S. Dimartino. 3D printed porous media columns with fine control of column packing morphology. *Journal of Chromatography A*, 1333:18–24, 2014.

M. Fellner, T. Lauer, U. Lübken, and P. Neyses. Manager mit situativer Führung. *Brauindustrie*, 10:50–53, 2012.

J. H. Ferziger and M. Perić. *Computational methods for fluid dynamics*. Springer, Berlin, 2002.

P. Flores and H. M. Lankarani. *Contact force models for multibody dynamics*. Springer, Switzerland, 2016.

G. P. Fulton. Filtration. In: M. J. Taras (Ed.), *The quest for pure water*, vol. II, pp. 47–79. American Water Works Association, Denver, 2nd ed., 1981.

R. Ge, M. Ghadiri, T. Bonakdar, and K. Hapgood. 3D printed agglomerates for granule breakage tests. *Powder Technology*, 306:103–112, 2017.

M. C. Georgiadis and M. Kostoglou. On the optimization of drug release from multi-laminated polymer matrix devices. *Journal of Controlled Release*, 77 (3):273–285, 2001.

S. Gerontas, T. Lan, M. Micheletti, and N. J. Titchener-Hooker. Evaluation of a structural mechanics model to predict the effect of inserts in the bed support of chromatographic columns. *Chemical Engineering Science*, 129:25– 33, 2015.

C. Goh and K. Teo. Control parametrization: A unified approach to optimal control problems with general constraints. *Automatica*, 24 (1):3–18, 1988.

S. Golmon, K. Maute, and M. L. Dunn. A design optimization methodology for Li+ batteries. *Journal of Power Sources*, 253:239–250, 2014.

J. Gostick, M. Aghighi, J. Hinebaugh, T. Tranter, M. A. Hoeh, H. Day, B. Spellacy, M. H. Sharqawy, A. Bazylak, A. Burns, W. Lehnert, and A. Putz. OpenPNM: A pore network modeling package. *Computing in Science Engineering*, 18 (4):60–74, 2016.

D. Gross, W. Hauger, J. Schröder, W. Wall, and J. Bonet. *Engineering mechanics 2*. Springer, Berlin, 2011.

J. Haba and R. Koch. Analyse des Filtrationsprozesses unter Einsatz von Filterhilfsmitteln. *Chemische Technik*, 30 (2):91–94, 1978.

I. Hacking. *Representing and intervening*. Cambridge University Press, Cambridge, 1983.

A. Hackl, E. Heidenreich, W. Höflinger, and R. Tittel. *Filterhilfsmittelfiltration*. VDI-Verlag, Düsseldorf, 1993.

R. Hannemann-Tamas and W. Marquardt. How to verify optimal controls computed by direct shooting methods? – A tutorial. *Journal of Process Control*, 22 (2):494–507, 2012.

J.-H. Hao, Q. Chen, and K. Hu. Porosity distribution optimization of insulation materials by the variational method. *International Journal of Heat and Mass Transfer*, 92:1–7, 2016.

F. Hebmüller. *Einflussfaktoren auf die Kieselgurfiltration von Bier*. Ph.D. thesis, Technischen Universität Bergakademie Freiberg, Fakultät für Maschinenbau, Verfahrens- und Energietechnik, 2003.

P. Heertjes and P. Zuideveld. Clarification of liquids using filter aids – Part I: Mechanisms of filtration. *Powder Technology*, 19 (1):17–30, 1978a.

P. Heertjes and P. Zuideveld. Clarification of liquids using filter aids – Part II: Depth filtration. *Powder Technology*, 19 (1):31–43, 1978b.

P. Heertjes and P. Zuideveld. Clarification of liquids using filter aids – Part III: Cake resistance in surface filtration. *Powder Technology*, 19 (1):45–64, 1978c.

D. Hekmat, M. Kuhn, V. Meinhardt, and D. Weuster-Botz. Modeling of transient flow through a viscoelastic preparative chromatography packing. *Biotechnology Progress*, 29 (4):958–967, 2013.

D. Hekmat, R. Mornhinweg, G. Bloch, Y. Sun, P. Jeanty, M. Neubert, and D. Weuster-Botz. Macroscopic investigation of the transient hydrodynamic memory behavior of preparative packed chromatography beds. *Journal of Chromatography A*, 1218 (7):944–950, 2011.

J. Herzig, D. LeClerc, and P. LeGoff. Flow of suspensions through porous media – Application to deep filtration. *Industrial & Engineering Chemistry Research*, 62 (5):8–35, 1970.

W. Hintz, S. Antonyuk, W. Schubert, B. Ebenau, A. Haack, and J. Tomas. Determination of physical properties of fine particles, nanoparticles and particle beds. In: E. Tsotsas and A. S. Mujumdar (Eds.), *Modern drying technology: Experimental techniques, Volume 2*, pp. 279–362. Wiley-VCH, Weinheim, 2008.

F. Horn. Optimale Temperatur- und Konzentrationsverläufe. *Chemical Engineering Science*, 14:77–89, 1961.

M. F. Horstemeyer. Multiscale modeling: A review. In: J. Leszczynski and M. K. Shukla (Eds.), *Practical aspects of computational chemistry*, pp. 87–135. Springer, Dordrecht, 2010.

X. Huang, Q. Wang, W. Zhou, D. Deng, Y. Zhao, D. Wen, and J. Li. Morphology and transport properties of fibrous porous media. *Powder Technology*, 283:618–626, 2015.

J. Hubbuch, T. Linden, E. Knieps, A. Ljunglöf, J. Thömmes, and M.-R. Kula. Mechanism and kinetics of protein transport in chromatographic media studied by confocal laser scanning microscopy. *Journal of Chromatography A*, 1021 (1):93–104, 2003a.

J. Hubbuch, T. Linden, E. Knieps, J. Thömmes, and M.-R. Kula. Mechanism and kinetics of protein transport in chromatographic media studied by confocal laser scanning microscopy. *Journal of Chromatography A*, 1021 (1):105–115, 2003b.

T. Hunt. Filter aids. In: M. C. Flickinger (Ed.), *Encyclopedia of industrial biotechnology*, pp. 1190–1197. John Wiley & Sons, 2009.

K. Husemann, F. Hebmüller, and M. Esslinger. Importance of deep bed filtration during kieselguhr filtration (Part 2). *Monatsschrift für Brauwissenschaft*, 56 (9-10):152–160, 2003.

J. N. Israelachvili. *Intermolecular and Surface Forces*. Academic Press, Waltham, 2011.

K. J. Ives (Ed.). *The scientific basis of filtration*. Noordhoff, Noordhoff, 1975.

T. Iwasaki. Some notes on sand filtration. *Journal of American Water Works Association*, 29 (10):1591–1602, 1937.

E. Johannessen and S. Kjelstrup. Minimum entropy production rate in plug flow reactors: An optimal control problem solved for SO2 oxidation. *Energy*, 29 (12-15):2403–2423, 2004.

D. Kahneman. *Thinking, fast and slow*. Penguin Books, London, 2012.

J. Kain. *Entwicklung und Verfahrenstechnik eines Kerzenfiltersystems (Twin-Flow-System) als Anschwemmfilter*. Ph.D. thesis, Technische Universität München, Fakultät Wissenschaftszentrum Weihenstephan für Ernährung, Landnutzung und Umwelt, 2004.

H. Kandra, A. Deletic, and D. McCarthy. Impact of filter design variables on clogging in stormwater filters. In: *WSUD 2012 - 7th International Conference on Water Sensitive Urban Design Conference 2012*. 2012.

H. S. Kandra, A. Deletic, and D. McCarthy. Assessment of impact of filter design variables on clogging in stormwater filters. *Water Resour. Manag.*, 28 (7):1873–1885, 2014a.

H. S. Kandra, D. McCarthy, T. D. Fletcher, and A. Deletic. Assessment of clogging phenomena in granular filter media used for stormwater treatment. *Journal of Hydrology*, 512:518–527, 2014b.

A.-R. Khaled and K. Vafai. The role of porous media in modeling flow and heat transfer in biological tissues. *International Journal of Heat and Mass Transfer*, 46 (26):4989–5003, 2003.

D. E. Kirk. *Optimal control theory*. Dover, Mineola, 2004.

J. Kozeny. Üeber kapillare Leitung des Wassers im Boden. *Sitzungsber Akad. Wiss., Wien*, 136 (2a):271–306, 1927.

M. Kuhn. Wo sind wir, wenn wir Technik treiben? – Über den Ursprung technischer Artefakte im Fiktiven. *fatum*, 3:75–78, 2015.

M. Kuhn. Fiktionale Variationen als Urprung technischer Artefakte. In: J. H. Franz and K. Berr (Eds.), *Welt der Artefakte*, pp. 43–54. Frank & Timme, Berlin, 2017.

M. Kuhn and H. Briesen. Dosage of filter aids in the case of pure surface filtration – An optimal control approach. *Computer Aided Chemical Engineering*, 37:1655–1660, 2015.

M. Kuhn and H. Briesen. Dynamic modeling of filter-aid filtration including surface- and depth-filtration effects. *Chemical Engineering & Technology*, 39 (3):425–434, 2016a.

M. Kuhn and H. Briesen. Optimal design of depth filters: A new model-based method. In: *Proceedings of the 12th World Filtration Congress*. 2016b.

M. Kuhn, C. Kirse, and H. Briesen. Improving the design of depth filters: A model-based method using optimal control theory. *AIChE Journal*, accepted, 2017a.

M. Kuhn, S. Lang, F. Bezold, M. Minceva, and H. Briesen. Time-resolved extraction of caffeine and trigonelline from finely-ground espresso coffee with varying particle sizes and tamping pressures. *Journal of Food Engineering*, 206:37–47, 2017b.

M. Kuhn, W. Pietsch, and H. Briesen. Clarifying thoughts about the clarification of liquids – Filtration and the philosophy of science. *Chemie Ingenieur Technik*, 89 (9):1126–1132, 2017c.

T. S. Kuhn. *The structure of scientific revolutions*. University of Chicago Press, Chicago, 1970. First published 1962.

J. Lee and J. Koplik. Microscopic motion of particles flowing through a porous medium. *Physics of Fluids*, 11 (1):76–87, 1999.

R. J. LeVeque. *Numerical methods for conservation laws*. Birkhäuser Verlag, Basel, 1992.

F. L. Lewis, D. L. Vrabie, and V. L. Syrmos. *Optimal control*. John Wiley & Sons, Hoboken, 2012.

M. Li and A. I. Liapis. Adsorption in a stratified column bed packed with porous particles having partially fractal structures and a distribution of particle diameters. *Journal of Separation Science*, 35 (8):947–956, 2012.

W. Liu, S. Chen, and S. Li. Influence of adhesion on random loose packings of binary microparticle mixtures. *AIChE Journal*, 63 (10):4296–4306, 2017.

Z. Liu, W. Wang, R. Xie, X.-J. Ju, and L.-Y. Chu. Stimuli-responsive smart gating membranes. *Chemical Society Reviews*, 45:460–475, 2016.

Z.-X. Low, Y. T. Chua, B. M. Ray, D. Mattia, I. S. Metcalfe, and D. A. Patterson. Perspective on 3D printing of separation membranes and comparison to related unconventional fabrication techniques. *Journal of Membrane Science*, 523:596–613, 2017.

B. Lu and S. Torquato. Chord-length and free-path distribution functions for many-body systems. *Journal of Chemical Physics*, 98 (8):6472–6482, 1993.

S. Lu, W. Ramirez, and K. Anseth. Modeling and optimization of drug release from laminated polymer matrix devices. *AIChE Journal*, 44 (7):1689–1696, 1998.

M. J. MacDonald, C.-F. Chu, P. P. Guilloit, and K. M. Ng. A generalized Blake-Kozeny equation for multisized spherical particles. *AIChE Journal*, 37 (10):1583–1588, 1991.

L. E. Malvern. *Introduction to the mechanics of a continuous medium*. Prentice-Hall, Englewood Cliffs, 1969.

L. McDowell-Boyer, J. Hunt, and N. Sitar. Particle transport through porous media. *Water Resources Research*, 22 (13):1901–1921, 1986.

R. N. Methekar, V. Boovaragavan, M. Arabandi, V. Ramadesigan, V. R. Subramanian, F. Latinwo, and R. D. Braatz. Optimal spatial distribution of microstructure in porous electrodes for Li-ion batteries. In: *Proceedings of the American Control Conference*, pp. 6600–6605. 2010.

M. Mirabolghasemi, M. Prodanović, D. DiCarlo, and H. Ji. Prediction of empirical properties using direct pore-scale simulation of straining through 3D microtomography images of porous media. *Journal of Hydrology*, 529, Part 3:768–778, 2015.

I. L. Molnar, W. P. Johnson, J. I. Gerhard, C. S. Willson, and D. M. O'Carroll. Predicting colloid transport through saturated porous media: A critical review. *Water Resources Research*, 51 (9):6804–6845, 2015.

K. Moroney, W. Lee, S. O'Brien, F. Suijver, and J. Marra. Modelling of coffee extraction during brewing using multiscale methods: An experimentally validated model. *Chemical Engineering Science*, 137 (0):216–234, 2015.

M. Mota, J. A. Teixeira, W. R. Bowen, and A. Yelshin. Binary spherical particle mixed beds: Porosity and permeability relationship measurement. *Transactions of the Filtration Society*, 1 (4):101–106, 2001.

S. Nawada, S. Dimartino, and C. Fee. Dispersion behavior of 3D-printed columns with homogeneous microstructures comprising differing element shapes. *Chemical Engineering Science*, 164:90–98, 2017.

B. F. Nielsen, O. Skavhaug, and A. Tveito. Penalty and front-fixing methods for the numerical solution of american option problems. *Journal of Computational Finance*, 5:69–97, 2002.

S. Noerpel, V. Siauw, and H. Nirschl. Filter cake washing of mesoporous particles. *Chemical Engineering & Technology*, 35 (4):661–667, 2012.

A. F. Ogunye and W. H. Ray. Optimal control policies for tubular reactors experiencing catalyst decay. Part 1. Single bed reactors. *AIChE Journal*, 17 (1):43–51, 1971.

M. Papageorgiou, M. Leibold, and M. Buss. *Optimierung – Statische, dynamische, stochastische Verfahren für die Anwendung*. Springer, Berlin, 2012.

K. H. Parker, R. V. Mehta, and C. G. Caro. Steady flow in porous, elastically deformable materials. *Journal of Applied Mechanics*, 54 (4):794–800, 1987.

R. Paulen. *Optimal operation of batch membrane processes*. Ph.D. thesis, Slovak University of Technology in Bratislava, Faculty of Chemical and Food Technology, 2012.

K. R. Popper. *Objective knowledge – An evolutionary approach*. Oxford University Press, Oxford, 1972.

K. R. Popper. *Conjectures and refutations*. Routledge, London, 2002a. First published 1962.

K. R. Popper. *The logic of scientific discovery*. Routledge, London, 2002b. First published 1959.

M. Rainer. *Aufbau und Eigenschaften von Precoatschichten auf Filtermedien für die Anschwemmfiltration*. Ph.D. thesis, Technischen Universität Wien, Fakultät für Maschinenbau, 2003.

V. Ramadesigan, R. N. Methekar, F. Latinwo, R. D. Braatz, and V. R. Subramaniana. Optimal porosity distribution for minimized ohmic drop across a porous electrode. *Journal of The Electrochemical Society*, 157 (12):A1328–A1334, 2010.

Raschig. Random packings. `http://www.raschig.de/-Random-Packings`, 2017. Last accessed: 21.06.2017.

S. Ripperger, W. Gösele, C. Alt, and T. Loewe. *Ullmann's Encyclopedia of Industrial Chemistry*, vol. 14, chap. Filtration, 1. Fundamentals, pp. 677–709. Wiley-VCH, Weinheim, 2012.

R. Sargent. Optimal control. *Journal of Computational and Applied Mathematics*, 124 (1-2):361–371, 2000.

M. Schäfer. *Computational engineering*. Springer, Berlin, 2006.

W. E. Schiesser and G. W. Griffiths. *A compendium of partial differential equation models: Method of lines analysis with Matlab*. Cambridge University Press, Cambridge, 2009.

L. Shampine and M. Reichelt. The MATLAB ODE suite. *SIAM Journal on Scientific Computing*, 18 (1):1–22, 1997.

A. P. Shapiro and R. F. Probstein. Random packings of spheres and fluidity limits of monodisperse and bidisperse suspensions. *Physical Review Letters*, 68:1422–1425, 1992.

B. Sorensen and P. Sorensen. Structure compression in cake filtration. *Journal of Environmental Engineering (ASCE)*, 123 (4):345–353, 1997.

M. Spijker. Stiffness in numerical initial-value problems. *Journal of Computational and Applied Mathematics*, 72 (2):393–406, 1996.

K. Stamatakis and C. Tien. Cake formation and growth in cake filtration. *Chemical Engineering Science*, 46 (8):1917–1933, 1991.

H. J. Sussmann and J. C. Willems. 300 years of optimal control: From the brachystochrone to the maximum principle. *IEEE Control Systems*, 17 (3):32–44, 1997.

D. H. Sutherland and P. Hidi. An investigation of filter-aid behaviour. *Transactions of the Institution of Chemical Engineers*, 44 (4):T122–T127, 1966.

K. Sutherland. *Filters and filtration handbook*. Elsevier, Oxford, 5th ed., 2008.

L. Svarovsky. *Solid-liquid separation*. Butterworth-Heinemann, Oxford, 2000.

N. N. Taleb. *The black swan*. Random House, New York, 2007.

J. Tansey and M. T. Balhoff. Pore network modeling of reactive transport and dissolution in porous media. *Transport in Porous Media*, 113 (2):303–327, 2016.

The MathWorks. Optimization decision table. `http://de.mathworks.com/help/optim/ug/optimization-decision-table.html`, 2017. Last accessed: 26.04.2017.

J. W. Tichy. *Zum Einfluss des Filtermittels und der auftretenden Interferenzen zwischen Filterkuchen und Filtermittel bei der Kuchenfiltration*. Ph.D. thesis, Technische Universität Kaiserslautern, Fachbereich Maschinenbau und Verfahrenstechnik, 2007.

C. Tien. *Introduction to cake filtration*. Elsevier B. V., Amsterdam, 2006.

C. Tien, R. Bai, and B. Ramarao. Analysis of cake growth in cake filtration: Effect of fine particle retention. *AIChE Journal*, 43 (1):33–44, 1997.

C. Tien and B. V. Ramarao. *Granular filtration of aerosols and hydrosols*. Elsevier, Amsterdam, 2007.

C. Tien and B. V. Ramarao. Can filter cake porosity be estimated based on the Kozeny-Carman equation? *Powder Technology*, 237:233–240, 2013.

C. Tien, R. Turian, and H. Pendse. Simulation of the dynamic behavior of deep bed filters. *AIChE Journal*, 25 (3):385–395, 1979.

F. M. Tiller and H. Cooper. The role of porosity in filtration: Part V. Porosity variation in filter cakes. *AIChE Journal*, 8 (4):445–449, 1962.

R. Tittel. *Die Anschwemmfiltration als ein Prozess zur Klärung von Flüssigkeiten*. Ph.D. thesis, Technische Universität Dresden, Sektion Verarbeituns- und Verfahrenstechnik, Dresden, 1987.

S. Torquato. Statistical description of microstructures. *Annual Review of Materials Research*, 32:77–111, 2002.

S. R. Upreti. *Optimal control for chemical engineers*. CRC Press, Boca Raton, 2013.

K. Vafai (Ed.). *Handbook of porous media*. CRC Press, Boca Raton, 2005.

A. van Boxtel, Z. Otten, and H. van der Linden. Dynamic optimization of a one-stage reverse-osmosis installation with respect to membrane fouling. *Journal of Membrane Science*, 65 (3):277–293, 1992.

B. van Leer. Towards the ultimate conservative difference scheme. II. Monotonicity and conservation combined in a second-order scheme. *Journal of Computational Physics*, 14 (4):361–370, 1974.

C. M. Van Wyk. A study of the compressibility of wool, with special reference to South African merino wool. *Onderstepoort Journal of Veterinary Science and Animal Industry*, 21 (1):99–127, 1946.

S. Venkataraman, R. Haftka, B. Sankar, H. Zhu, and M. Blosser. Optimal functionally graded metallic foam thermal insulation. *AIAA Journal*, 42 (11):2355–2363, 2004.

Verein Deutscher Ingenieure. Mechanical solid-liquid-separation by cake filtration, Part 2: Determination of filter cake resistance. Tech. rep., VDI-Gesellschaft Verfahrenstechnik und Chemieingenieurwesen, Fachausschuss Mechanische Flüssigkeitstrennung, Düsseldorf, 2006.

K. Vollmari, T. Oschmann, S. Wirtz, and H. Kruggel-Emden. Pressure drop investigations in packings of arbitrary shaped particles. *Powder Technology*, 271 (0):109–124, 2015.

R. Wakeman and E. Tarleton. *Filtration – Equipment selection, modelling and process simulation*. Elsevier, Oxford, 1999.

K. Wegner. *Hydrodynamische Modellierung der Klärfiltration mit körnigen Stoffen unter besonderer Berücksichtigung der Anschwemmfiltration mit Schichtzunahme*. Ph.D. thesis, Technische Universität Dresden, Fakultät für Maschinenwesen, 1985.

S. Whitaker. The equations of motion in porous media. *Chemical Engineering Science*, 21 (3):291–300, 1966.

S. Whitaker. Flow in porous media I: A theoretical derivation of darcy's law. *Transport in Porous Media*, 1 (1):3–25, 1986.

S. Whitaker. *The method of volume averaging*, vol. 13 of *Theory and applications of transport in porous media*. Springer, Dordrecht, 1999.

L. Wittgenstein. *Tractatus logico-philosophicus*. Routledge, London, 2001. First published in Annalen der Naturphilosophie 1921; english edition first published 1922.

A. V. Wouwer, P. Saucez, and C. Vilas. *Simulation of ODE/PDE Models with MATLAB, OCTAVE and SCILAB*. Springer, Cham, 2014.

Q. Xiong, T. G. Baychev, and A. P. Jivkov. Review of pore network modelling of porous media: Experimental characterisations, network constructions and applications to reactive transport. *Journal of Contaminant Hydrology*, 192:101–117, 2016.

W.-C. Yang (Ed.). *Handbook of fluidization and fluid-particle systems*. Marcel Dekker, New York, 2003.

J. Yoon, J. Germaine, and P. Culligan. Visualization of particle behavior within a porous medium: Mechanisms for particle filtration and retardation during downward transport. *Water Resources Research*, 42 (6):1–16, 2006.

A. B. Yu, R. P. Zou, and N. Standish. Packing of ternary mixtures of nonspherical particles. *Journal of the American Ceramic Society*, 75 (10):2765–2772, 1992.

A. Zamani and B. Maini. Flow of dispersed particles through porous media – Deep bed filtration. *Journal of Petroleum Science and Engineering*, 69 (1-2):71–88, 2009.

H. Zhu, B. Sankar, R. Haftka, S. Venkataraman, and M. Blosser. Optimization of functionally graded metallic foam insulation under transient heat transfer conditions. *Structural and Multidisciplinary Optimization*, 28 (5):349–355, 2004.

E. Zondervan. *Intermediate to long term optimization of dead-end ultrafitration*. Ph.D. thesis, Groningen University, Chemical Engineering Department, 2007.

E. Zondervan and B. Roffel. Dynamic optimization of chemical cleaning in dead-end ultra filtration. *Journal of Membrane Science*, 307 (2):309–313, 2008.